University of Groningen

Polystyrene - poly (sodium methacrylate) amphiphilic triblock copolymers by ATRP for Enhanced Oil Recovery;

Synthesis, characterization and effect of structure on rheology of aqueous solutions

By Marc Meijerink

A thesis submitted in partial fulfillment for the

degree of Master of Science

in the

Faculty of Mathematics and Natural Sciences

Chemical Engineering Department

December 2015

This page intentionally left blank

Polystyrene - poly (sodium methacrylate) amphiphilic triblock copolymers by ATRP for Enhanced Oil Recovery

Justification

Title	:	Polystyrene - poly (sodium methacrylate) amphiphilic triblock copolymers by ATRP for Enhanced Oil Recovery
Subtitle	:	Synthesis, characterization and effect of structure on rheology of aqueous solutions
Status	:	Final version
Date of Publication	:	16/12/2015
Author	:	Marc Meijerink

Contact	:	Marc Meijerink	(marcmij92@gmail.com)
Student number	:	2022176	

Institution	:	University of Groningen
Faculty	:	Faculty of Mathematics and Natural Sciences
Address	:	Nijenborgh 4, 9747 AG Groningen
Department	:	Chemical Engineering
Project	:	Part of the Research Program of the Dutch Polymer Institute DPI, Eindhoven, The Netherlands, project #716

Thesis Assessors	:	Prof. dr. Francesco Picchioni[a]	(f.picchioni@rug.nl)
	:	Dr. P.P. Pescarmona[b]	(p.p.pescarmona@rug.nl)
Supervisor	:	ir. Frank van Mastrigt[c]	(f.van.mastrigt@rug.nl)

[a] Professor – Chemical Engineering and Polymer Science, [b] Assistant Professor – Sustainable Chemical Products and Catalysis, [c] PhD candidate

Acknowledgement

This report is a thesis written as partial fulfillment for the degree of Master of Science in the Faculty of Mathematics and Natural Sciences. The thesis should reflect the acquired learned skills in the master degree program of Chemical Engineering at the University of Groningen.

The project started at 14 November 2014 and it took 12 months to complete this thesis. It has been a challenging learning process where I gained a lot of knowledge in the field of polymeric surfactants. The work described in this thesis was performed in the research group Product Technology of the Engineering and Technology Institute at the University of Groningen, the Netherlands.

This report would not have been possible without the support and guidance of many people. I would like to thank professor dr. Francesco Picchioni for accepting me in his group, his feedback and support. Furthermore, I would like to express my gratitude to my daily supervisor ir. Frank van Mastrigt for his assistance, help and advice during the project. Also I would like to thank dr. Patrizio Raffa for suggestions, feedback and helpful discussions about the experiments. The negative stain and cryo transmission electron microscopy images would not have been possible without the help of Linda Franken. Finally, I would like to thank my fellow students and G.T.D Bernoulli for the great time at coffee hours, Friday afternoon drinks and activities.

Marc Meijerink

Abstract

Well-defined amphiphilic triblock poly(sodium methacrylate)-polystyrene-poly(sodium methacrylate) (PMAA-*b*-PS-*b*-PMAA) copolymers characterized by a different length of either the hydrophilic or the hydrophobic block have been synthesized by ATRP. In solution the micelle-like aggregates consists of a collapsed PS core surrounded by charged hydrated PMAA chains which are fully stretched. The micelles are kinetically 'frozen' and as a consequence the triblock copolymers do not show any surface activity. At higher polymer concentrations the micelles interpenetrate and shrink, forming a polymer network. A mathematical model is used to describe the micelle radius and the results were in good agreement with the experimentally obtained radius in transmission electron microscopy. A systematic investigation of the triblock copolymers concerning their rheological behavior in water showed that the hydrophilic block length has a major influence on the rheology where the short PMAA blocks yield the strongest gels at the same weight concentration. The hydrophobic block length has only a minor influence until a certain threshold (35 monomeric units) below which the hydrophobic interactions are too weak resulting in the formation of weak gels. When the polymers are used in EOR, they improve the oil recovery between 40-60% in a 2D flow-cell, which simulates the residual oil in dead-end pores. The oil recovery in high permeable Bentheim sandstone cores was significantly improved with an additional oil recovery of 6% for the triblock copolymer compared with 4% for a commercial HPAM polymer.

Keywords: amphiphilic block copolymers, ATRP, rheology, Enhanced Oil Recovery

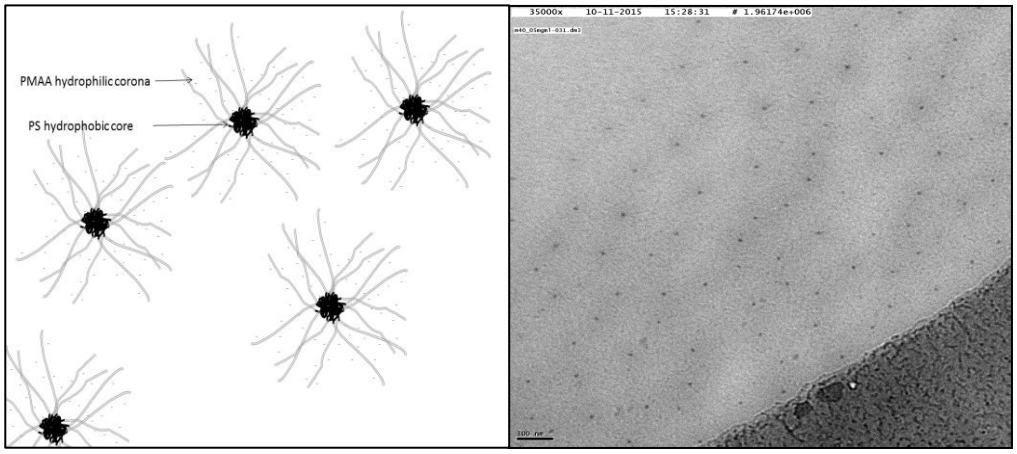

Figure: Schematic + cryo-TEM image of PS-PMAA triblock copolymers in solution

University of Groningen – Department of Chemical Engineering │Nijenborgh 4, 9747 AG Groningen

Table of Contents

Acknowledgement 4

Abstract 5

Table of Contents 6

List of Figures 7

List of Tables 8

List of Abbreviations 9

1. Introduction 10

2. Background information 14

2.1 Oil recovery 14

2.2 Controlled/living radical polymerization 16

3. Materials and Methods 18

4. Results and Discussion 25

4.1 Synthesis of triblock copolymers of polystyrene and poly(methacrylic acid) 25

4.2 Rheology of aqueous solution with PMAA-*b*- PS-*b*-PMAA block copolymers 34

4.3 Oil recovery simulation 55

4.3.1 Flow-cell experiments 55

4.3.2 Core-flood experiment 57

5. Conclusion 62

6. Recommendations 64

References 65

Appendix I 71

Appendix II 72

Appendix III 73

Appendix IV 74

Appendix V 75

Appendix VI 76

List of Figures

Figure 1: Viscous fingering (left) and polymer flooding (right) in an oil reservoir 14
Figure 2: ATRP polymerization of styrene 17
Figure 3: A schematic (a) and photo (b) presentation of the flow-cell (top view) 23
Figure 4: Schematic presentation of the experimental set-up for the core-flood experiments 24
Figure 5: Polymerization of EBIB and styrene to form a polystyrene macroinitiator 25
Figure 6: Polymerization of tBMA and PS-Br macroinitiator to form a block copolymer 26
Figure 7: Hydrolysis of the block copolymers resulting in PMAA-*b*-PS-*b*-PMAA triblock copolymer 28
Figure 8: Synthesis of poly(methacrylic acid) by RAFT polymerization 28
Figure 9: Synthesis of the sodium salt by adding NaOH where after the excess base is removed by dialysis 30
Figure 10: Synthesis and structure of a polymer prepared in this report (entry 11; PS45-PMAA598) 30
Figure 11: Overview of the synthesized PMAA-*b*-PS-*b*-PMAA block copolymers 31
Figure 12: a) Proton NMR spectra for entry 2 (styrene]/[EBIB] ratio = 70/1). b) Proton NMR spectra for entry 7 ([MAA]/[PS-Br] ratio = 2061/1) 32
Figure 13: Hydrolysis step for entry 7 from PS75-tBMA463 to PS75-PMAA463 33
Figure 14: Evolution of the molecular weight distributions for tBMA ATRP polymerizations using PS-Br macroinitiator entry 1 (a), entry 2 (b) and entry 4 (c) as initiator and ME6TREN as ligand. d) The GPC traces for the molecular weight distribution of the produced PS-tBMA triblock copolymers. 34
Figure 15: Viscosity as function of the shear rate for different PMAA-*b*-PS-*b*-PMAA block copolymers. Polymers were measured at a concentration of 1wt%. 35
Figure 16: The apparent viscosity (at $\gamma = 9.63\ s^{-1}$; 1 wt%) as a function of the hydrophobic and hydrophilic block length 36
Figure 17: The apparent viscosity (at $\gamma = 9.63\ s^{-1}$) as a function of the concentration and schematic representation of micelles overlapping and shrinking in the different regions 37
Figure 18: Schematic representation of the arrangement of the amphiphilic triblock copolymers into micelles 38
Figure 19: Tube inversion tests. Concentration = 1 wt%. Entry 8: PS75-PMAA629 ; Entry 11: PS45-PMAA598 38
Figure 20: a,b,c) G' and G'' versus the frequency for 1 wt% polymer solutions. d) G' and G'' versus the frequency at different polymer concentration for entry 11: PS45-PMAA598 39
Figure 21: a,b) Cross-over point for the different polymer solutions at G' and G'' versus the frequency for 1 wt% and 0.1 wt% polymer solutions. c,d) Phase angle as a function of the frequency at 1 wt% and 0.1 wt% polymer concentration 40
Figure 22: Surface tension vs the polymer concentration of various triblock copolymers 41
Figure 23: Schematic of the exchange mechanisms between the bulk and the interface for a solution of (a) PMAA-*b*-PS-*b*-PMAA and (b) PDEGA-*b*-PAA 42
Figure 24: Negative stain EM pictures of 1 wt% solutions of: entry 7 (a), entry 8 (b), entry 11 (c), entry 9 (e), entry 10(e) and entry 12(f) 44
Figure 25: Cryo-TEM image of an amphiphilic triblock copolymer at 0.3 wt % (a,b) and 0.5 wt% (c,d) (entry 8: PS75-PMAA629) 45
Figure 26: Stern model describing the ionic conc. as a function of the distance from the charged surface of a particle 46
Figure 27: The zeta potential of the PS-PMAA triblock copolymer systems in water (conc. $2\ 10^{-5}$M) 47
Figure 28: a) Shear viscosity of 1 wt% PS45-PMAA598 solutions at different NaCl concentrations b) Viscosity (measured at $\gamma = 9.63\ s^{-1}$ at 20 °C) as a function of the polymer concentration in salt water (30.000 ppm NaCl) 48
Figure 29: Star-like micelle of PS-PMAA triblock copolymer in water without (left) and with (right) the addition of salt 49
Figure 30: a) Shear viscosity of entry 11 (PS45-PMAA598, 1 wt%) as function of the shear rate at different temperatures. B) Shear viscosity of entry 11 as function of temperature at $\gamma = 9.63\ s^{-1}$ 50
Figure 31: Shear viscosity of entry 11 (PS45-PMAA598, 1 wt%) at different pH 50
Figure 32: pH dependency of the zeta potential for PS45-PMAA598 solutions (conc. $2 * 10^{-5}$ M) 51

Figure 33: Phase separation of oil and polymer solution (with the same viscosity) at given times 52
Figure 34: Light microscopy images (magnification 40x) after emulsification for (a) water (b) Entry 7: PS75-PMAA463, 58.6 kDa (c) Entry 8: PS75-PMAA629, 76.7 kDa (d) Entry 9: PS45-PMAA2210, 245.9 kDa (e) Entry 10: PS45-PMAA1047, 119.2 kDa (f) Entry 12: PS35-PMAA1564, 174.5 kDa and (g) Entry 11: PS45-PMAA598, 70.2 kDa 53
Figure 35: Comparison between the reference (water/oil) and polymer emulsion (entry 11/oil) directly and after 5 days of emulsification 54
Figure 36: Phase separation of oil and polymer solution (at the same molar concentration) at given times 54
Figure 37: Oil recovery out of dead-end zones in the 2D flow-cell (molecular weight in Da) 56
Figure 38: Oil recovery from high permeable Bentheim sandstone cores 59
Figure 39: Viscosity as function of the shear rate (PS75-PMAA629) before and after the polymer flood in the core-flood experiment 59

List of Tables

Table 1: Results of polymerization reaction of styrene by ATRP 25
Table 2: Synthesis of block copolymers (PtBMA-*b*-PS-*b*-PtBMA) by ATRP (90 °C) 27
Table 3: Characterization of the triblock copolymers by ^{1}H-NMR, GPC and gravimetric analysis 27
Table 4: Synthesis of PMAA by RAFT polymerization 29
Table 5: Overview of the synthesized PMAA-*b*-PS-*b*-PMAA block copolymers 31
Table 6: Calculated $r_{A,}$ r_B and p according to equation 12 and 15 43
Table 7: Average radius of a micelle in solution at different concentrations 45
Table 8: The calculated micelles radius, r_{mic}, with and without the addition of salt 48
Table 9: Comparison between theoretical and experimentally found micelle radius 49
Table 10: Physical properties of the sandstone cores used in the core-flood experiments 57
Table 11: Oil recovery from Bentheim sandstone cores (brine concentration 2000 ppm) 58
Table 12: Permeability results of the core-flood experiment 60

List of Abbreviations

ACVA	4,4'- Azobis(4-cyanovaleric acid)
API	American petroleum institute
ATRP	Atom transfer radical polymerization
BzMA	Benzyl methacrylate
CMC	Critical micelle concentration
CPADB	4-Cyano-4- (phenylcarbonothioylthio)pentanoic acid
CTA	Chain transfer agent
EOR	Enhanced Oil Recovery
EBIB	Ethylene bis(2-bromoisobutyrate)
GPC	Gel permeation chromatography
HPAM	Hydrolyzed polyacrylamide
IOR	Improved oil recovery
MAA	Methacrylic acid
Me6TREN	Tris[2-(dimethylamino)ethyl]-amine
Mn	Molecular weight distribution
NMP	Nitroxide-mediated polymerization
NMR	Nuclear magnetic resonance
OOIP	Original oil in place
PAA	Poly acrylic acid
PBA	Poly (n-butyl acrylate)
PCL	Polycaprolactone
PDEGA	Poly (diethylene glycol ethyl ether acrylate)
PDI	Polydispersity index
PEB	Poly (ethylene-co-butene)
PMAA	Poly methacrylic acid
PEG	Poly (ethylene glycol)
PEO	Poly (ethylene oxide)
PMDETA	N,N,N′,N″,N″-Pentamethyldiethylenetriamine
PPO	Poly (propylene oxide)
ppm	Parts per million
PS	Polystyrene
RAFT	Reversible addition−fragmentation chain-transfer
RF	Resistant factor
RRF	Residual resistant factor
tBA	Tert-butyl acrylate
tBMA	Tert-butyl methacrylate
TEM	Transmission electron microscopy
THF	Tetrahydrofuran
TMEDA	Tetramethylethylenediamine

1. Introduction

Amphiphilic block copolymers are of great industrial importance due to their adjustable rheological behavior and formation of self-assembled structures in a specific solvent (mostly water)[1-4]. The possibility exist to introduce responsive behavioral groups into the blocks, which respond to parameters such as pH[5], temperature[6] or UV irradiation[1]. The versatility in properties has resulted in an increased attention in the last decades for application in several fields including smart materials[6,7], micro emulsion stabilization[8] and polymerization[9,10], coatings[11], drug delivery[12-14] and Enhanced Oil Recovery[15-18]. In the application of Enhanced Oil Recovery (EOR) the additional oil recovery is mainly influenced by the viscosity of the displacement fluid and the interfacial tension between the water phase and the oil[19]. Recently, it was discovered that the viscoelastic properties of the polymeric solution also influence the oil recovery[20-23]. Nowadays, a combination of a high molecular weight polymer (thickening agent) and surfactant (lower the interfacial tension) is used in EOR applications. However, amphiphilic block copolymers can affect both the rheology and the interfacial properties and therefore are a promising alternative[1,24].

Amphiphilic block copolymers have the ability to form shear-dependent transient association in water, which results in thickening of the solution (increase of viscosity). The thickening capability of a polymer depends on several parameters such as the concentration, molecular weight, charged moieties and hydrophobic groups[25]. An increase in concentration leads to more entanglements and thus a higher viscosity. According to the well-known Mark-Houwink equation a higher molecular weight polymer results in an increase of the hydrodynamic radius of the polymer coils and subsequently a higher viscosity[26]:

$$[\eta] = KM^{\alpha} \qquad \text{[Eq. 1]}$$

Where η is the viscosity, M is the molecular weight and K and α are parameters that depend on the particular polymer-solvent system. The introduction of charged moieties along the backbone of the polymer leads to more electrostatic repulsion thus increasing the hydrodynamic volume, which results in a higher solution viscosity. This is only the case in the absence of salts (ions), which give a strong screening effect and decrease the hydrodynamic radius and as a consequence the viscosity. An increase in viscosity can also be achieved by the introduction of hydrophobic groups, which give either intra or intermolecular hydrophobic associations[27]. Furthermore, amphiphilic block copolymers may lower the surface tension of water depending on the nature of the blocks[28]. Amphiphilic block copolymers can thus be considered as the macromolecular counterparts of small-molecule surfactants and are therefore called polymeric surfactants[1,29].

Amphiphilic block copolymers can be synthesized with a large variety of monomers, but the most studied are copolymers in which the hydrophilic block is constituted by poly (ethylene oxide) (PEO), poly (ethylene glycol) (PEG), poly (acrylic acid) (PAA) and poly (methacrylic acid) (PMAA). In these

systems the hydrophobic block is mainly constituted by polystyrene (PS)[1]. The first and most studied are the Pluronic systems (diblock copolymers of PEO and poly(propylene oxide) (PPO)), which were commercialized by BASF as industrial detergents[30]. Besides the composition, the molecular architecture of block copolymers is also widely studied[31]. A lot of different molecular architectures of block copolymers such as the AB diblock, ABA and ABC triblock to more complex graft/comb/brush/star structures can be synthesized with the ongoing development of controlled radical polymerizations[32]. The main synthetic methods used to prepare amphiphilic block copolymers are atom transfer radical polymerization (ATRP)[33,34], reversible addition-fragmentation chain transfer polymerization (RAFT)[35] and nitroxide-mediated polymerization (NMP)[36]. These methods exhibit excellent control over the structure and molecular weight distribution. However, limitations exist related to functional groups tolerance, which lead to the use of protecting groups and as a consequence additional polymerization transformations[37].

Amphiphilic block copolymers exhibit interesting properties in an aqueous solution. Aggregates are formed due to the hydrophobic and hydrophilic nature of the block. In the case of a short hydrophobic and a long polyelectrolyte block the copolymers form star-like polyelectrolyte micelles[38]. The use of a polyelectrolyte such as PAA or PMAA is particularly interesting because repulsive electrostatic interactions lead to a highly stretched formation[39]. The rheological properties of a polymer solution are mainly derived from the inter-micellar interactions[40]. The rheology of diblock PS-*b*-PAA copolymers in water has been intensely studied[41,42] and it has been shown that the aggregates are constituted by a dense rigid PS core surrounded by a hydrophilic corona of PAA brushes. The aggregation number of the micelles depends on the morphology for which Raffa et al.[15] found that the aggregation number decreased for di, tri and star block copolymers of PS and PMAA, respectively. This behavior was attributed to the more difficult arrangement by steric hindrance. Rheological studies observe that amphiphilic block copolymers form viscoelastic solutions and turn into gels after a critical concentration[3,27,43]. PS-PAA and related block copolymers form a gel structure that can be described as a disordered state similar to colloidal glass[44]. However, evidence was found with PEO triblock copolymers that the micelles in the gel are arranged in an ordered array[45]. For example PEG-*b*-poly(ethylene-co-butene) (PEB) block copolymer form micelles that are arranged in body-centered or face-centered cubic lattices depending on the block composition[46].

The dynamic nature of the block copolymer aggregates in solution is interesting as several polymeric surfactants do not show a critical micelle concentration (CMC). Observations indicate that these block copolymer systems behave as kinetically “frozen” micelles[47-49]. An extreme low CMC is advantageous for many applications, since only traces of polymer are required to form micelles. The morphology of the micelles is primarily determined by a balance among three main forces: core-chain stretching, corona-chain repulsion and interfacial tension[50,51]. For neutral block copolymers the so called hydrophilic-lipophilic balance (HLB) plays an important role and predicts the properties of the

surfactant. Polymeric electrolytes behave differently due to the lower diffusion coefficient and the more complex conformations at interfaces (compared to their low-molar mass counterparts)[52,53].

The ability of amphiphilic block copolymers to stabilize emulsions is an interesting research field[54]. Emulsions are normally thermodynamically unstable and the two phases will separate over time because of a tendency for the emulsion to reduce its interfacial energy. Several breakdown processes occur such as coalescence, creaming, Ostwald ripening, sedimentation and flocculation[55]. A surface active agent like amphiphilic block copolymers can increase the kinetic stability of an emulsion and as a consequence the droplet size does not change[56]. The triblock copolymers can adsorb at the droplet surface to form thick layers, which prevent the droplets from coalescing by mechanisms such as electrostatic repulsion and/or steric hindrance[2,57].

Although many papers document the synthesis and self-assembly of amphiphilic block copolymers, to the authors best knowledge only relatively little work has been carried out on the systematic study of the rheology, gel structure, emulsification and surface properties of such polymers. A deeper knowledge of these parameters is crucial to optimize the design for the application in EOR. The field of polymeric surfactants is relatively new and a full understanding of the structure-property relationship is still missing. In this work we present an investigation concerning the rheological behavior of a series of amphiphilic PMAA-*b*-PS-*b*-PMAA triblock copolymers with different lengths of the hydrophilic and hydrophobic block. Especially the effect of a short hydrophobic block has not been investigated before. The amphiphilic triblock copolymers are synthesized by ATRP. Methacrylic acid cannot be polymerized directly because of poisoning effects of the copper(II) species, which are formed in the reaction media[58]. Therefore tert-butyl methacrylate is used as a monomer which can later be converted into the free acid by a post-polymerization reaction such as hydrolysis[59]. This research is a continuation of the work by Raffa et al.[16] on PS-*b*-PMAA diblock copolymers. It is expected that different architecture (triblock instead of diblock) of the block copolymer will display an effect on the rheological and interfacial properties. Moreover, the additional methyl group on the monomer increases the hydrophobicity of PMAA compared to PAA[60,61]. Subsequently, this can influence the aggregation behavior of the block copolymers in water. Kimerling et al.[41] showed that the use of hydrophobic groups on the hydrophilic block in PS-*b*-(AA-co-EA) copolymers decreased the gelation concentration and increased the viscosity due to increased inter-micellar attraction.

Furthermore, the rheological behavior of the triblock copolymer solutions at different temperatures, pH and concentrations of NaCl has been studied. It is expected that the rheological properties change dramatically due to the screening effect of the salt, which results in a collapsed conformation of the hydrophilic corona. The degree of electrostatic repulsion at different pH is quantified with zeta-potential measurements. Furthermore, the gel structure of the micelles in solution was investigated with cryo and negative stain transmission electron microscopy. A theoretical model was used to

compare the micelle radius with the microscopy images. Finally, the emulsification properties and the surface tension of the triblock systems are preliminary investigated. Besides the rheological properties, also the Enhanced Oil Recovery performance of the PMAA-*b*-PS-*b*-PMAA triblock copolymers is evaluated by flow-cell and core-flood experiments. The flow-cell experiment gives valuable information of the polymers capability to recover oil out of dead-end zones in a reservoir. The core-flood experiment simulates a highly permeable sandstone reservoir in which a comparison is made with a commercial polymer to test its application in the field.

2. Background information

2.1 Oil recovery

The conventional techniques for extracting oil out of a reservoir consist of primary and secondary methods which recover at most 55 % of the original oil in place (OOIP)[25]. In practice, the recovery is typically much lower and varies between 20-40%[62]. The primary technique uses natural forces such as the aquifer drive, the gas cap drive and the gravity flow to produce oil. The aquifer drive is the most efficient mechanism where the driving force is represented by the pressure that is exerted on the oil by the aquifer[63]. The secondary methods involves the injection of gas or water where the increased pressure drives the oil out of the reservoir[19]. However, an enormously large quantity of the OOIP remains embedded in oil reservoirs, due to the limited recovery. The last few decades, many different methods have been developed to increase the oil recovery. These methods belong to the category improved oil recovery (IOR) which also includes operational strategies, such as infill drilling, horizontal wells and intelligent reservoir management[24]. A subset of IOR called Enhanced Oil Recovery (EOR) is more specific and implies a reduction in oil saturation in the reservoir below the residual oil saturation to extend the lifetime of the reservoir[19]. Commonly, two categories of EOR technology exist: thermal and non-thermal methods. Thermal methods are most advanced among EOR methods due to a lot of field experience and are best suited for heavy oils (10-20° API) and tar sands (≤ 10° API). The mechanism includes a reduction of the viscosity (hence increase mobility ratio) by heating the oil in the reservoir[19]. The needed temperature is delivered by steam with different methods such as cyclic steam injection or steam flooding. Non-thermal methods (the focus of this thesis) include the injection of gas (CO_2)[64,65] or chemicals (polymer and/or surfactant solutions)[24,66]. Chemical EOR consists of several methods such as polymer flooding, surfactant flooding, alkaline flooding or a combination of the three called Alkaline-Surfactant-Polymer (ASP) flooding. These methods are more suitable for light oils and have been implemented in several oil reservoirs with mixed results[66-68]. The need for chemical flooding arises due to several problems when a water flood is used as secondary recovery method. Not all of the oil is contacted by the displacing fluid during a water flood, which results in a low volumetric sweep and displacement efficiency of oil. A phenomena called viscous fingering (see Figure 1, adapted from Ref.[25]) occurs due to the instabilities created by the difference in viscosity of oil and the displacement fluid.

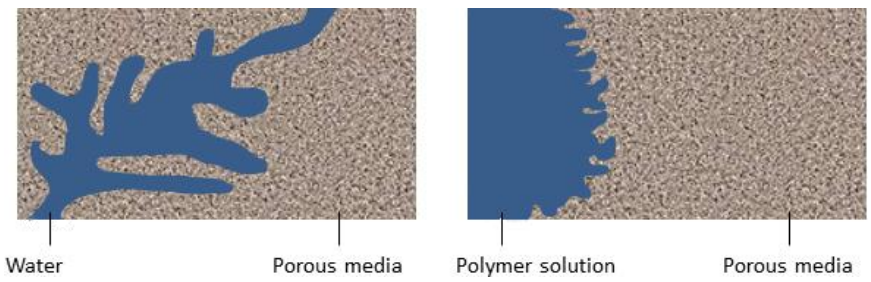

Figure 1: Viscous fingering (left) and polymer flooding (right) in an oil reservoir

The sweep efficiency of an oilfield is limited while early breakthrough of the displacing fluid occurs. The residual oil in the reservoir can be classified into four types[69]: oil film on rock surface, oil trapped in dead-ends, oil in pore throats by capillary forces and oil upswept in micro-scale heterogeneous portions of the porous media. In current polymer flooding, the polymer enhances the viscosity of the displacement fluid and consequently decreases the water/oil mobility ratio [31,70]. The mobility ratio is defined by equation 2.

$$M = \frac{k_w}{\eta_w}\frac{\eta_o}{k_o} \qquad \text{[Eq. 2]}$$

Where k_w and k_o being the permeability of the porous media to water and oil and η_0 and η_w are the viscosity of the oil and water, respectively. A low mobility ratio results in an increase of the macroscopic displacement and volumetric sweep efficiency. Recently, it was discovered that the viscoelastic nature of the polymer also increases the microscopic sweep of the reservoir while the displacement efficiency is improved[20-23]. The viscoelastic fluid provides greater stress and velocity at the changed section of pores, which results in dispersing and entraining the residual oil[69]. Moreover, the use of polymers generates a greater pressure drop and stronger vortices, which also increase the microscopic sweep efficiency[20]. Overall, polymer flooding is capable of reducing the residual oil film, increase the oil recovery out of dead-ends pores and increases the sweep efficiency, which reduces the unswept oil in heterogeneous porous media. Therefore the use of elastic polymers is a challenging and promising research field. Moreover, several EOR methods are devised with the goal of overcoming the capillary forces, which retain a high amount of residual oil in pore throats of the reservoirs[71]. Polymer flooding with polymeric surfactants aims to increase the oil recovery on all residual oil types. Besides, decreasing the mobility ratio, the use of polymeric surfactants in polymer flooding also lowers the interfacial tension and therefore tackles the capillary forces problem. These capillary forces are normally quantified by the Young-Laplace equations in interfacial sciences[72]:

$$P = \mathrm{C} * \gamma = \frac{2\gamma cos\theta}{R} \qquad \text{[Eq. 3]}$$

Where P is the capillary force, γ the interfacial tension, C the curvature of the interface which is determined by the pore radius (R), and the contact angle (θ). The contact angle is intrinsically related to surface wettability. The microscopic displacement efficiency can be increased by reducing the capillary effects, by reducing the oil-water interfacial tension and modifying the rock wettability. Furthermore, the use of polymers can reduce the rock's permeability due to adsorption of the polymer chains on the surface of the rock[73,74]. The reduction of the permeability of the reservoir can be measured by the resistant factor (RF). The RF is defined as[75]:

$$RF = \frac{\lambda_w}{\lambda_p} = \left(\frac{k_w}{\eta_w}\right) * \left(\frac{\eta_p}{k_p}\right) \qquad \text{[Eq. 4]}$$

Where k_p and η_p are the polymer solution permeability and viscosity, and k_w and η_w are the water solution permeability and viscosity, respectively. The residual resistant factor (RRF) is a measure to evaluate the permanent reduction in the permeability of the rock formation due to adsorption of the polymeric chains. It can be determined using the differential pressure during a brine flood (ΔP_w) before and after polymer injection ($\Delta P_{w,p}$)[18]:

$$RRF = \frac{\Delta P_{w,p}}{\Delta P_w} \quad \text{[Eq. 5]}$$

The average absorbed polymer thickness (e) on the rock surface can be determined using the RRF[76]:

$$e = r * (1 - RRF^{-\frac{1}{4}}) \quad \text{[Eq. 6]}$$

Where e is the absorbed layer thickness (μm), r is the average pore radius (μm) and RRF is the residual resistant factor. The advantage of adsorption is that the permeability is decreased such that the flow is diverted from high permeable zones towards low permeable unswept areas. However, the high increase of pressure can lead to injection problems. This must be investigated to examine if these polymers can be applied in EOR. Overall, the use of polymeric surfactants enables to use the advantages of both polymeric and surfactant flooding.

2.2 Controlled/living radical polymerization

Amphiphilic block copolymers combine the structural features of polyelectrolytes, block copolymers and surfactants. In literature a wide variety of block copolymers with MAA or AA as hydrophilic block and polystyrene (PS)[16], poly(n-butyl acrylate) (PBA)[77] or polycaprolactone (PCL)[78] as hydrophobic block are synthesized by living radical polymerization. Moreover, the polyacid block can function as a responsive behavioral group due to the strong dependency on the degree of protonation of the carboxylic moieties and thus on the solution pH[79]. The main synthetic methods used to prepare amphiphilic polymers are atom transfer radical polymerization (ATRP), reversible addition-fragmentation chain transfer polymerization (RAFT) and nitroxide-mediated polymerization (NMP). These polymerization systems are based on establishing a rapid dynamic equilibrium between a minute amount of growing free radicals and a large majority of dormant species. This result in high molecular weight distributions, narrow polydispersity's and high degrees of chain end functionalities[37]. Moreover, ATRP offers a tight control over the molecular architecture. A typical ATRP reaction of styrene is shown in the following scheme:

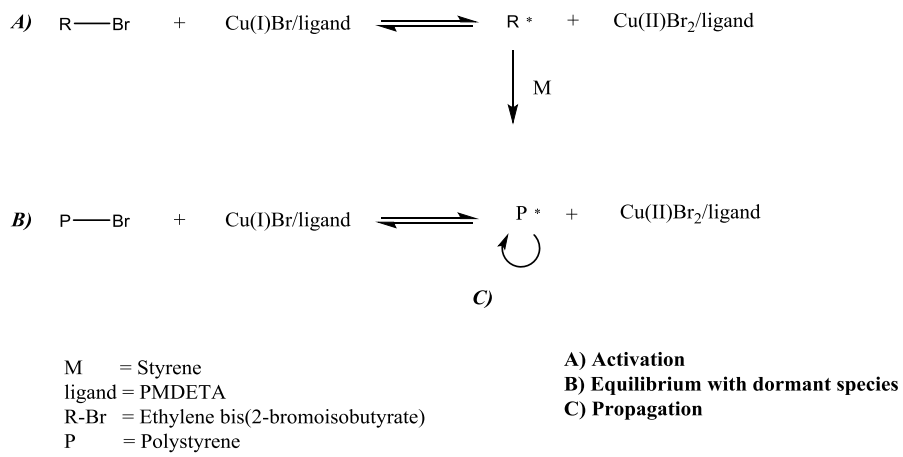

Figure 2: ATRP polymerization of styrene

ATRP uses a transition metal complex such as $CuBr_2$ or $CuCl_2$ as the catalyst and an alkyl halide R-X (X= Cl, Br) such as ethyl α-bromoisobutyrate (monofunctional), ethylene bis(2-bromoisobutyrate) (difunctional) or pentaerythritol tetrakis(2-bromoisobutyrate) (tetrafunctional) as the initiator. The most used ligands are N,N,N′,N″,N″-Pentamethyldiethylenetriamine (PMDETA) and tris[2-(dimethylamino)ethyl]-amine (ME6TREN). The metal complex can exist in two different oxidation states. The lower oxidation state metal complex, Cu(I)Br/ligand, reacts with the initiator to yield a radical R* and the corresponding higher oxidation state metal complex. This step is called activation and the reversible process establishes an equilibrium that is shifted to low radical concentrations. The radicals can react: with the monomer (M) generating a polymer, with each other which results in termination or with the metal/ligand complex, which yields the halogen-terminated polymeric dormant state. This process is reversible and if the deactivation process is efficient narrow molecular weight distribution polymers are obtained[33,34]. Acidic monomers such as MAA are challenging to synthesize due to the non-compatibility of the free carboxylic group with the catalyst system. Only RAFT can polymerize these acidic monomers without needing a protective group such as ter-butyl acrylate (tBA), ter-butyl methacrylate (tBMA) or benzyl methacrylate (BzMA)[59]. However, the formation of triblock copolymers of styrene and PMAA by RAFT have not been reported in literature yet and therefore ATRP is used in this research.

3. Materials and Methods

Chemicals. Tert-butyl methacrylate (tBMA, Aldrich, 98%) was vacuum-distilled over CaH_2 and kept under nitrogen before use. CuCl (Sigma-Aldrich, ≥ 99%) and CuBr (Sigma-Aldrich, ≥ 98%) were stirred in glacial acetic acid for 6 hours and then filtered, washed with acetic acid, ethanol, ethyl acetate and dried under vacuum before use. Styrene (Sigma-Aldrich, ≥ 99%) was filtered through a short column of basic alumina to remove inhibitors and then kept under nitrogen before use. Glacial acetic acid, ethanol, ethyl acetate, THF, methanol, dioxane and acetone were used without further purifications. Anisole (Sigma-Aldrich, anhydrous, 99.7%) was deoxygenated by bubbling with nitrogen for 60 minutes. N,N,N′,N″,N″-Pentamethyldiethylenetriamine (PMDETA, Aldrich, 99%), Ethylene bis(2-bromoisobutyrate) (EBIB, Aldrich, 97%), tetramethylethylenediamine (TMEDA, Aldrich, ≥ 99.5%), and tris[2-(dimethylamino)ethyl]-amine (Me6TREN, Aldrich), 4,4′-Azobis(4-cyanovaleric acid) (ACVA, Aldrich, ≥ 75%), 4-Cyano-4- (phenylcarbonothioylthio)pentanoic acid (CPADB, Aldrich, 97%), Methacrylic acid (MAA, Aldrich, 99%) were used as received, without further purifications. The crude oil used for the oil recovery experiments was heavy oil, which was supplied by Shell Global Solution International B.V. The viscosity of the oil was 1023 mPa.s at 20 °C which corresponded to API gravity below 22.3°.

Synthesis of polystyrene macroinitiator (PS-Br). PS-Br macroinitiators were synthesized as follows: 1 mmol of initiator EBIB, CuBr (2 mmol), and styrene (20−50 mmol) were introduced under nitrogen in a 100 mL round-bottomed flask equipped with a magnetic stirring bar and a reflux condenser, previously purged with nitrogen. The mixture was further degassed by purging with nitrogen gas (N_2) for at least 45 minutes under vigorous stirring (1050 rpm). After deoxygenation, the flask was put in an oil bath set to a temperature of 100 °C (750 rpm). After 1 min, TMEDA (2 mmol) was introduced under nitrogen to initiate the reaction. The solution turned light green as complex formation occurred and remained heterogeneous. After 1 hour, the reaction was stopped by cooling down, introducing air and diluting with around 50 mL of THF. The THF solution was filtered through a short column of basic alumina to remove the copper catalyst. The solution was then precipitated in a 20-fold excess of methanol. The precipitate was filtered, re-dissolved in THF, and re-precipitated in 2:1 v/v methanol/water and washed with methanol. The obtained white solid was dried overnight at 70 °C. The conversion and the molecular weight were determined gravimetrically and by GPC respectively. The theoretical molecular weight was determined using the following equation[59]:

$$Mn_{th} = Mn_{EBIB} + (Mn_{st} * \frac{[St]_o}{[EBIB]_o} * X) \quad \text{[Eq. 7]}$$

where $Mn_{,th}$ is the theoretical molecular weight of the synthesized PS-Br macroinitiator (g/mol); $Mn_{,EBIB}$ and Mn_{st} are the molecular weights of the initiator ethylene bis(2-bromoisobutyrate) and monomer styrene (g/mol), $[St]_0$ and $[EBIB]_0$ are the initial concentrations of the monomer styrene and

the initiator EBIB (mol) and X represents the fractional monomer conversion (x/100%). The PS-Br macroinitiator was further characterized by using proton nuclear magnetic resonance (^{1}H-NMR) spectroscopy with chloroform ($CDCl_3$) as solvent.

Synthesis of Block Copolymers (PtBMA-*b*-PS−*b*-PtBMA). Block copolymers PtBMA-*b*- PS-*b*-PtBMA were synthesized as follows: PS-Br macroinitiator (0.5 g), deoxygenated anisole (10 mL), the copper catalyst CuCl, and tBMA (according to stoichiometry) were introduced under nitrogen in a 250 mL round-bottomed flask equipped with magnetic stirring bar and reflux condenser, previously purged with nitrogen. The mixture was further degassed by purging with nitrogen gas (N_2) for at least 45 minutes under vigorous stirring (1050 rpm). After deoxygenation and complete dissolution of the macroinitiator, the flask was put in an oil bath at 90 °C and the ligand (Me6TREN) was added under nitrogen. After a given time, the reaction was stopped by cooling down, introducing air, and diluting with around 50 mL of THF. The THF solution was filtered through a short column of alumina to remove the copper catalyst, then precipitated in a 20-fold excess of methanol, re-dissolved in THF and re-precipitated in 2:1 methanol/water mixture twice, washed with methanol, and dried overnight at 70 °C, affording a white solid. The conversion and the molecular weight were determined both gravimetrically and by GPC and NMR (solvent $CDCl_3$). The theoretical molecular weight was determined using the following equation[59]:

$$Mn_{th} = Mn_{PS-Br} + (Mn_{tBMA} * \frac{[tBMA]_o}{[PS-Br\ macroinitiator]_o} * X) \quad \text{[Eq. 8]}$$

where Mn_{th} is the theoretical molecular weight of the synthesized triblock copolymer (g/mol); $Mn_{PS\text{-}Br}$ and Mn_{tBMA} are the molecular weights of the PS-Br macroinitiators and the monomer tBMA (g/mol), $[tBMA]_0$ and $[PS\text{-}Br\ macroinitiator]_0$ are the initial concentrations of the monomer tBMA and the initiator (mol) and X represents the fractional monomer conversion (x/100%).

Hydrolysis. 3 gram of PtBMA-*b*-PS-*b*-PtBMA block copolymer was dissolved in 100 ml dioxane in a 250 ml round bottomed flask equipped with a magnetic stirring bar and reflux condenser. The dissolution is quite slow at low temperatures, therefore the temperature was set on 100 °C. After complete dissolution, an excess of concentrated HCl (10 ml) was added. The solution turns from transparent to cloudy in about 1 hour. After 3-4 hours the reaction was stopped by cooling where after the solution turns back to transparent. The solution was precipitated in an excess of acetone (1 L). The precipitate was filtered and dried overnight at 70 °C. The polymers were recovered as glassy transparent whitish solids. The extent of hydrolysis was determined by ^{1}H-NMR in d_6-DMSO.

Neutralization. The hydrolyzed polymers were converted to their corresponding sodium salts by neutralization. The polymers were dissolved in an excess of NaOH in water. Because of the high viscosity, the solutions were stirred overnight to ensure homogeneity. The excess base was removed

by dialyzing against Milli-Q water. The water was changed at least 3 times over a period of 3 days. Subsequently, the obtained polymers were dried at 70 °C for 3 days. The polymers were recovered as glassy transparent white-yellowish solids.

Synthesis of homopolymer PMAA. Homopolymers of PMAA were synthesized via the RAFT process as follows: CPADB (1 mmol) and MAA (500−1500 mmol) were dissolved in 4:1 v/v water/1,4 dioxane mixture (pH = 4). The mixture was introduced under nitrogen in a 100 mL round-bottomed flask equipped with a magnetic stirring bar and a reflux condenser, previously purged with nitrogen. The mixture was further degassed by purging with nitrogen gas (N_2) for at least 45 minutes under vigorous stirring (1050 rpm). After deoxygenation, the flask was put in an oil bath set to a temperature of 80 °C (750 rpm). After 1 min, ACVA (0.25 mmol) was introduced under nitrogen to initiate the reaction. After addition of the reactants, the ultimate pH of the solution was 2.8. After a given time, the reaction was stopped by cooling and exposing the solution to air. The polymer was recovered by precipitation in an excess of stirring diethyl ether. The precipitate was filtered and dried overnight (70 °C) obtaining a pink glassy solid. The conversion and the molecular weight were determined both gravimetrically and by GPC. The theoretical molecular weight was determined using the following equation[80]:

$$Mn_{th} = Mn_{CPADB} + (Mn_{MAA} * \frac{[MAA]_o}{[CPADB]_o} * X) \quad \text{[Eq. 9]}$$

where Mn_{th} is the theoretical molecular weight of the synthesized polymer (g/mol); Mn_{CPADB} and Mn_{MAA} are the molecular weights of the RAFT agent and the monomer (g/mol), respectively, $[MAA]_0$ and $[CPADB]_0$ are the initial concentrations of MAA and CPADB (mol) and X represents the fractional monomer conversion (x/100%). The PMAA homopolymers were activated by the neutralization step as described above.

Characterization.

GPC measurements. Samples for the PS-Br macroinitiator and the triblock copolymers were prepared by dissolving the polymers in in THF (99+%, extra pure, stabilized with BHT) at 10 mg/ml concentrations. The samples were filtered over a 0.45 μm PTFE filter prior to injection. GPC measurements for the PS-Br macroinitiator were performed with a HP1100 from Hewlett-Packard, equipped with three 300 x 7.5 mm PLgel 3 μm MIXED-E columns in series. Detection was made with a GBC LC 1240 IR detector. The samples were eluted with THF at a flow rate of 1 mL/min at a pressure of 140 bar. The PDI and molecular weights were determined using the software PSS WinGPC Unity. GPC measurements for the triblock copolymers were performed at 30 °C (1 mL/min) using triple detection, consisting of a Viscotek Ralls detector, Viscotek Viscometer Model H502 and

Shodex RI-71 Refractive Index detector. The separation was carried out by utilizing a guard column (PLgel 5 μm GUARD, 50 mm and two columns PLgel 5 μm MIXED-C, 300 mm from Agilent Technologies). Data acquisition and calculations were performed using Viscotek OmniSec Software using a refractive index increment (dn/dc) from the samples. Molecular weight were determined based on a universal calibration curve generated from narrow dispersity polystyrene standards (Mw from 645 to 3001000 g/mol). For the homopolymer PMAA Gel permeation chromatography (GPC) was performed with an Agilent 1200 system with Polymer Standard Service (PSS) columns (guard, 100 Å and 3000 Å, 8 x 300 mm). The eluent solution was a 50 mM of sodium nitrate ($NaNO_3$) aqueous solution. The elution was conducted with a flow rate of 1.00 mL/min. at 40 °C. As a baseline calibration linear polyacrylamide was used. The apparent molecule weight and polydispersity index (PDI) were calculated with WINGPC software (PSS).

NMR measurements. ^{1}H NMR spectra in $CDCl_3$ and d_6-DMSO were recorded on a Varian Mercury Plus 300 MHz spectrometer operating at room temperature.

Transmission Electron Microscopy. Three μl of each sample at 1 mg/ml was pipetted onto a glow-discharged copper grid covered with carbon film. Due to the viscosity of the samples obtaining a thin layer of sample proved difficult and various repetitions of washing with miliQ water and 2% uranyl acetate solution were applied before letting the final stain layer rest for 30 seconds prior to blotting. Blotting was done with different types of paper, because of their varying absorbing properties. The grids were visualized with either of two microscopes. One is a Tecnai G2 20 Twin electron microscope (FEI, Eindhoven, the Netherlands), that was equipped with an LaB6 cathode, an UltraScan 4000 UHS CCD camera (Gatan, Pleasanton, CA, USA) and operated at 200 kV. The other is a Philips CM120 electron microscope (FEI, Eindhoven, the Netherlands) equipped with a LaB6 cathode, 4000 SP 4K slow-scan CCD camera (Gatan, Pleasanton, CA, USA) and operated at 120 kV. Micrographs were cropped and their levels, brightness and contrast were optimized in Adobe Photoshop CS6.

Cryo-Transmission Electron Microscopy. Three μl of entry 8 at 0.3 or 0.5 mg/ml was applied to a glow-discharged copper grid with holey carbon film (quantifoil 3.5/1) and plunge-frozen with a Vitrobot (FEI, Eindhoven, The Netherlands) in liquid ethane after blotting for 20 and 28 seconds respectively. Because of the viscosity of the samples, the general filter paper in the Vitrobot was replaced with a double layer of paper towel on each site. The specimen was then inserted into a cryo-transfer holder (Gatan model 626) and transferred to a Philips CM120 electron microscope (FEI, Eindhoven, the Netherlands) equipped with a LaB6 cathode, 4000 SP 4K slow-scan CCD camera (Gatan, Pleasanton, CA, USA) and operated at 120 kV using low-dose mode. Micrographs were cropped and their levels, brightness and contrast were optimized in Adobe Photoshop CS6.

Zeta potential. The size and zeta potential measurements were performed in a ZetaPALS zeta potential analyzer (Brookhaven Instruments Corporation) using Phase Analysis Light Scattering, to

determine the electrophoretic mobility of charged, colloidal suspensions in an electric field. The particle size was measured by dynamic light scattering. The samples were prepared by dissolving the amphiphilic triblock copolymers in water solutions with different pH. The pH was adjusted with hydrochloric acid (HCl). Prior to each experiment the pH was measured on a UltraBasic Denver Instrument and took half an hour for equilibration. The glass electrode was calibrated with buffer solutions of pH 4 and pH 7.

Rheology characterization.

Viscosity and viscoelastic measurements. Rheological measurements were performed on a HAAKE Mars III (ThermoScientific) rotational rheometer using a 2 mL solution at 20 °C. The rheometer was equipped with a cone-and-plate geometry (diameter 60 mm, angle 2°). A trap for the solvent was used in order to avoid water evaporation during the experiments. Solutions at 0.1, 0.5 and 1.0 wt% concentrations were prepared by dissolving the triblock copolymer sodium salts in demineralized water, followed by stirring for at least 10 hours before the measurement in order to get homogeneous solutions. All the prepared polymers were soluble in water in their sodium salt form without the need for co-solvents or heating. Viscosimetric measurements, such as shear viscosity and viscoelasticity measurements were performed with shear rate variations of 0.1 – 500 s^{-1} and frequency ranges of $6.37*10^{-3}$ – 15.92 Hz (0.04 – 100 rad/s), respectively. For the application in EOR, the polymer's ability to increase the viscosity at shear rates between 5-10 s^{-1} is most important, since these are the shear rates encountered in the porous media where the oil resides[81]. Prior to all viscoelasticity measurements, a stress amplitude sweep experiment was performed in order to establish the regime of viscoelastic response; the linear viscoelastic region (LVR). Hereafter, oscillation frequency sweep measurements were performed at constant stress.

Surface tension experiments. Surface tension was measured using the pendant drop method on a Dataphysics OCA15EC tensiometer equipped with a CCD video camera (752*582 pixels). A 1 ml syringe was attached to a needle with a capillary radius of 1.36 mm. The drop was measured on its maximum size. Two sets of three measurements were taken and then averaged. Graphically the critical micelle concentration (CMC) can be obtained from the plot of the surface tension against the concentration by taking the line of best fit in two places and noting the concentration at the intersection[82].

Kinetic stability. O/W emulsions were prepared according to the following method: 10 ml oil (102.2 mPa, $\gamma = 9.63$ s^{-1}) and 10 ml surfactant solution (concentration adjusted to match the viscous state of crude oil) were mixed on a stirring plate (750 rpm) for 30 minutes to obtain a homogenous emulsion. The emulsion droplets were observed under bright-field illumination with a Nikon light microscope

(Nikon, Eclipse 600, New York, USA) using a 4x objective lens and 10 x ocular lens (magnification 40x). Images were captured with a high resolution color camera (Nikon, COOLPIX 500, MDC Lens, Japan). Phase separation was observed visually at room temperature over a given time span.

Enhanced Oil Recovery performance experiments.

Flow-cell experiments. Flow-cell experiments were performed using a 2-Dimensional flow-cell (see Figure 3) to simulate dead-end pores in oil reservoirs. The bottom part of the flow-cell is made out of aluminum and the cover is glass. The flow-cell setup has been adapted from the original, presented by Niu et al[83] and shown by Wever et al[22]. It must be noted that for the calculation of the oil recovery only chamber 2, 3 and 4 were used as examples for dead-end pores. The flow-cell chambers are first filled with oil and afterwards flooded with water (reference) or polymer solution. The crude oil (1023 mPa, γ = 9.63 s^{-1}) supplied by Shell Global Solution International B.V. has been diluted with cyclooctane to a viscosity of 102.2 mPa (γ = 9.63 s^{-1}) at 20 °C. The polymer concentration was adjusted for every polymer solution to match the viscosity of the crude oil. The flow rate was set at 1.00 mL/hour and the run-time was continued for at least 24 hours at room temperature. The oil recovery out of the different cells was visually determined by taking high definition pictures after the flood. The image was analyzed using Adobe Photoshop CS6 via the "pixel count" option, which allows the calculation of the amount of oil left behind in the flow-cell and consequently calculation of the oil recovery according to the following equation:

$$Add.Oil\ rec.\% = \left(100 - \frac{100 * Pixel_{Total}}{Pixel_{Remaining}}\right)_{Pol.flood} - \left(100 - \frac{100 * Pixel_{Total}}{Pixel_{Remaining}}\right)_{Water\ flood} \quad \text{[Eq. 10]}$$

Where additional oil recovery (%) is the percentage oil recovered during polymer flood minus the water flood reference.

a)

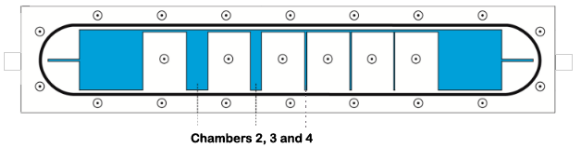

b)

Figure 3: A schematic (a) and photo (b) presentation of the flow-cell (top view)

Core-flow experiments. An oil recovery experiment using a polymer flood in a simulated oil reservoir was conducted with Bentheim sandstone cores (5 x 30 cm, Kocurek Industries). The experimental setup can be seen in Figure 4 (adapted from Ref[22]). First the sandstone core was fixed in a core holder and flooded with carbon dioxide (CO_2) to remove any oxygen. Hereafter, brine (2000 ppm) was injected (water flood) at a low flow rate (12 ml/h) for several hours to be certain that all the remaining CO_2 was dissolved. The pressure drop at different flow rates of brine solution (2000 ppm) was measured with GS4200-USB digital pressure transducers from ESI Technology Inc.. The brine permeability of sandstone core was calculated as stated in literature using Darcy's law[84]. The stone was filled with oil (102.2 mPa.s, γ = 9.63 s^{-1}) at a flow rate of 12 ml/h and afterwards flooded (12 ml/h) with brine solution (2000 ppm) until no additional oil was recovered to simulate a secondary oil recovery method. Finally, the polymer flood was performed with a flow rate of 12 ml/h until no additional oil was recovered. The pressure was recorded as a function of time during both the brine and polymer flooding. Polymer solution and oil out of the core stone were collected and visually analyzed by calculating the cumulative volume. Hereafter, the Enhanced Oil Recovery was calculated according to the following equation:

$$Oil\ recovery\ (\%\ of\ OOIP) = \frac{oil\ produced\ by\ polymer\ flood\ (ml)}{Oil\ original\ in\ place\ (ml)} * 100 \qquad \text{[Eq. 11]}$$

Where the Enhanced Oil Recovery is defined as the volume of oil produced by the polymer flood divided by the total volume of oil original in place (as percentage).

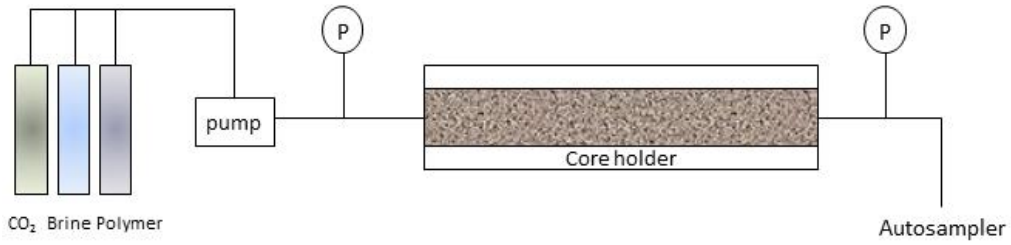

Figure 4: Schematic presentation of the experimental set-up for the core-flood experiments

4. Results and Discussion

4.1 Synthesis of triblock copolymers of polystyrene and poly(methacrylic acid)

The synthesis of difunctional PS-Br macroinitiators were performed in bulk at 100 °C, using CuBr as catalyst and TMEDA or PMDETA as ligand. Both ligands are commercially available, relatively inexpensive, and result in well controlled ATRP polymerizations[15,59]. The polymerization process was performed according to Figure 5.

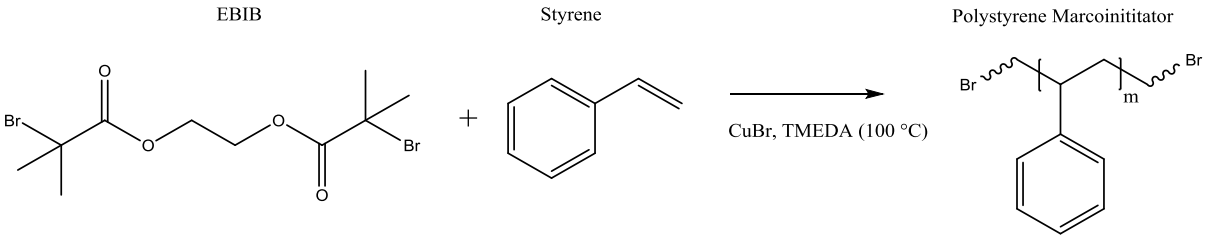

Figure 5: Polymerization of EBIB and styrene to form a polystyrene macroinitiator

The goal of this step was to synthesize styrene with different block lengths. The results are summarized in Table 1. The molecular weight averages determined by GPC analysis indicate the synthesis of polystyrene block lengths between 23 and 75 units. The poly polydispersity indices (PDI) of the PS-Br macroinitiators are low and differ between 1.14 and 1.44, which supports the fact that the ATRP polymerization is a controlled/"living" radical polymerization[85]. Entry 4 and 5 used TMEDA as a ligand to have a better control over the reaction where the use of PMDETA resulted in much faster reaction times than TMEDA. Moreover, anisole (entry 6) was tried as a solvent, but the conversion decreased dramatically.

Table 1: Results of polymerization reaction of styrene by ATRP

Entry	$[ST]_0 : [CuBr]_0 : [PMDETA]_0 : [EBIB]_0$ [a]	T (°C)	Time (min.)	Conv. [b] (%)	Mn_{theor} [c] (g/mol)	Mn_{GPC} [d] (g/mol)	ST_{GPC} (units)	PDI (-)
1	49 : 2 : 2.0 : 1	100	35	25.2	1659	8166	75	1.34
2	26 : 2 : 1.8 : 1	100	30	46.6	1628	5047	45	1.30
3	21.5 : 2 : 2.0 : 1	100	30	31.8	1074	6483	59	1.39
4	22.5 : 2 : 2.1 : 1	100	150	31.5	1097	4044	35	1.44
5	21.8 : 2 : 2.2 : 1	100	60	9.1	564	2767	23	1.14
6	21 : 2 : 2.3 : 1	100	120	14.0	667	4040	35	1.22

a. Molar ratio in feed, entry 4 and 5 used TMEDA instead of PMDETA, entry 6 was performed with anisole as solvent
b. Calculated by gravimetric analysis
c. Calculated from the theoretical molecular weight formula proposed by Davis et al. using equation 7
d. Calculated from GPC analysis in THF against linear p(St) standards

There is quite a high discrepancy between the theoretical molecular weight (determined gravimetrically) and the molecular weight by GPC analysis. An explanation could be that the initiator does not dissolve completely in styrene or that it is not completely functional In both cases this results

in a higher monomer/initiator ratio and subsequently a higher molecular weight average. Also, gravimetric methods are often inaccurate for synthesis reactions with tiny amounts of starting products and several purifications steps. Therefore, in this case the GPC results are more accurate and will be used in the report.

Chain extension of the PS-Br macroinitiators with tBMA was performed in anisole at 90 °C using CuBr as catalysts and Me6TREN or PMDETA as ligand. The polymerization process was performed according to Figure 6.

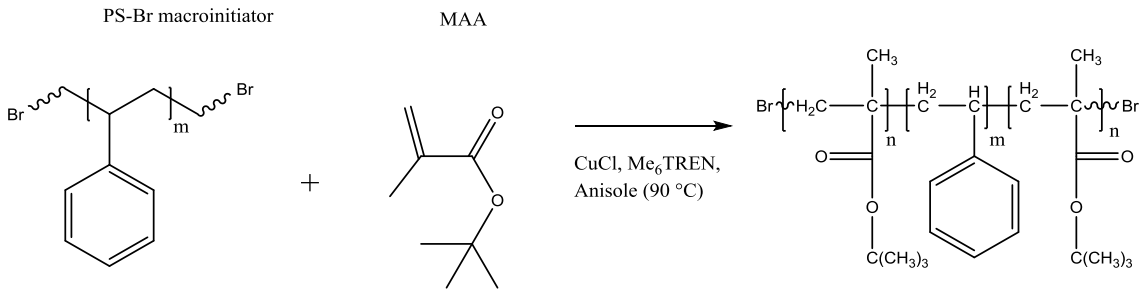

Figure 6: Polymerization of tBMA and PS-Br macroinitiator to form a block copolymer

The goal of this step was to perform a chain extension with tBMA on the hydrophobic polystyrene blocks. Three PS-macroinitiators with varying block length, entry 1, 2 and 4, (75, 45 and 35 monomeric units, respectively) were found to be suitable to obtain triblock copolymers with a significant different hydrophobic core. The results are summarized in Table 2. A Cu(I)/PMDETA or (Me6TREN) catalyst system was used to give narrow molecular weight distributions[59]. The PDI of the PS-PtBMA triblock copolymers are around 2 which again supports the fact that the ATRP polymerization is a controlled/"living" radical polymerization. Also, the monodisperse distributions confirmed a successful chain extension. The total monomer conversions varied for the different entries, but after 17 hours most polymers reach a conversion of ≈ 55 %. The results are in good agreement with the results obtained by comparable studies by Davis et al.[59] and Raffa et al.[15].

Table 2: Synthesis of block copolymers (PtBMA-*b*-PS-*b*-PtBMA) by ATRP (90 °C)

Experiment	$[tBMA]_0$: $[CuCl]_0$: $[Me6TREN]_0$: $[macroinitiator]_0$ [a]	Time (h)	Conv. [b] (%)	Mn_{theor} [c] (g/mol)	Mn_{GPC} [d] (g/mol)	Mn_{NMR} [e] (g/mol)	PDI (-)
7 (entry 1)	2064 : 2 : 4 : 1	5.0	22.9	69361	73086	81321	2.18
8 (entry 1)	1978 : 2 : 4 : 1	4.5	34.7	105819	96327	105758	1.95
9 (entry 2)	3200 : 2 : 2 : 1	16	59.5	275408	314847	225503	1.71
10 (entry 2)	1986 : 2 : 2 : 1	5.0	47.9	140258	151889	119022	1.72
11 (entry 2)	995 : 2 : 3 : 1	17	59.5	91691	88862	93608	2.27
12 (entry 4)	3187 : 2 : 4 : 1	17	43.9	203253	223353	250346	2.05
13 (entry 4)	2175 : 2 : 4 : 1	4.0	12.9	43962	85710	63162	2.16
14 (entry 4)	1053 : 2 : 3 : 1	17	28.9	47455	77139	50893	2.42

a. Molar ratio, entry 7 and 8 used PMDETA instead of Me6TREN as ligand
b. Calculated by gravimetric analysis
c. Calculated from the theoretical molecular weight formula proposed by Davis et al. using equation 8
d. Calculated from GPC analysis in THF against linear p(St) standards
e. Calculated on the basis of the DP determined by ^{1}H NMR

The final copolymers were characterized by ^{1}H-NMR, GPC and gravimetric analysis. The results of the composition (in monomeric units) and molecular weight are summarized in Table 3 and were in good agreement.

Table 3: Characterization of the triblock copolymers by ^{1}H-NMR, GPC and gravimetric analysis

Experiment	$[tBMA]_0$: $[CuCl]_0$: $[Me6TREN]_0$: $[macroinitiator]_0$	PS_{GPC} (units)	$PtBMA_{GPC}$ [a] (units)	$PtBMA_{NMR}$ [b] (units)	$PtBMA_{gravi.}$ [c] (units)	PS-$PtBMA_{GPC}$ (units)
7	2064 : 2.2 : 3.8 : 1	75	463	569	437	75-463
8	1978 : 2.2 : 3.6 : 1	75	629	741	659	75-629
9	3200 : 2.3 : 2.3 : 1	45	2210	1583	1916	45-2210
10	1986 : 2.0 : 2.0 : 1	45	1047	834	947	45-1047
11	995 : 2.1 : 3.3 : 1	45	598	656	587	45-598
12	3187 : 2.2 : 4.0 : 1	35	1564	1758	1407	35-1564
13	2175 : 2.3 : 4.0 : 1	35	582	442	260	35-582
14	1053 : 2.0 : 3.1 : 1	35	521	355	289	35-521

a. Calculated from GPC analysis in THF against linear p(St) standards
b. Calculated on the basis of the DP determined by ^{1}H NMR
c. Calculated by gravimetric analysis

Discrepancies observed in the GPC can be ascribed to the use of PS standards for calibration and to the deviation from linearity at high molecular weight[16]. Discrepancies observed in gravimetric analysis can be ascribed to the multiple purification steps, where not all polymer is recovered and subsequently the calculated molecular weight by gravimetric analysis is lower for all experiments. Discrepancies in the ^{1}H-NMR can be ascribed to the fact that a baseline correction is applied. This baseline correction is necessary, but influences the integral area significantly due to the fact that the integral of the peaks for the PS block is very small compared to the integral of the peaks for the PMAA block.

The PtBMA-*b*-PS-*b*-PtBMA block copolymers have been selectively hydrolyzed with concentrated HCl in refluxing 1,4-dioxane. The amount of 1,4-dioxane and concentrated HCl (threefold excess) added was based on the mass of the polymer and on the moles of ester groups present, respectively. According to the literature, primary ester groups in the difunctional initiator are stable under the adopted hydrolysis conditions[59,86]. The tert-butyl esters of the polymer are unstable and therefore hydrolyzed. This can be seen afterwards on ^{1}H-NMR spectra where there is no signal of the ter-butyl ester (see Figure 13). Hydrolysis gives the acidic form of the polymers, which do not dissolve in water, but swell very slowly.

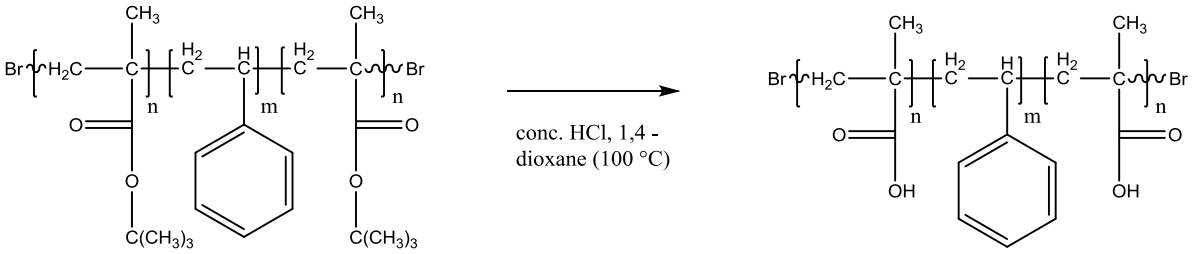

Figure 7: Hydrolysis of the block copolymers resulting in PMAA-*b*-PS-*b*-PMAA triblock copolymer

A poly(methacrylic acid) PMAA homopolymer is synthesized to act as a reference polymer for comparing its properties with the triblock copolymers. For this polymerization not ATRP, but reversible addition fragmentation chain transfer (RAFT) polymerization is used while there is no need for blocking the methacrylic acid. Polymerization was performed in a water/1,4-dioxane system (pH = 4) at 80 °C using CPADB as the RAFT agent and ACVA as the initiator. The polymerization process was performed according to Figure 8.

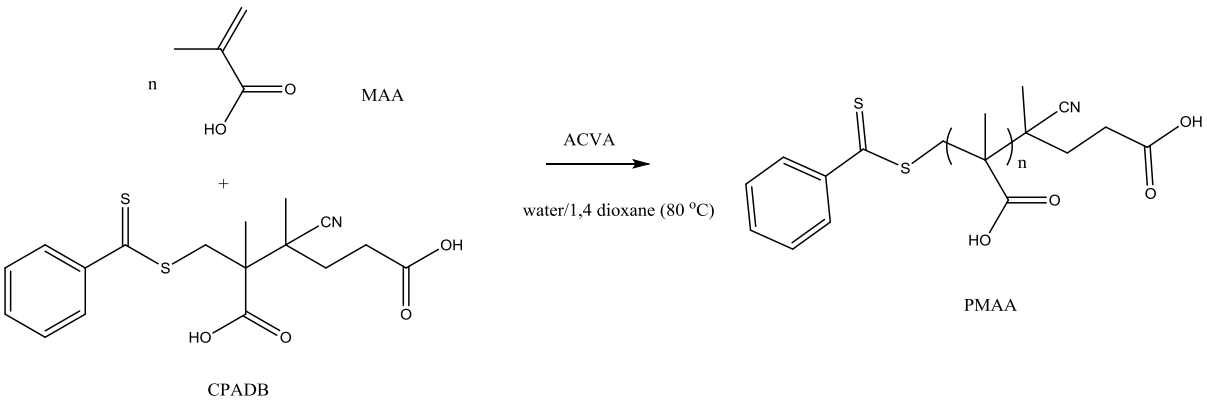

Figure 8: Synthesis of poly(methacrylic acid) by RAFT polymerization

The synthesized homopolymers were characterized by ^{1}H-NMR, GPC and gravimetric analysis. The results summarized in Table 4.

Table 4: Synthesis of PMAA by RAFT polymerization

Entry	$[MAA]_0$: $[ACVA]_0$: $[CPADB]_0$:	T (°C)	Time (hours)	Conv.[b] (%)	Mn_{theor}[c] (g/mol)	Mn_{GPC}[d] (g/mol)	$PMAA_{GPC}$ (units)	PDI (-)
15	1306 : 0.27 : 1	80	24	48.6	54758	275100	3196	2.26
16	580 : 0.25 : 1	80	2	54.3	27144	115000	1336	1.42
17	571 : 0.25 : 1	80	1	26.9	13274	74229	863	1.47

a. Molar ratio
b. Calculated by gravimetric analysis
c. Calculated from the theoretical molecular weight formula using equation 9
d. Calculated from GPC analysis in water against linear polyacrylamide

PMAA with different block lengths were synthesized via RAFT polymerization. Two different $[MAA]_o/[CTA]_o$ ratios (1306/1 and 580/1) were evaluated and compared. It was shown that a higher ratio, yields a higher molecular weight due to more free monomer available relative to the CTA initially present. The results in table 4 show that a high monomer conversion and a low polydispersity are obtained which is characteristic for controlled/living polymerization[85]. Moreover, entry 16 and 17 indicate that the molecular weight linearly increases with the conversion, which is also a characteristic of a controlled/"living" radical polymerization. The effect of the solvent (water/1,4-dioxane) has a dramatic effect on the molecular weight distribution. This solvent combination was chosen because CPADB is not soluble in water at room temperature and needs a water-miscible organic solvent such as 1,4 dioxane. However, due to the solvent the theoretical and the experimental molecular weight differ significantly. This deviation can be ascribed to the poor stability of the reactants, where in water-based systems there is the chance of potential hydrolysis of the dithioester group of CPADB. The CTA hydrolysis results in inactivation, which generates fewer reactive species where after the Mn increases dramatically. The same observations were found by Pelet et al.[80] and by Thomas et al.[87,88]. For further research a different CTA such as 4-cyano-4-thiothiopropylsulfanyl pentanoic acid (CTPPA) should be used. Chaduc et al.[35] observed that with this CTA no hydrolysis occurs and a good control of the polymerization of MAA in water was obtained. Nonetheless, the obtained polymers have sufficient molecular weight or block length to compare these with the amphiphilic triblock copolymers.

The sodium salt of the prepared triblock copolymers and the PMAA homopolymer is obtained after addition of NaOH. The excess base is removed by dialyzing the resulting solution in water. The water was changed at least 3 times over a period of 3 days. The sodium salt form is readily soluble in water, forming clear colorless solutions with high viscosity. The neutralization reaction is shown in Figure 9.

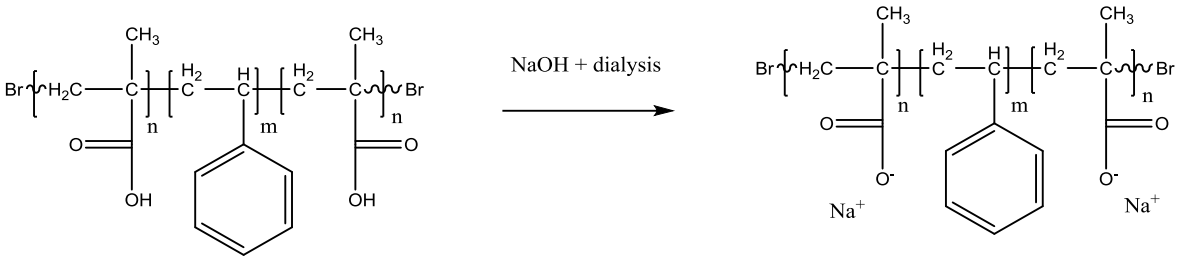

Figure 9: Synthesis of the sodium salt by adding NaOH where after the excess base is removed by dialysis

The synthesis and the structure of the obtained polymers are sketched in Figure 10. The numbers indicate the polymer composition in terms of monomeric units.

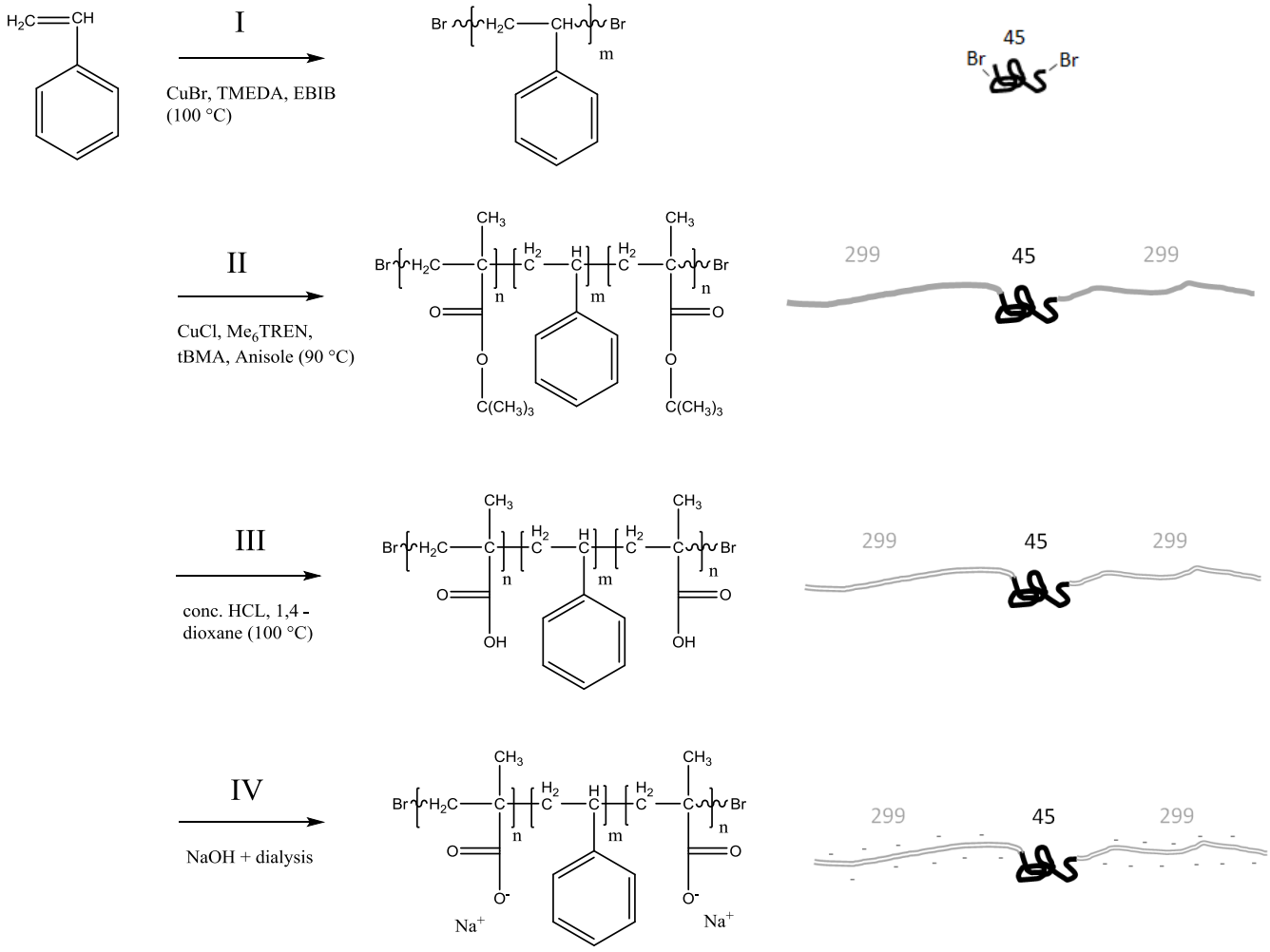

Figure 10: Synthesis and structure of a polymer prepared in this report (entry 11; PS45-PMAA598)

In Table 5 and Figure 11 an overview is given of the obtained polymers with different PS and PMAA block lengths. The diversity in the prepared polymers offers interesting comparison opportunities. Obviously, the trends for the different hydrophobic and hydrophilic block lengths can be examined. Moreover, it is interesting to compare polymers with the same MAA/ST ratio but different total molecular weight, for example entry 9 & 11 or 11, 13 and 14.

Table 5: Overview of the synthesized PMAA-*b*-PS-*b*-PMAA block copolymers

Entry	$Mn_{salt\ form}$ [a]	PS_{GPC} [b] (units)	$PMAA_{GPC}$ [c] (units)	MAA/ST (-)	Styrene (mol %)	MAA (mol%)
7	58638	75	463	6.1	17.0	83.0
8	76708	75	629	8.3	13.1	86.9
9	245904	45	2210	48.4	2.6	97.4
10	119211	45	1047	22.9	5.3	94.7
11	70210	45	598	14.6	8.9	91.1
12	174548	35	1564	43.6	2.9	91.1
13	67536	35	582	12.5	7.5	92.5
14	60872	35	521	10.0	8.3	91.7

a. MW initiator +109($[tBMA]_0/[I]_0$ x conversion)
b. Calculated from GPC analysis in THF against linear p(St) standards
c. Calculated from GPC analysis in THF against linear p(St) standards

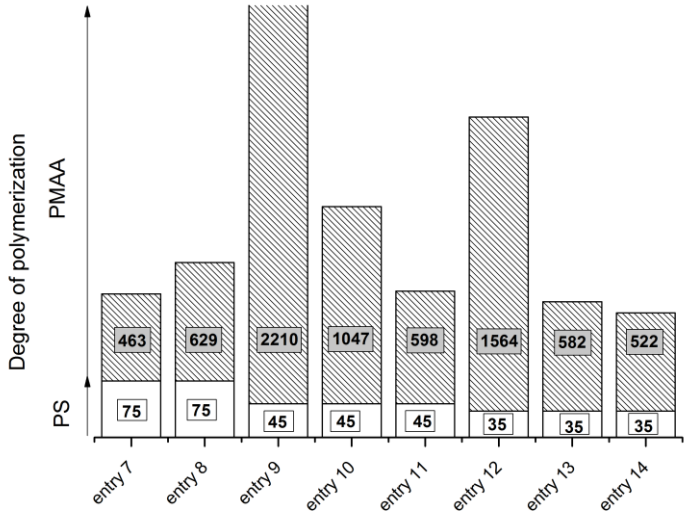

Figure 11: Overview of the synthesized PMAA-*b*-PS-*b*-PMAA block copolymers

NMR spectroscopy - ^{1}H-NMR. The synthesis of the PS-Br macroinitiator and the triblock copolymer PS-PtBMA were characterized by ^{1}H-NMR to determine the degree of polymerization. Examples of ^{1}H-NMR spectra ($CDCl_3$) of a PS-Br macroinitiator (entry 2) and a PtBMA-*b*-PS-*b*-PtBMA block copolymer (entry 7) can be found in Figure 12a and Figure 12b, respectively.

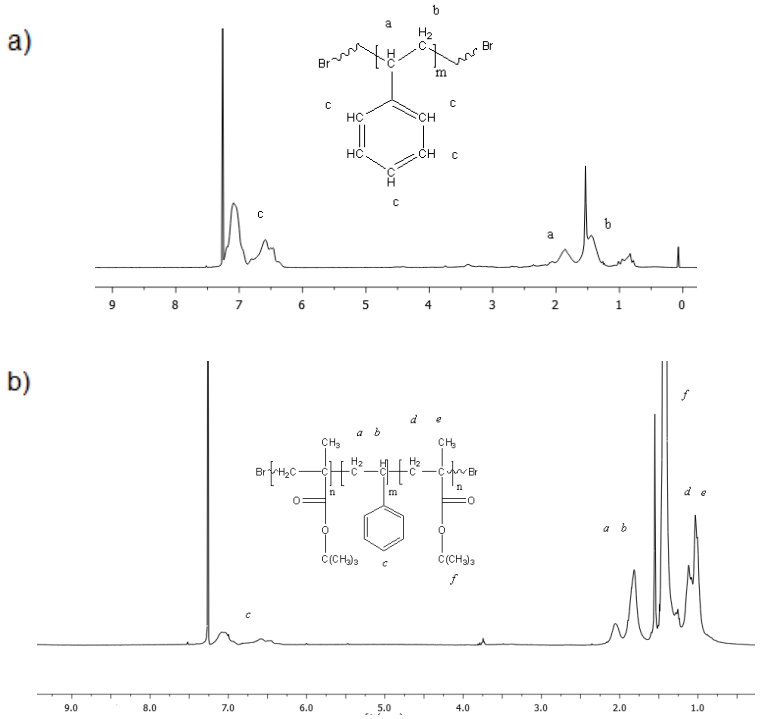

Figure 12: a) Proton NMR spectra for entry 2 (styrene]/[EBIB] ratio = 70/1). b) Proton NMR spectra for entry 7 ([MAA]/[PS-Br] ratio = 2061/1)

Figure 12a: ^{1}H NMR (400 MHz, $CDCl_3$, δ): 0.56-2.05 (m, a+b), 6.23-7.22 (m, c). Impurities: 0 (grease), 1.56 (H_2O)

Figure 12b: ^{1}H NMR (400 MHz, $CDCl_3$, δ): 0.69-2.19 (m, a+b+d+e+f), 6.23-7.22 (m, e). Impurities: 1.56 (H_2O)

Moreover, the extent of the hydrolysis step with concentrated HCl in refluxing dioxane to PMAA-*b*-PS-*b*-PMAA was determined by ^{1}H-NMR. In the experimental conditions, the hydrolysis reach completeness after 3 hours. This is also shown in Figure 13, where it can be seen in that there is no signal of the of the tert-butyl ester anymore. It can be assumed that the degree of hydrolysis is greater than 95%[59].

Figure 13: ^{1}H NMR (400 MHz, d_6-DMSO, δ): 0.69-2.19 (m, 8H), 6.23-7.22 (m, 5H). Impurities: 2.1 (acetone), 3.33 (H_2O), 3.6 (1,4-dioxane)

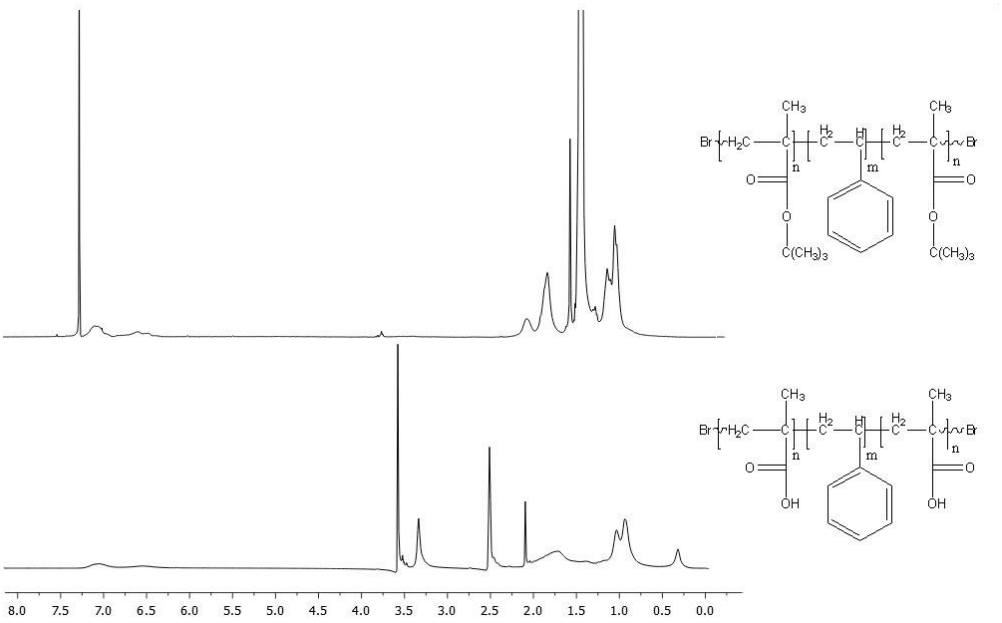

Figure 13: Hydrolysis step for entry 7 from PS75-tBMA463 to PS75-PMAA463

GPC measurements. The polydispersity index (PDI) and molecular weights of the PS-Br macroinitiators and the PS-PtBMA triblock copolymers were determined by GPC measurements. High molecular weight polymers with a narrow polydispersity index (PDI) are desired for optimal use in rheology applications. In Figure 14 the evolution of the molecular weight distribution after chain extension of the different PS-Br macroinitiators is shown. The narrow monodisperse molecular weight distribution (PDI ≈ 2) for the synthesized PS-PtBMA triblock copolymers indicates a controlled radical polymerization and confirms the chain extension on the PS block[85].

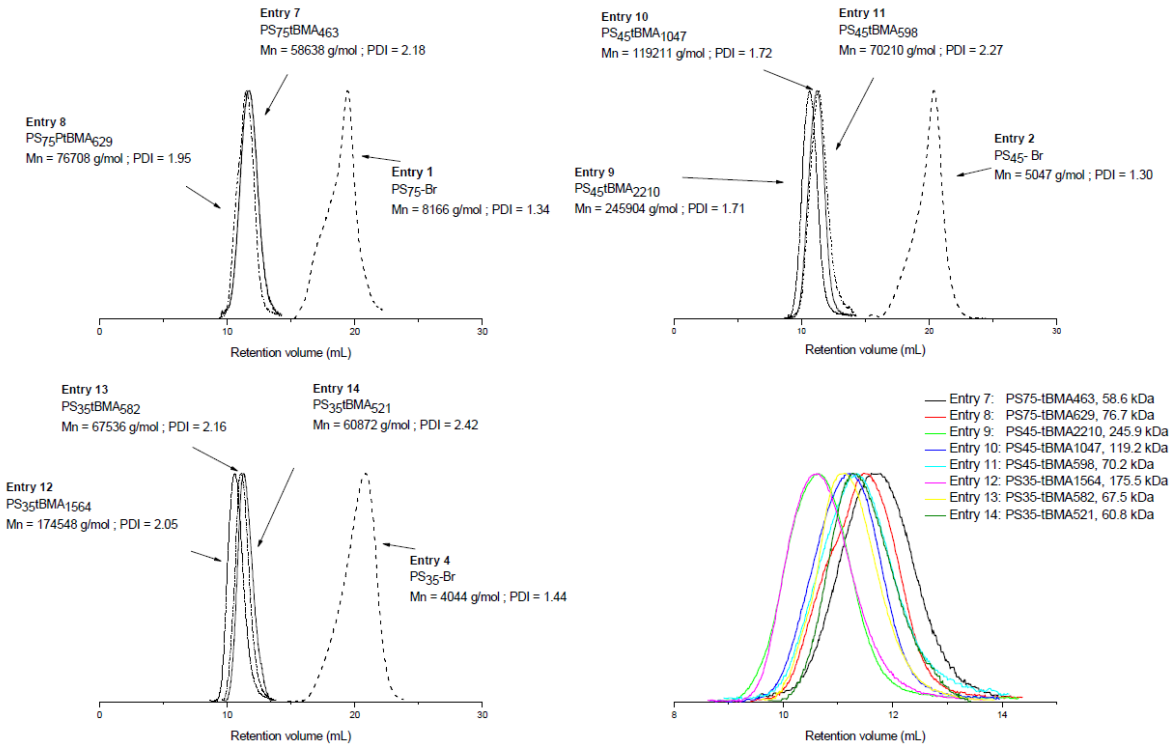

Figure 14: Evolution of the molecular weight distributions for tBMA ATRP polymerizations using PS-Br macroinitiator entry 1 (a), entry 2 (b) and entry 4 (c) as initiator and ME6TREN as ligand. d) The GPC traces for the molecular weight distribution of the produced PS-tBMA triblock copolymers.

4.2 Rheology of aqueous solution with PMAA-*b*- PS-*b*-PMAA block copolymers

The rheological characteristics of the associated amphiphilic triblock copolymers were determined by shear viscosity and viscoelastic measurements. All measurements were performed at 20 °C. The synthesized polymers possess interesting thickening capabilities. As observed in Figure 15, all the polymers solutions (1 wt%) are shear thinning. At lower shear rates ($< \gamma = 10\ s^{-1}$) most polymers reach an apparent Newtonian plateau with exception of entry 8 & 11, with no apparent Newtonian plateau in the frequency range investigated. The absence of a Newtonian plateau supports the fact that these amphiphilic block copolymers already form strong polyelectrolyte gels, which is a typical behavior for hydrophobic modified polymers[15,89]. Shear thinning is primarily determined by the molecular weight and is related to the disruption of the associating polymer network with increasing shear rate which results into the isolation of the polymeric structure. The shear viscosity profiles of the solutions can be fit with a power-law fluid model ($\eta = K\gamma^{n-1}$) and provides an n value of approximately 0.3 for the polymers of entry 8 & 11. This value was also found for diblock copolymers of PS-*b*-PAA by Kimerlang et al.[41] and for block copolymers of PS-PMAA by Raffa et al.[15]. The polymers with a longer PMAA block have an even higher n value of 0.6-0.8. For these polymers, at low shear rates a Newtonian plateau is reached which was also observed by Korobko et al.[42] with PS_{20}-PAA_{85} diblock copolymers. It can also be observed that the high molecular weight polymers, entry 3, 4 and 6, which

have long PMAA arms, are less shear thinning and have longer Newtonian regions. An explanation for this phenomena lies in the nature of the aggregates in solution, where polymers with longer hydrophilic blocks form micelles with a larger PMAA corona. This results in stronger interaction (electrostatic forces and entanglement) between the micelles, which are less easily disrupted by shear[16]. However, for these high molecular weight polymers it was expected that the viscosity was higher due to the higher amount of charged moieties along the backbone of the polymer. The charged nature of the backbone can lead to electrostatic repulsions and therefore increases the hydrodynamic volume of the polymer coil which results in higher viscosity[90]. An explanation could be that these high molecular weight triblock polymers have more difficulty to aggregate, which results in weaker intra or intermolecular hydrophobic associations. The same observations related to the viscosity were also made by Raffa et al.[16] for diblock copolymers of PS and PMAA. The polymers of entry 7, 8 and 11 have a moderate hydrophobic and hydrophilic block and can form strong aggregates which results in high viscosities. Finally, it can be seen that the homopolymer give much lower viscosities compared to the amphiphilic triblock copolymers. An explanation for this is the absence of the hydrophobic block, which has a major effect on the rheological properties. In Appendix II, the viscosity as a function of the shear rate for different polymer concentrations (1, 0.5, 0.1 wt%) can be found. As expected, the viscosity profile decreased in magnitude with decreasing concentration.

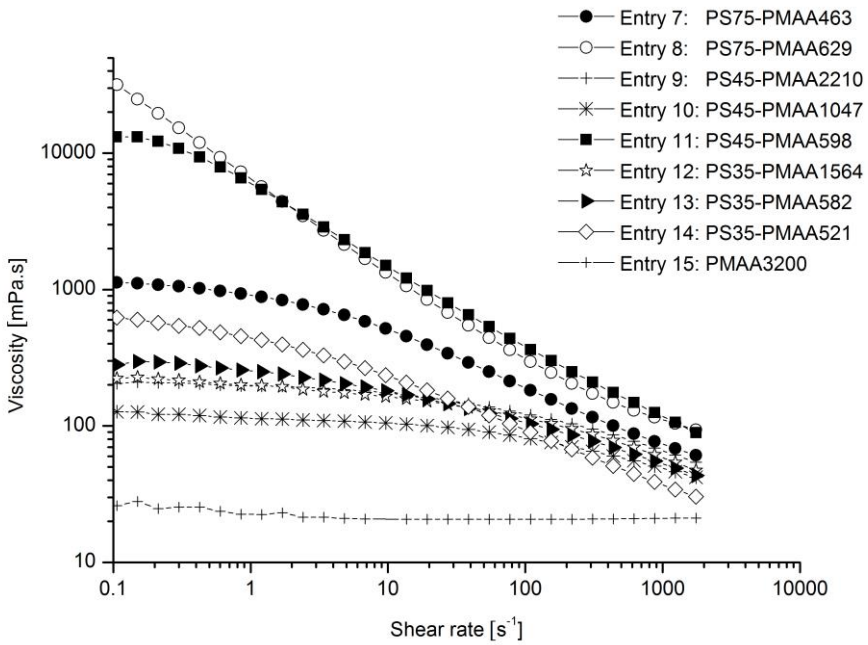

Figure 15: Viscosity as function of the shear rate for different PMAA-*b*-PS-*b*-PMAA block copolymers. Polymers were measured at a concentration of 1wt%.

In Figure 16, the apparent viscosity (at γ = 9.63 s^{-1}; 1 wt%) as a function of the hydrophobic and hydrophilic block length (in monomeric units) is given. The total hydrophilic block length is given above each block in the diagram. For the polymers with the same hydrophobic block length, the hydrophilic block length increases from left to right. In the figure several trends are observed. First, it

can be noted the viscosity decreases dramatically with a total hydrophilic block larger than approximately 600 repeating units. An explanation for this could be that a longer hydrophilic arm with more charges on the backbone leads to the fact that the amphiphilic triblock copolymers have more difficulty to aggregate, which results in less stronger intra or intermolecular hydrophobic associations[3,15,16]. It is also observed that after a certain hydrophilic block length, the viscosity increases slightly again. This can be attributed to the additional molecular weight which influences the viscosity according to the Mark–Houwink equation[91]. Another trend that is observed, is that the viscosities of the polymers with a PS35 block are very low compared with polymers with a larger PS block (with similar hydrophilic blocks). This could be explained by the fact that there is a certain threshold below which the hydrophobic block is too short for strong intra and intermolecular hydrophobic associations. Moreover, for the PS75 block copolymers it appears that a too short hydrophilic block is also not beneficial for the viscosity. An explanation for this is the decrease in electrostatic repulsion with a decreasing hydrophilic block length. From the plot below, it can be concluded that an optimum is reached with amphiphilic triblock polymers with a PS block larger than 35 monomeric units and a hydrophilic block of approximately 600 monomeric units.

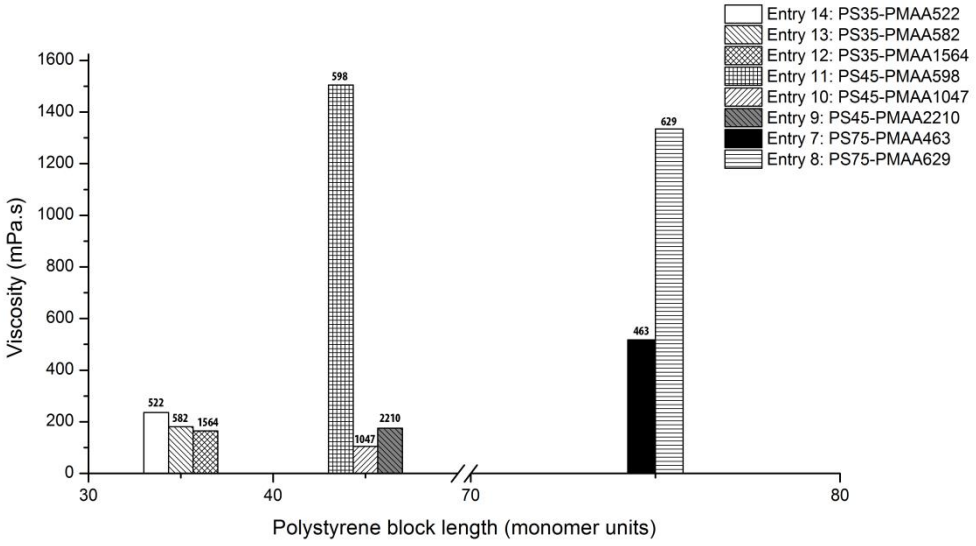

Figure 16: The apparent viscosity (at $\gamma = 9.63\ s^{-1}$; 1 wt%) as a function of the hydrophobic and hydrophilic block length

In Figure 17, the apparent viscosity at shear rate 9.63 s^{-1} as a function of the molar concentration is given for the polymers of entry 7, 8, 9 and 11. In all cases, sigmoidal curves are obtained. At very low concentrations the viscosity is slightly higher than that of water and nearly constant. According to the theory this is the diluted regime[3]. In this regime, the polymers are non-interacting and form isolated micelles with the hydrophilic block fully stretched into the solution. Stretching is the result of the osmotic pressure exerted by the counter ions trapped in the corona by Coulombic interaction[16]. Micelles are formed because the short PS block provides a strong driving force for association of the

copolymer chains into micelle-like aggregates. These micelles consist of a collapsed PS core surrounded by a charged hydrated PMAA coronae[92]. The stability of the micelles is ensured while the strong hydrophobicity of the core-forming PS overcomes the electrostatic repulsion between the PMAA chains. With a higher concentration, the micelles start to interact and after a critical value (the overlapping concentration c*) the viscosity increases sharply. This region is called the semi-diluted regime where the micelles start to interpenetrate and shrink. At even higher concentrations, the slope of the curve does not increase sharply anymore, but remains almost constant. In this region a sol-gel transition occurs and an interpenetrating polymer network (gel) is formed. The typical viscosity profile described above is similar to that observed in star and micellar systems[93] and for PS-PAA-PnBA terpolymers[94]. Also Raffa et al.[16] described the same behavior for PS-PMAA diblock copolymers.

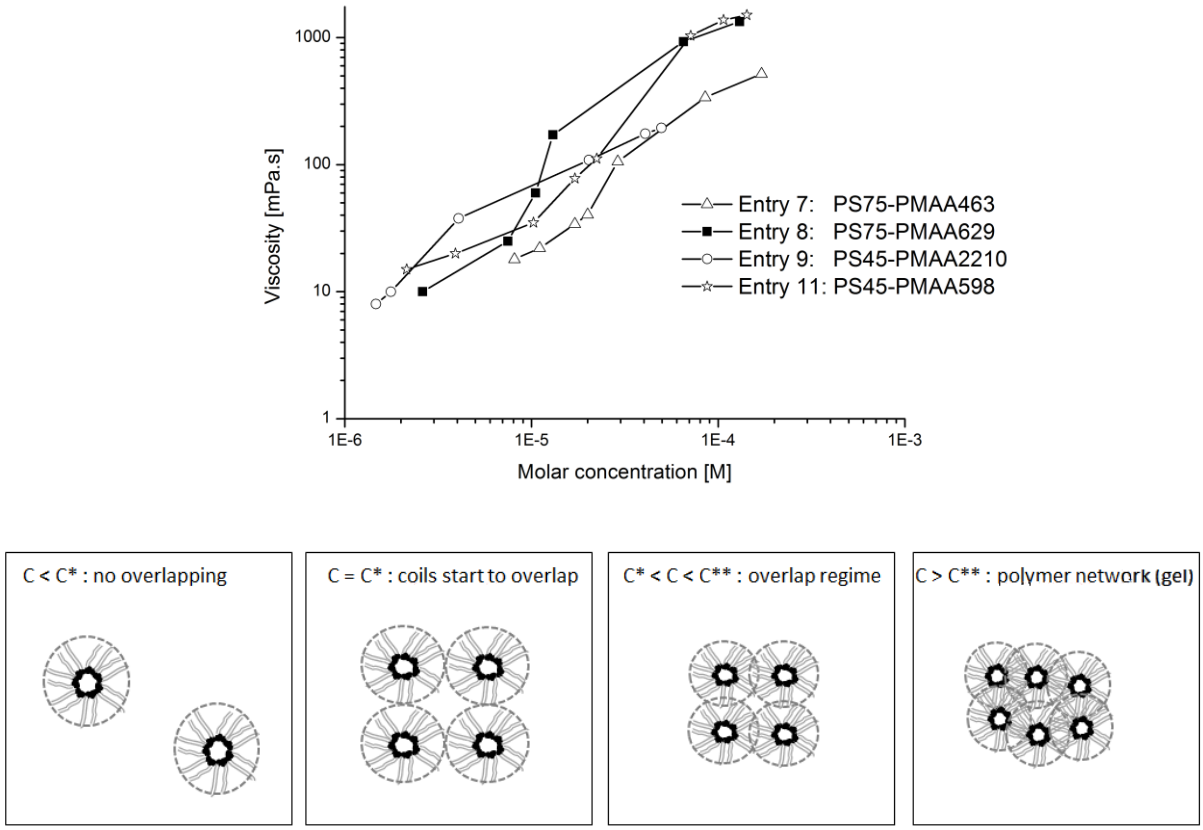

Figure 17: The apparent viscosity (at $\gamma = 9.63\ s^{-1}$) as a function of the concentration and schematic representation of micelles overlapping and shrinking in the different regions

In Figure 17, it can be observed that the overlapping concentrations are almost the same. This can be explained by looking at the hypothetic structure of the micelles, which is depicted in Figure 18. The overlapping concentration is primarily determined by the length of the hydrophilic arm. Polymers with longer hydrophilic blocks form micelles with longer arms and therefore overlap at lower concentrations. For entry 8 & 11 the PMAA block is approximately the same and therefore also the overlapping concentration. Entry 9 has long hydrophilic arms and start to overlap at a lower

concentration as is shown in the above figure. The same results were found by Raffa et al. with diblock copolymers of PS and PMAA[16] and was already reported for neutral amphiphilic copolymers[95]. It can also be observed that in the concentrated region, the polymers with the shortest PMAA blocks form stronger gels at the same weight concentration.

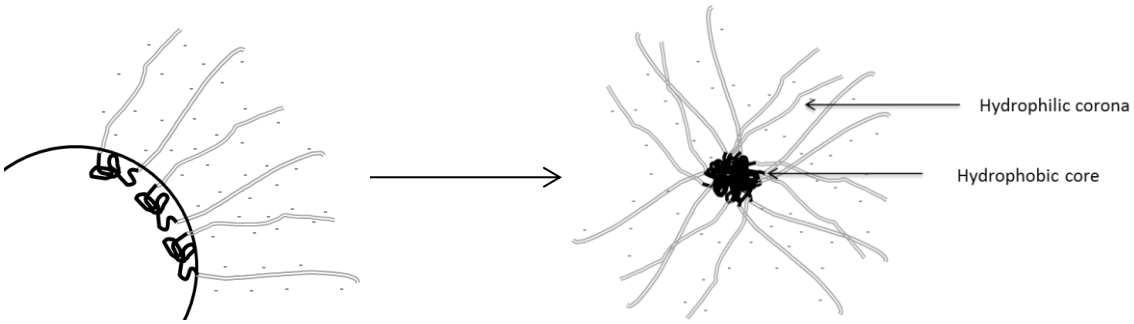

Figure 18: Schematic representation of the arrangement of the amphiphilic triblock copolymers into micelles

Viscoelasticity. This section describes the loss/elastic (G') and storage/viscous (G'') modulus measurements. The results are presented as a function of the frequency, under amplitude oscillatory shear of 1 mPa at a reference temperature of 20 °C. All the polymer samples were tested at polymer concentrations of 0.1, 0.5 and 1 wt%.

The elastic response of an aqueous polymeric solution is dependent on several parameters such as the molecular weight, the concentration and the presence of hydrophobic groups[96,97]. In Figure 20 a,b,c the G' and G'' versus the frequency are plotted for 1 wt% polymer solutions. It can be observed that entry 8 and 11 form viscoelastic gels with G'> G'' over a broad frequency range. Moreover, it is observed that the modulus is nearly independent from the frequency. This is due to the fact that the 1 wt% polymer solutions of 8 & 11 do not flow in tube inversion tests. The results of these tests are shown in Figure 19 and confirm that entry 8 and 11 present a yield stress at concentrations above 1 wt%. The other polymer solutions flow at the bottom of the tube at any investigated concentration. This was also observed by Raffa et al. for di, tri and star block copolymers of PS and PMAA[15,16].

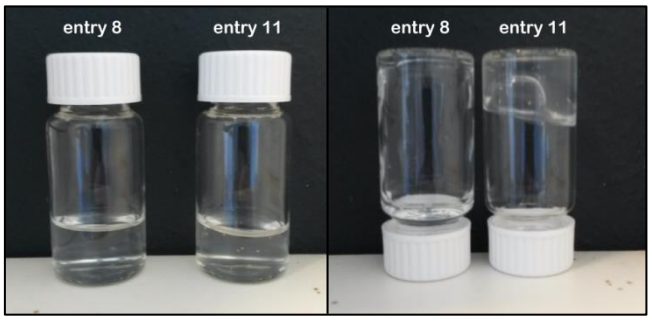

Figure 19: Tube inversion tests. Concentration = 1 wt%. Entry 8: PS75-PMAA629 ; Entry 11: PS45-PMAA598

The polymers with exception of entry 8 and 11 form viscoelastic solutions with a long viscous region where the cross over point occurs at high frequency rates. Moreover, for these solutions the

dependency on the frequency is more pronounced. This shows that the polymer network in solution is weak and easily disturbed. For entry 8 & 11 at lower concentration the same results are found, which indicates the transition from elastic gels to viscoelastic solutions (see Figure 20d).

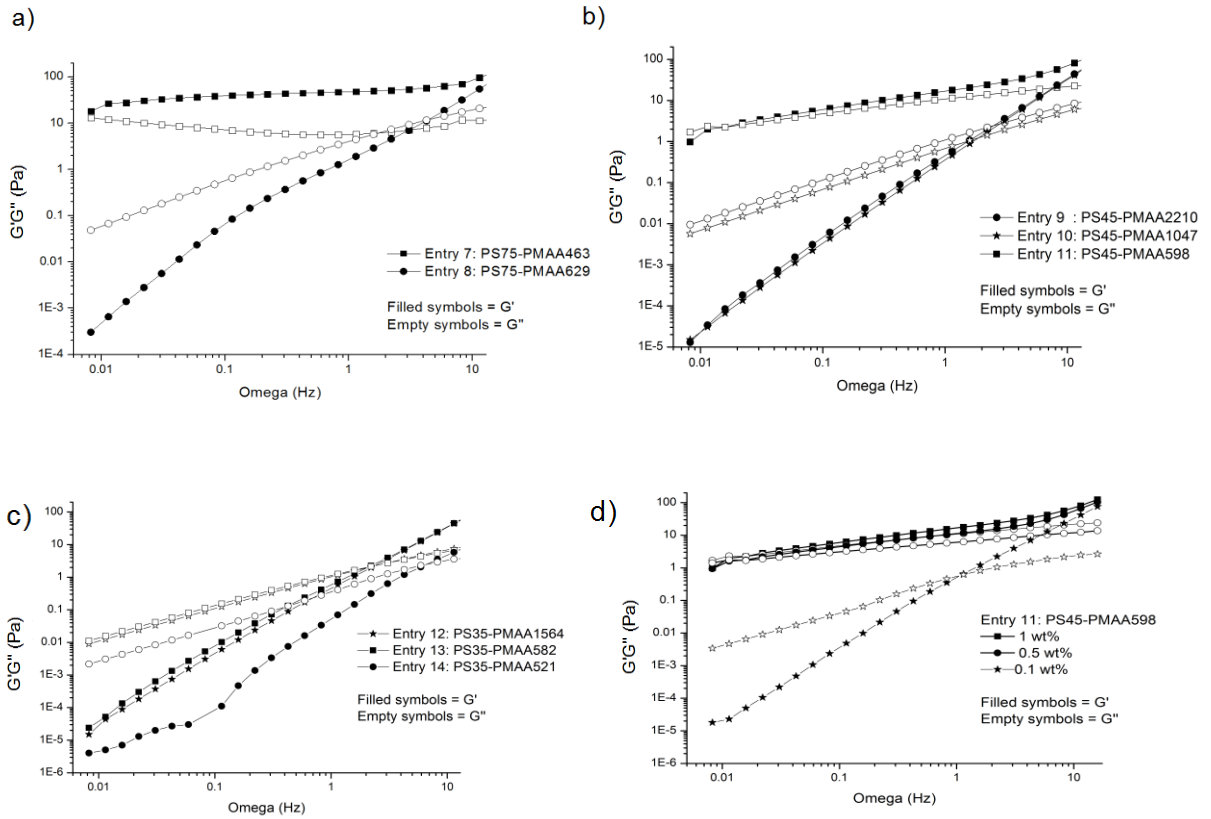

Figure 20: a,b,c) G' and G'' versus the frequency for 1 wt% polymer solutions. d) G' and G'' versus the frequency at different polymer concentration for entry 11: PS45-PMAA598

For a better comparison, the viscoelastic behavior is compared between the dilute/semi-dilute (0.1 wt%) and the concentrated regime (1 wt%). It is expected that in the dilute/semi-dilute regime the molecular weight becomes the controlling factor while micelle interactions are minimized. In Figure 21 the phase angle and the cross over point of G' and G'' versus the frequency for 1 wt% and 0.1 wt% polymer solutions are shown. It can be seen that the polymer solutions giving a high viscosity at 1 wt% polymer solutions (entry 8 & 11) exhibit a high elastic response. The more pronounced elastic response results in a lower phase angle and cross-over point at low frequencies. Apparently, the inner network formed by gelation for these polymers is highly elastic. Moreover, the high viscosity results in an increase in both the loss and storage modulus, which indicates the formation of strong gels. The other polymers do not form strong gels due to the fact that in the 1 wt% regime, longer hydrophilic arms leads to more steric hindrance and electrostatic repulsion, which results in less hydrophobic interactions between the hydrophobic polystyrene chains. The results are quite masked by the differences in viscosity. The high viscosity shifts the phase angle transition from the terminal to the plateau zone at lower frequencies. Therefore the results in the semi dilute regime are more interesting

because in the semi dilute regime the length of the arms have more influence on the elastic response. In this regime, a higher elastic response is more pronounced (except entry 8, where the viscosity is still high) for the polymers with a high molecular weight i.e. long hydrophilic arms. An explanation lies in the length of the hydrophobic and hydrophilic blocks. In the dilute regime, there exist no inner gel network, thus the elastic response is primarily determined by the length of the hydrophilic block. Longer hydrophilic arms have more interactions which gives a higher elastic response. This is shown in Figure 21 c and d with lower phase angles at given frequencies and the cross-over points at low frequencies.

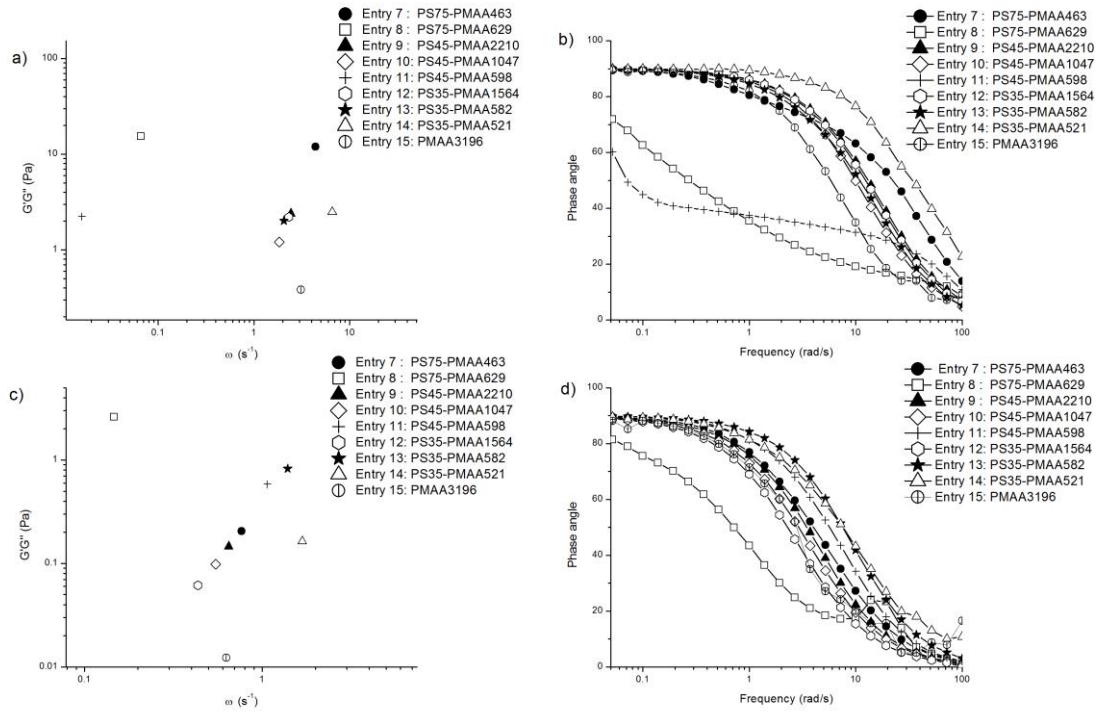

Figure 21: a,b) Cross-over point for the different polymer solutions at G' and G'' versus the frequency for 1 wt% and 0.1 wt% polymer solutions. c,d) Phase angle as a function of the frequency at 1 wt% and 0.1 wt% polymer concentration

Surface tension. The surface tension (against air) of different polymer solutions was measured using the pendant drop method on a Dataphysics OCA15EC tensiometer. The obtained results are plotted in Figure 22 where the surface tension versus the polymer concentration is shown. For clarity, only several results are shown, which represent the results of all polymer solutions.

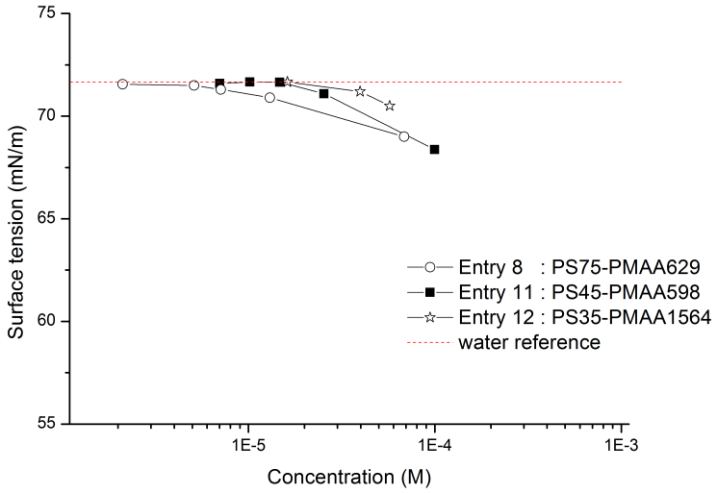

Figure 22: Surface tension vs the polymer concentration of various triblock copolymers

For low polymer concentrations, the solutions move towards the surface tension of demineralized water (measured to be 71.66 mN/m). As the concentration increases, the surface tension reaches a region where it start to decrease. Unfortunately, after a certain concentration ($<10^{-4}$ wt%) due to the high viscosity of the polymer solutions, the droplet size did not remain constant due to relaxation, which resulted in inaccurate measurements. Moreover, it can be argued that the small differences in the measured surface tensions are experimental errors and the amphiphilic triblock copolymers are not surface active. In literature it is described that amphiphilic block copolymers have low diffusion coefficients and subsequently equilibrium situations between the unimers and micelles are reached only after a very long time period[32,98]. The same observations were made by Théodoly et al.[99], who demonstrated on a series of diblock copolymers (PS-*b*-PAA, PBA-*b*-PAA, and poly(diethylene glycol ethyl ether acrylate) (PDEGA)-*b*-PAA) with similar charged hydrophilic blocks of PAA, that the kinetics of adsorption are slower when the copolymers are more hydrophobic. It was shown that for PS-PAA diblock copolymers adsorption was totally hampered. The same observations were made for diblock and triblock copolymers of PS and PEO[98], diblock copolymers of PS and PAA[100] and diblock copolymers of PS and PMAA[47]. It must be noted that the kinetically "frozen" micelles are only obtained in a very poor solvent for polystyrene. An explanation for this phenomena is that due to the strong hydrophobic interactions in the micelles there is a very slow or no exchange between unimers and micelles in solution. Inherently there is no overall diffusion from the bulk to the interface[48]. The PMAA-*b*-PS-*b*-PMAA block copolymers behave as physically/kinetically "frozen" micelles and do

not lower the surface tension of the droplets. This is illustrated in Figure 23, where an exchange mechanism between the bulk and the interface for a solution of PMAA-*b*-PS-*b*-PMAA (a) and PDEGA-*b*-PAA (b) is shown. For the PS-PMAA triblock copolymer solution, due to the relatively high glass transition temperature (T_g) of polystyrene, the core exists in a glassy state that causes a large activation energy barrier for molecular exchange and subsequently does not allow restructuring of the aggregates. For the PDEGA-PAA polymer the hydrophobicity of PDEGA is much lower which allows an equilibrium between micelles and unimers and subsequently results in surface activity of the polymer in solution.

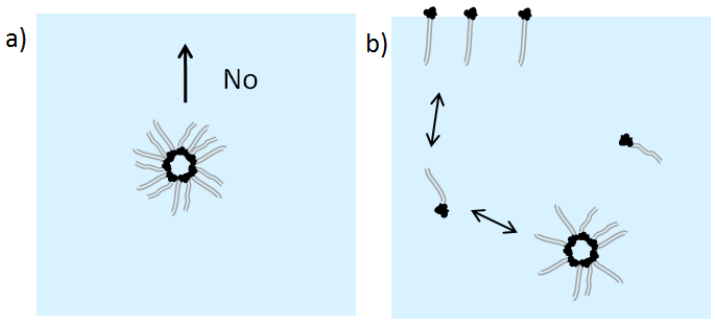

Figure 23: Schematic of the exchange mechanisms between the bulk and the interface for a solution of (a) PMAA-*b*-PS-*b*-PMAA and (b) PDEGA-*b*-PAA

Electron microscopy and modelling of the micelles. The gelation of the triblock copolymers can be quantified with small calculations of the micelle radius and the aggregation number. The gelation of polymeric micellar systems, i.e. the volume fraction of the micelles, depends on the molar polymer concentration c, the micelle radius r_{mic} and the aggregation number p according to the following equation[44]:

$$\varphi = \frac{4\pi r_{mic.}^3}{3}\frac{cN}{p} \qquad \text{[Eq. 12]}$$

Where N is the Avogadro's number. The authors assume that gelation occurs at a volume fraction of φ = 0.6. Computer simulations of PS−PAA block copolymers have shown that for suspensions of hard spheres φ = 0.56 - 0.6 and even higher values were obtained for polydisperse samples[44]. The triblock copolymer is composed by N_A and N_B hydrophilic and hydrophobic monomers, respectively. For triblock copolymers the appropriate scaling has to be applied where $N_A' = N_A/b$ and $N_B' = N_B/b$ with n = the number of arms. It is assumed that both monomers have the same length l. The value l = 0.25 nm is taken as repeating unit length because this is the length of a segment of three sp^3-hybridized connected carbon atoms. Below the critical micelle concentration, the micelle arms are completely stretched and the micelle core is formed by completely collapsed hydrophobic chains. Therefore the core radius r_B is given by:

$$r_B = l * (p * N_B)^{1/3} \quad \text{[Eq. 13]}$$

Where l is the monomer length, p the aggregation number and N_B the degree of polymerization of the hydrophobic block. The hydrophilic chain radius[16] r_A is given by:

$$r_A = l * N_A \quad \text{[Eq. 14]}$$

Where l is the monomer length and N_A the degree of polymerization of the hydrophilic block. This results that the micelle radius can be simply expressed as:

$$r_{mic} = r_{A+}r_B = l(pN_B)^{1/3} + lN_A \quad \text{[Eq. 15]}$$

The aggregation number p, r_A and r_B can be calculated substituting equation 12 in equation 15. The results are shown in Table 6.

Table 6: Calculated r_A, r_B and p according to equation 12 and 15

Entry	N_B	N_A	Molecular weight (g/mol)	gel conc. (M)[a]	r_{mic} (nm)	r_B (nm)	r_A (nm)	p
7	75	463	58638	$3.41\ 10^{-5}$	60.5	2.7	57.9	32
8	75	629	76708	$1.30\ 10^{-5}$	81.2	2.6	78.6	29
9	45	2210	245904	$4.07\ 10^{-6}$	281.4	6.5	276.3	772
10	45	1047	119211	$1.68\ 10^{-5}$	134.8	3.9	130.9	173
11	45	598	70210	$1.42\ 10^{-5}$	76.9	2.1	74.8	27
12	35	1564	174548	$1.15\ 10^{-5}$	200.2	4.7	195.5	387
13	35	582	67536	$2.96\ 10^{-5}$	75.2	2.4	72.8	53
14	35	521	60872	$3.29\ 10^{-5}$	67.4	2.3	65.1	42

a. Polymer molar concentration

The calculated values for the micelle radius, r_{mic}, show that the total radius is increased with longer hydrophilic chains. This also increases the aggregation number where in bigger micelles, more polymers can aggregate. Interestingly, Raffa. et al.[16] estimated the aggregation number p, for diblock copolymers of PS and PMAA using the same equations as above. The diblock copolymers gave much higher aggregation numbers. For example for a diblock copolymer PS45-*b*-PMAA555 which corresponds to entry 11 (PS45-PMAA598) the obtained aggregation number was 195, which is almost 7 times higher. This is in line with the expectation that diblock copolymers arrange into micelles much easier due to less steric hindrance. Moreover, Huh et al. [101] showed for A-B(n) block copolymers that there is an inverse relationship between the number of arms and the aggregation number. Thus the more arms (star > tri > di), the more steric hindrance which results in a low aggregation number. However, it must be noted that several assumptions are made in the calculation. For example it is assumed that the system is based on a dynamic equilibrium between the unimers and the micelles in solution. As shown with the surface tension experiments, the micelles behave as kinetically 'frozen'

micelles. Moreover, it is difficult to determine at which concentration a sol-gel transition occurs, but for the calculations the same reference point is taken, which allows to make a comparison.

The structure of the gels has also been characterized by transmission electron microscopy measurements. In Figure 24 negative stain TEM images (scale = 50 nm) from 1 wt% solution of the polymers can be seen. The images show a micellar structure where white spots are the spherical hydrophobic cores consisting of polystyrene. The PS core is surrounded by the PMAA hydrophilic corona which is depicted as the dark regions due to adsorption of the stain. The images show that polymers giving a high viscosity (Figure 24 a,b,c) have a smaller micelle radius and a more dense packing, indicating a gel network. The images also show that the hydrophilic domains are highly linked together (especially for the polymers with long PMAA chains) which is expected in a gel structure. The gel structure appears disordered in all cases which was also found for PS-PAA and related block copolymers[44].

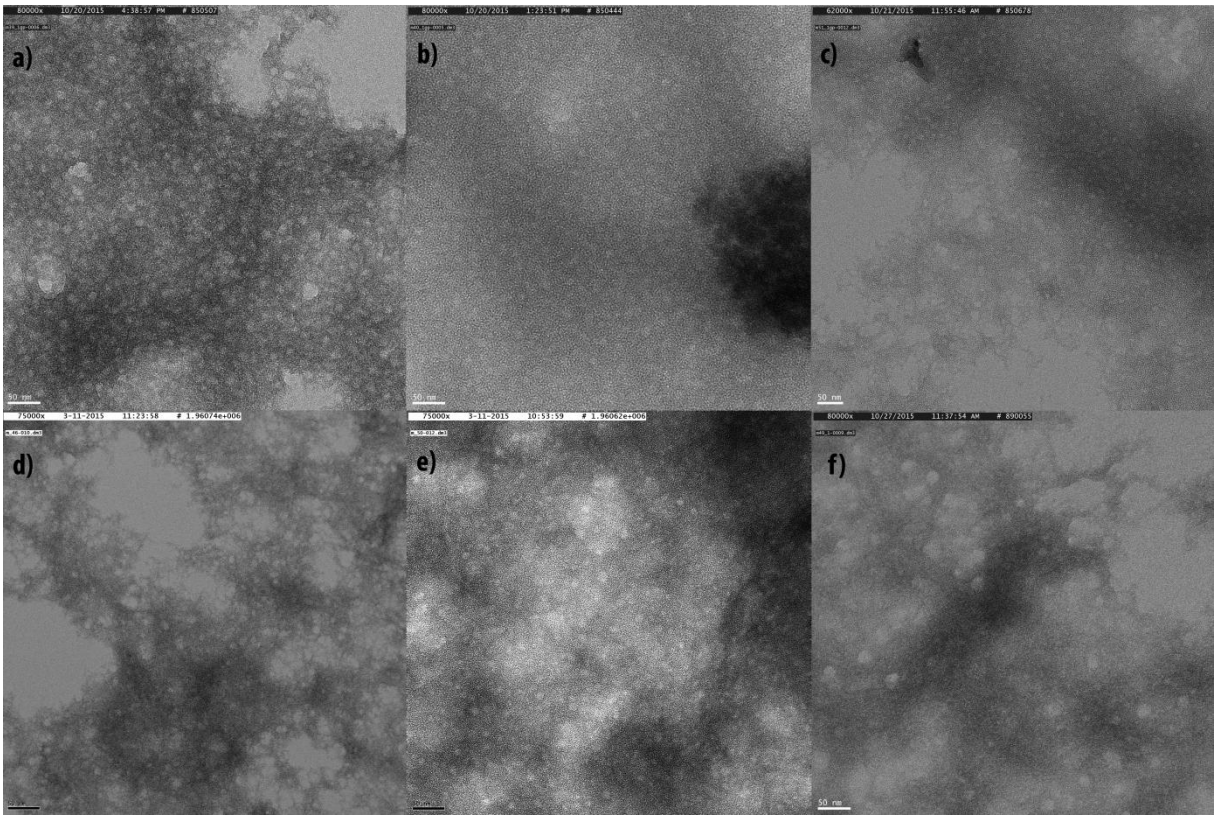

Figure 24: Negative stain EM pictures of 1 wt% solutions of: entry 7 (a), entry 8 (b), entry 11 (c), entry 9 (d), entry 10(e) and entry 12(f)

Furthermore, the gel structure of entry 8 (PS75-PMAA629) was investigated using cryo-transmission electron microscopy. A cryo-TEM image of PS-PMAA block copolymers has never been seen before. A cryo-TEM image shows the amphiphilic block copolymer in their native environment, which results in more accurate interpretation of the structure. A typical cryo-TEM image (entry 8) is displayed in Figure 25 with a concentration of 0.3 (Figure 25 a, b) and 0.5 wt% (Figure 25 c, d).

The cryo TEM images show that the gel structure can be described as a disordered state similar to colloidal glass. The average radius can be calculated using the Ruler tool in Adobe Photoshop CS6. The cryo TEM results and the theoretical calculated radius according to equation 15 are shown below.

Table 7: Average radius of a micelle in solution at different concentrations

conc. (wt%)	r_{mic} (nm)
0.5	51.4
0.3	61.1
0.1	81.2[a]

a. Calculated r_{mic} fully stretched in solution below gelation concentration (according to equation 15)

The experimentally obtained results are in good agreement with the theory of percolation and the calculated micelle radius. The results show that with an increase of the concentration, the micelles start to interpenetrate, which leads to a decrease in the micellar radius (shrinking of the hydrophilic corona) due to the screening effect of the interpenetrating charged coronas.

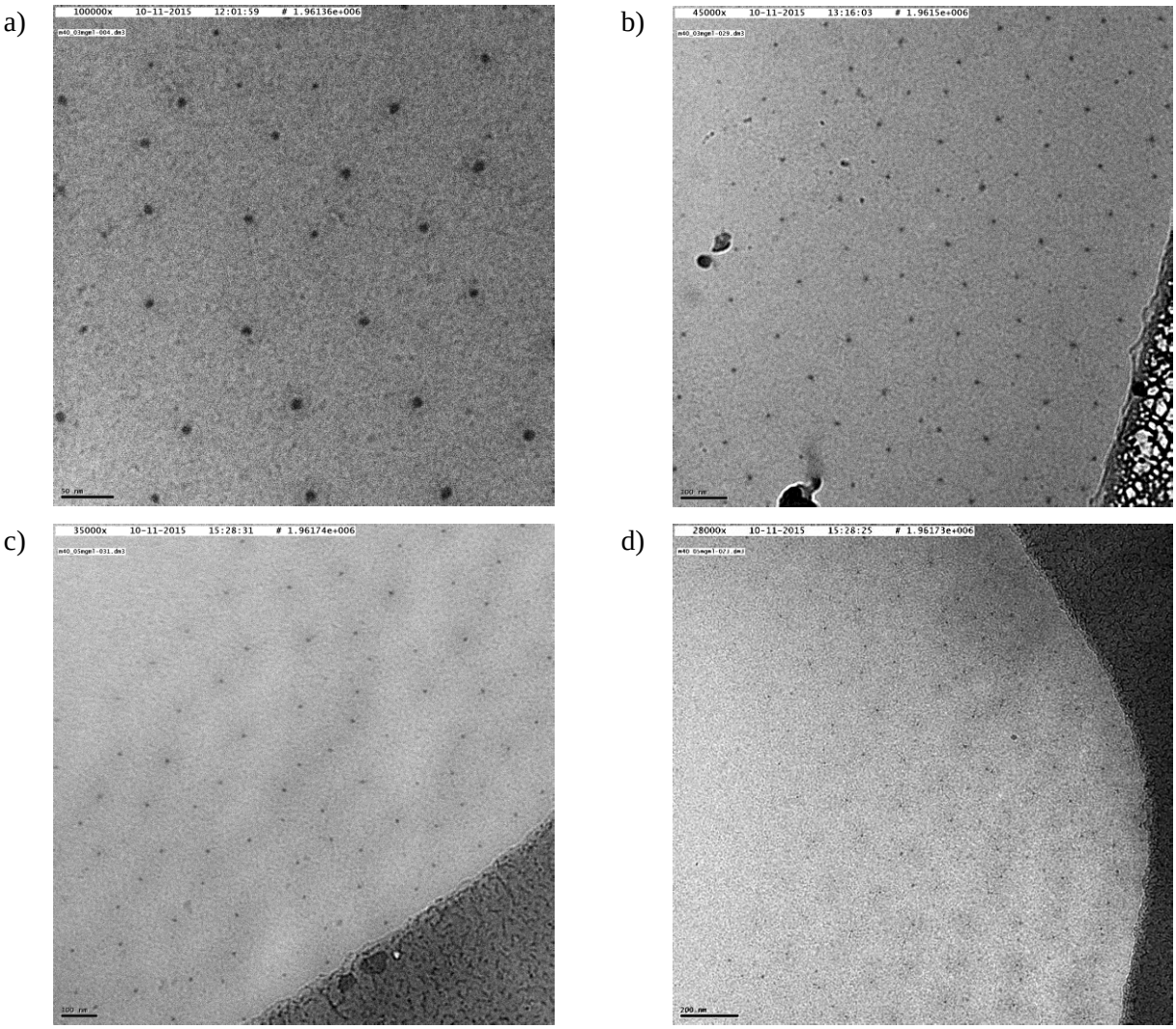

Figure 25: Cryo-TEM image of an amphiphilic triblock copolymer at 0.3 wt % (a,b) and 0.5 wt% (c,d) (entry 8: PS75-PMAA629)

Zeta-potential. Colloidal particles accumulate charge at their surface that can be expressed as a surface potential, which is an important factor for determining the electrostatic repulsion between particles[102]. The surface electrical potential is an immeasurable quantity, but the so-called zeta potential can be measured. The Stern model as shown in Figure 26 describes the zeta potential as follows: at the particle surface, a tightly bound layer of counter-ions (i.e. of opposing charge) accumulates, which is called the Stern layer. Beyond this layer, the ionic concentration decreases with increasing distance from the particle surface (diffuse layer). The zeta potential is the electric potential at the location of the slipping plane which is dependent on the characteristics of the particle[103].

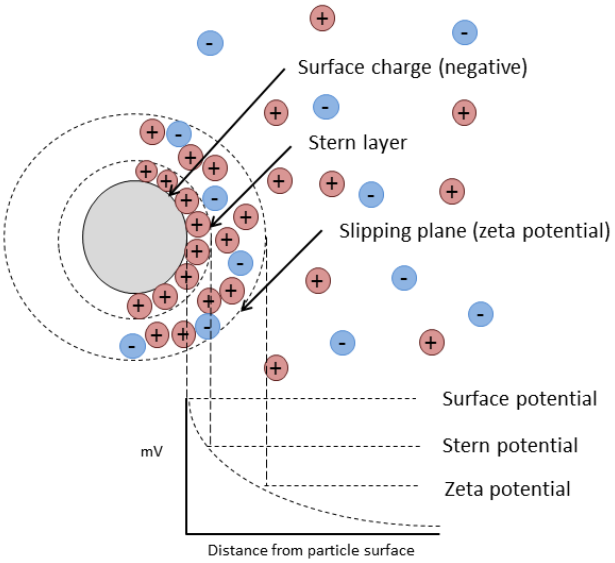

Figure 26: Stern model describing the ionic conc. as a function of the distance from the charged surface of a particle

The zeta potential was measured on a ZetaPALS zeta potential analyzer. Figure 27 shows the zeta potential for the different amphiphilic PS-PMAA triblock copolymer systems in water with a concentration of $2*10^{-5}$ M. Most of the zeta potentials obtained in this study are very high and within the range of ± 65-75 mV. The negative potential indicates that the surface of the particles are negatively charged, as expected from ionized methacrylic acid groups[5]. Systems with the zeta potential in this range exhibit excellent stability of the colloid whereby the magnitude of the zeta potential indicates the degree of electrostatic repulsion between charged particles[104]. The stability of water/oil emulsion will be discussed later in this report. The particle size was measured using dynamic light scattering at 90°. The measured particles sizes can be found in Appendix IV. It can be seen that the particle size is much higher than the calculated estimations in Table 6 or the size obtained from transmission electron microscopy. Therefore, the magnitude of the calculated zeta-potential can only be used relatively. Nonetheless, it can be seen that the magnitude of the electrostatic repulsion for the polymeric systems is almost equal and is slightly dependent on the viscosity. The magnitude of the zeta-potential decreases with a higher viscosity. A higher viscosity indicates that micelles have more interaction and an interpenetrating network is formed. This results in shrinking of the hydrophilic

corona and subsequently screening of the charges which results in less electrostatic repulsion which determines the zeta potential. Moreover, it can be argued that the higher viscosity reduces the diffusion coefficient and therefore according to the electrical mobility equation of the Einstein relation, the "mobility", or the ratio of the particle's terminal drift velocity to an applied force is decreased[105].

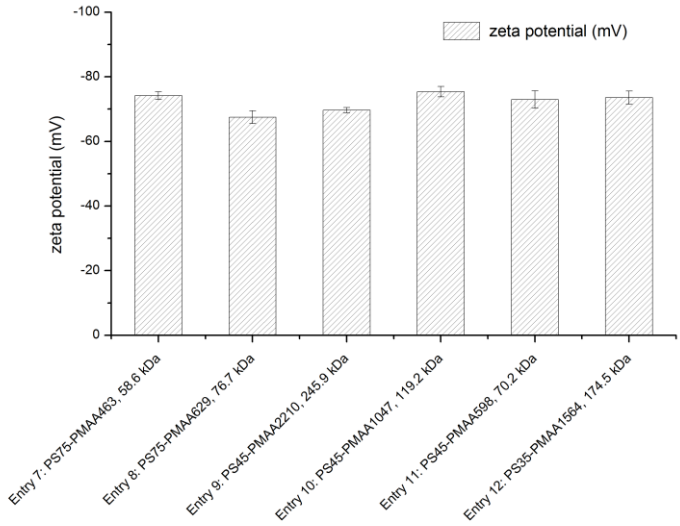

Figure 27: The zeta potential of the PS-PMAA triblock copolymer systems in water (conc. 2 10^{-5}M)

Salt effect. The presence of NaCl on the shear viscosity of 1 wt% PMAA-*b*-PS-*b*-PMAA block copolymer solutions has been investigated using entry 11: PS45-PMAA598 in different concentration of NaCl solutions. In Figure 28, the viscosity versus the shear rate at different NaCl concentrations is shown. The viscosity drops dramatically upon addition of salt. An explanation for this is the fact that the salt ions shield the charges on the PMAA block, which results in chain collapse, shrinking of the corona and weaker intermicellar interactions[15,41,42]. Consequently, this results in a decrease in viscosity and elasticity. Also the viscosity as function of the concentration was investigated using entry 11 (PS45-PMAA598) in 30.000 ppm of NaCl solution. As it can be seen from Figure 28, the dependency shows now a more exponential curve with much lower viscosities compared with the entry 11 solution without 30.000 ppm NaCl. However, the system still presents the characteristics of a gel. This shows that the polyelectrolyte screening shrunk the PMAA chains, but did not affect the hydrophobic association. This was also observed by Hietala et al.[89] for PS-PAA star polymers.

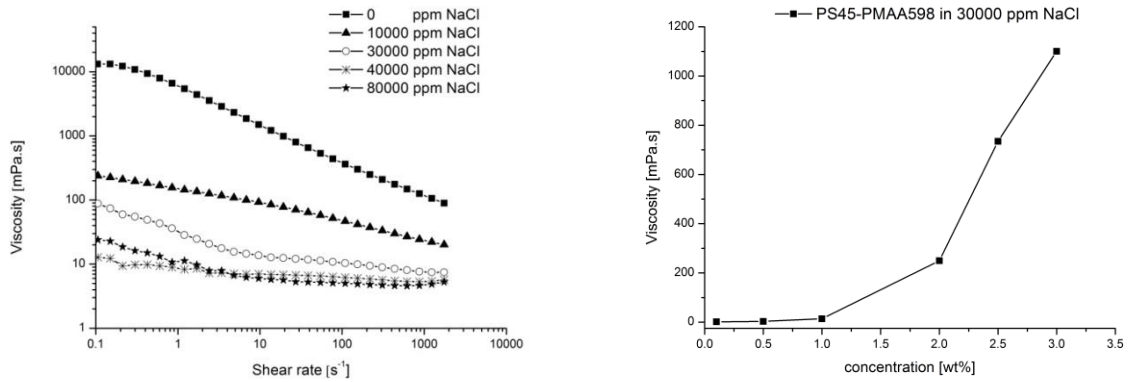

Figure 28: a) Shear viscosity of 1 wt% PS45-PMAA598 solutions at different NaCl concentrations b) Viscosity (measured at γ = 9.63 s^{-1} at 20 °C) as a function of the polymer concentration in salt water (30.000 ppm NaCl)

A small calculation can be made to model the size of the micelles upon addition of salt. In the regime of high salt concentration, the stretching of the polyelectrolyte arms should disappear due to screening of the charges. This is schematically shown in Figure 29. The corona radius scales with $p^{1/5}N_A^{3/5}c_s^{-1/5}$ where c_s is the salt concentration[106]. For a completely collapsed corona, the c_s value can be written that the concentration of Na^+ equals the concentration of MAA units; $c_s = c^* N_A$. The micelle radius for micelles upon salt addition is given by:

$$r_{mic} = r_{A+}r_B = l(pN_B)^{\frac{1}{3}} + lp^{\frac{1}{5}}N_A^{\frac{3}{5}}(cN_A)^{-\frac{1}{5}} \qquad \text{[Eq. 16]}$$

$$r_{mic} = l[(pN_B)^{\frac{1}{3}} + p^{\frac{1}{5}}N_A^{\frac{2}{5}}c^{-\frac{1}{5}}]$$

We assume that p is constant because the micelles are kinetically "frozen", thus for entry 11, p = 27, the following results are obtained:

Table 8: The calculated micelles radius, r_{mic}, with and without the addition of salt

Entry	N_B	N_A	Molecular weight (g/mol)	conc. (M)	r_{mic} (nm)	r_B (nm)	r_A (nm)	p
11[a]	45	598	70210	$1.42\ 10^{-5}$	76.9	2.1	74.8	27
11[b]	45	598	70210	$4.26\ 10^{-3}$	5.6	2.1	3.54	27

a. Without the addition of salt, c = gel concentration
b. With addition of salt, c_s= salt concentration

The calculations show that the radius of the micelle decreases dramatically upon addition of salt. The decreased radius also results in less interaction between the aggregates and subsequently a lower viscosity.

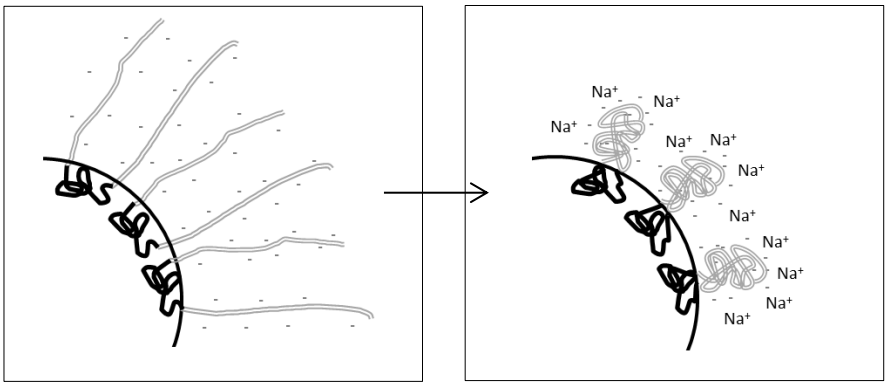

Figure 29: Star-like micelle of PS-PMAA triblock copolymer in water without (left) and with (right) the addition of salt

Interestingly, it can be argued that the micelle structure when salt is added is comparable to the gel structure at high polymer concentrations. In both cases, the hydrophilic corona is shrunk. At the gel point, the coronas are interpenetrating and the osmotic effect that stretches the polyelectrolyte brush has disappeared. This can be proofed by the fact that the micelle radius as estimated above (5.6 nm) is approximately the same as observed in the negative stain electron microscopy image (see Figure 24c, Table 9).

Table 9: Comparison between theoretical and experimentally found micelle radius

	r_{mic} (nm)
Theoretical	5.6
TEM	9.8

a) According to equation 16

b) Experimentally found radius with negative stain TEM

Temperature effect. The effect of temperature on the shear viscosity of 1 wt% PMAA-*b*-PS-*b*-PMAA block copolymer solutions has been investigated using entry 11 (PS45-PMAA598, 70.2 kDa). In Figure 30 the viscosity as a function of the temperature and shear rate (at several temperatures) is reported. It can be seen that the viscosity for example at shear rate y = 9.63 s^{-1} hardly decreases. This was not expected since in literature the viscosity is highly dependent on the temperature. For example for PMAA-PEG[107] diblock copolymers and $PAA_{54}PS_6$ starpolymers[89] the viscosity decreases significantly with increasing temperature while the inner network is broken. Apparently, the micellar structure is strong enough to resist breakage of the inner network. Moreover, this polymer shows promising thickening capabilities at high temperatures, which is an important requirement in Enhanced Oil Recovery applications where the temperature in a reservoir can rise up to 120 °C[24].

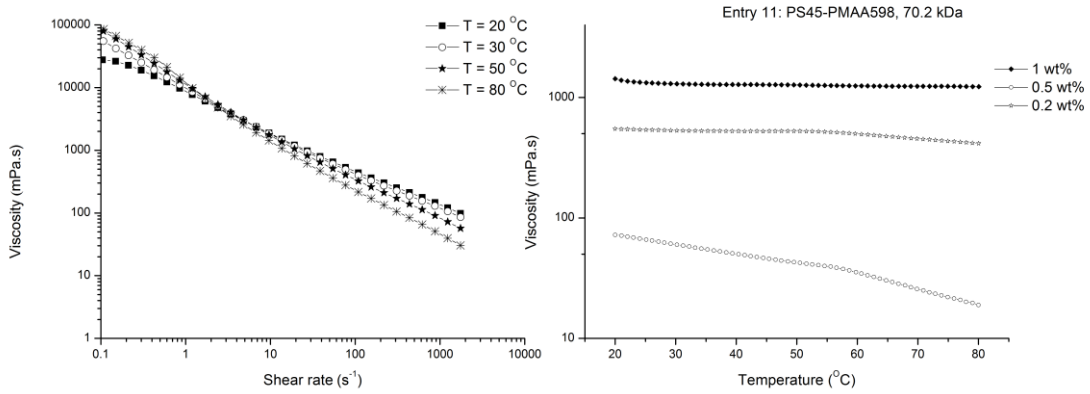

Figure 30: a) Shear viscosity of entry 11 (PS45-PMAA598, 1 wt%) as function of the shear rate at different temperatures. B) Shear viscosity of entry 11 as function of temperature at $\gamma = 9.63\ s^{-1}$

pH effect: The effect of the pH on the shear viscosity of 1 wt% PMAA-*b*-PS-*b*-PMAA block copolymer solutions has been investigated using entry 11 (PS45-PMAA598, 70.2 kDa). In Figure 31 the viscosity as a function of the shear rate at different pH is displayed. The samples were made by dissolving the amphiphilic triblock copolymers in water and adding a predetermined amount of 1 M hydrochloric acid. The potentiometric measurements of the pH were done on a UltraBasic Denver Instrument. The solutions show a decrease in viscosity with a lower pH. At a high pH the hydrophilic PMAA chains are deprotonated and highly stretched in solution which causes high electrostatic repulsion between the chains[5]. Gradually decreasing the pH results in neutralizing the charges and subsequently the polymer chains collapse. This is the same viscosity profile as can be seen with the addition of salt. The pH and salt dependency of the amphiphilic triblock copolymers yield interesting opportunities in the application of smart materials[5].

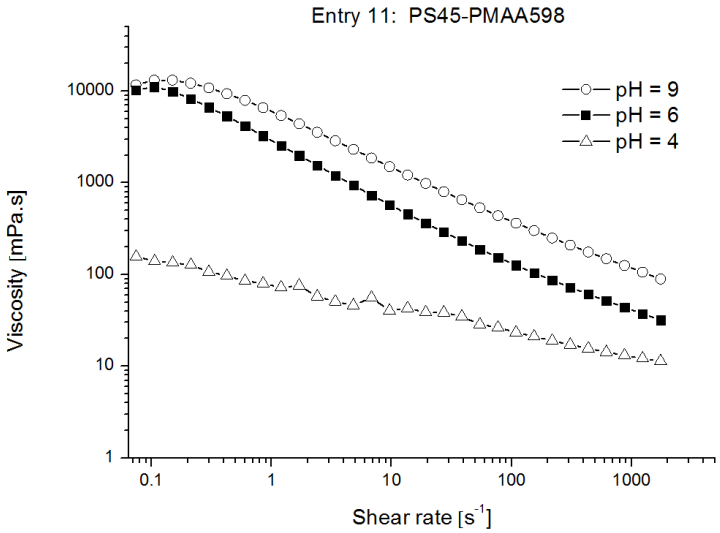

Figure 31: Shear viscosity of entry 11 (PS45-PMAA598, 1 wt%) at different pH

The effect of the pH can also be quantified by zeta-potential measurements. pH-Sensitive micellization was realized with the amphiphilic triblock copolymers of PS-PMAA in aqueous solution. Figure 32

shows the zeta-potential of entry 11: PS45-PMAA598 (concentration: 2 * 10^{-5} M) at different pH. Observations show a transition from collapsed to stretched PMAA polymer chains judged from the fact that the zeta-potential increases with increasing pH due to the ionization of the PMAA blocks[108]. At pH = 1.0-2.0, the zeta potential is almost zero which indicates that the micelles are almost electrically neutral. At this pH, the insoluble polymer complex precipitates. In Appendix IV more results of the zeta-potential measurements can be found. Here the average diameter of the micelles is reported as well, from which it can be seen that the diameter decreases with a decreasing pH. This is in line with the expectation that the micelle collapses due to neutralization of the charges. At pH =1.0 – 3.0 the measured micelle radius is larger again, but this is due to precipitation of the micelle in solution which results in more light scattering and thus a larger diameter. Sun et al.[109] reported the same pH dependency of the zeta potential for amphiphilic triblock copolymers of PAA-*b*-PEO-*b*-PAA. Fernyhough et al.[5] found for polybutadiene–poly(methacrylic acid) (PMAA) block copolymers the same results, but only when the solution was changed from high to low pH. They reported that the aggregates in solution (measured by TEM) transformed from vesicles to cylinders to spheres by changing the pH. For further research it would be interesting to see if this change in structure is also obtained for PS-PMAA block copolymers. The polystyrene block might inhibit change of the structure due to the high glass transition temperature.

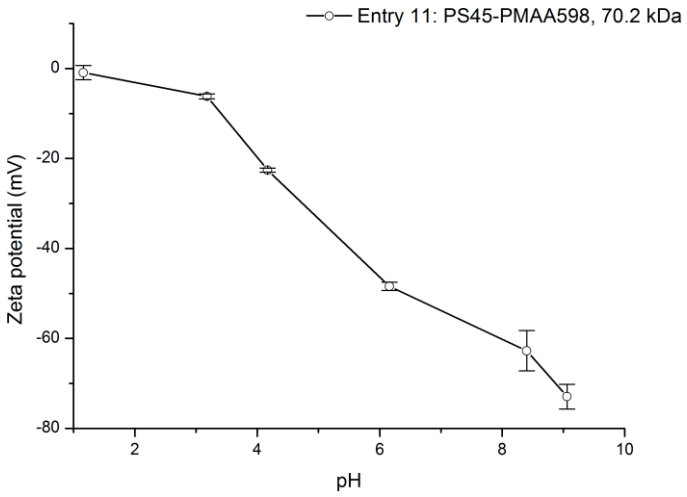

Figure 32: pH dependency of the zeta potential for PS45-PMAA598 solutions (conc. 2 * 10^{-5} M)

Kinetic stability emulsion experiment. The stability of emulsions consisting of an equal amount of oil (102.2 mPa, $\gamma = 9.63\ s^{-1}$) and polymer solution were tested by phase separation experiments. Three important parameters influence the stability of the emulsion: the viscosity, the composition and the concentration. In the first experiment the concentration of the polymer solution was adjusted to match the viscous state of the crude oil in order to investigate the effect of the concentration on emulsion stability. Also, at these concentrations a comparison can be made with the performance in the flow-

cell. In the second experiment the molar concentration of the polymer solution was held constant and the effect of the viscosity on the emulsion stability was tested. The oil in water (O/W) macro emulsions (droplet size ≈ $1*10^{-3}$ m) were made by mixing oil and polymer solution for 30 minutes at 750 rpm on a stirring plate. The obtained O/W emulsion are in line with the Bancroft rule which states that the phase in which an emulsifier is more soluble constitutes the continuous phase[110]. A water in oil (W/O) emulsion was obtained with entry 7 with a different emulsion preparation technique. This emulsion was created by mixing oil and polymer solution for 30 minutes at 750 rpm on a stirring plate and putting the solution for 10 minutes in an ultrasonic bath. It is known that sonication can break the inter-micellar associations, disrupting the micelles which leads to fragmentation of large aggregates. Reorganization of these micelles was not observed by Zhao et al. for PEO- PS diblock copolymers[111]. Explanation and further research about these mechanisms is outside the scope of this thesis, but it opens a challenging research field and gives multiple options for interesting applications. Phase separation was determined visually at given times during the experiment. The results are shown in Figure 33 with the solution characteristics (viscosity and concentration) in appendix IV.

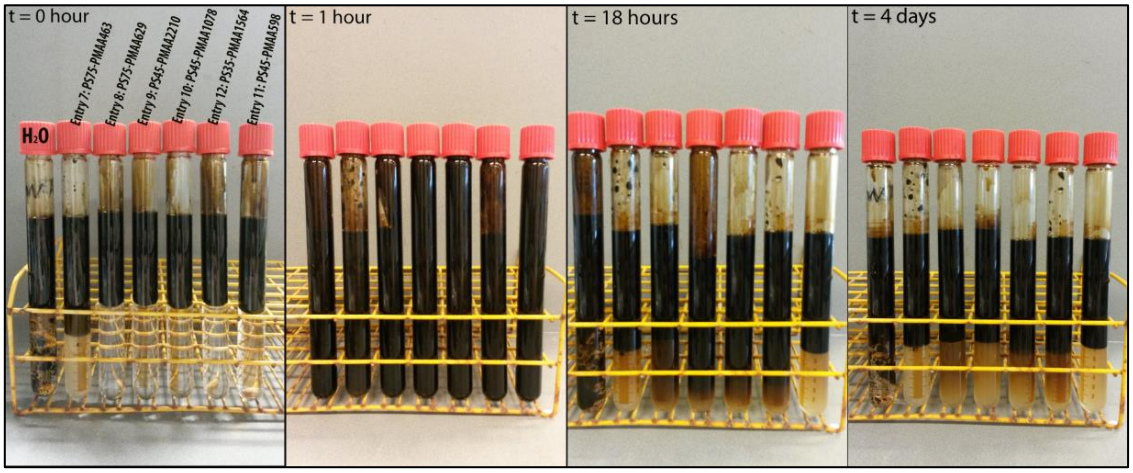

Figure 33: Phase separation of oil and polymer solution (with the same viscosity) at given times

Observations show that after 18 hours most emulsions have phase separated to some extent. This phenomena is clearly shown in the above figure where phase separation for the reference emulsion (water/oil) is complete after 18 hours whereas the other emulsions are not completely separated. The emulsion stability is enhanced due to the fact that the polymers act as a surfactant, lowering the interfacial tension. Phase separation is most pronounced for the low molecular weight polymer solutions; especially entry 7, 8 and 11 with the short PMAA arms. This can be justified considering that the concentrations of the polymer solutions differ completely and affect the degree of phase separation. The higher the polymer concentration, the higher the stability of the emulsion. The more concentrated polymer solutions (entry 9, 10 and 12) show higher emulsion stability. This can be explained by the fact that the triblock copolymers in these solutions have more interaction with each other (steric hindrance, electrostatic repulsion) which results in a more kinetically stabilized emulsion.

The formation of stable oil/water emulsions with an amphiphilic triblock copolymer was also shown by Huang et al.[112] which synthesized a $PDMA_{22}$-$PPMA_{27}$-$PLMA_{36}$ (poly[N,N-(dimethylamino) ethyl methacrylate-*b*-poly(ethylene glycol)methyl ether methacrylate-*b*-lauryl methacrylate) triblock copolymer with a hydrophobic core and hydrophilic arms. These copolymers reduced the dodecane/water interfacial tension significantly and could be tuned by adjusting the solution pH.

An optical microscope (magnification 40x) was utilized to image the emulsion droplets to check the influence of copolymer concentration and composition on the size of the dispersed droplets in emulsions formed with PS-PMAA triblock copolymers. As shown in Figure 34, a decrease in average diameter of droplets was clearly observed compared with the reference emulsion (water/oil). The differences in droplet size can be attributed to two factors: the polymer concentration and the hydrophobic/hydrophilic block length. It is expected that a high concentration results in small droplets. At low concentrations, the block copolymer is not capable to absorb on the large surface area of small droplets, which results that the dispersed droplets lower their surface area by having a large size with wide diameter distribution[9,112,113]. This trend is not clearly observed in the results in Figure 34. Apparently, a very short PS block (35 units) and a long PMAA block (1564 units) gives the best emulsification and stabilization efficiency (Figure 34f)

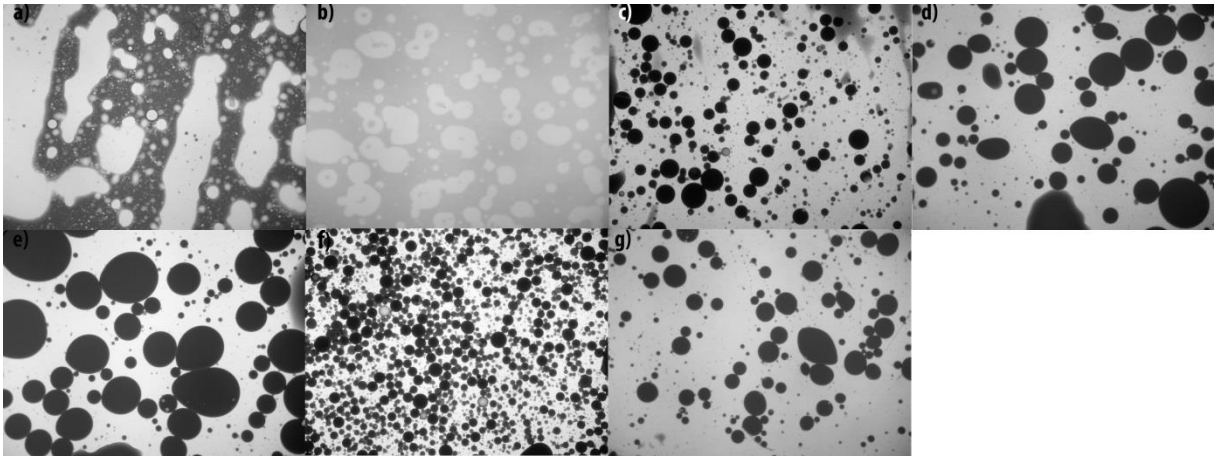

Figure 34: Light microscopy images (magnification 40x) after emulsification for (a) water (b) Entry 7: PS75-PMAA463, 58.6 kDa (c) Entry 8: PS75-PMAA629, 76.7 kDa (d) Entry 9: PS45-PMAA2210, 245.9 kDa (e) Entry 10: PS45-PMAA1047, 119.2 kDa (f) Entry 12: PS35-PMAA1564, 174.5 kDa and (g) Entry 11: PS45-PMAA598, 70.2 kDa

The results indicate that all polymer solutions influence the interfacial properties in some extent that different sized droplets are formed. After 5 days, the emulsions show (almost) complete phase separation. A comparison was made between the reference emulsion (water/oil) and a polymer emulsion (entry 11/oil) directly and after 5 days of emulsification. Complete phase separation occurred for the reference emulsion where in both phases no other phase was found. Interestingly, for the polymer emulsion in the water phase still small oil droplets could be found. The results are shown in Figure 35.

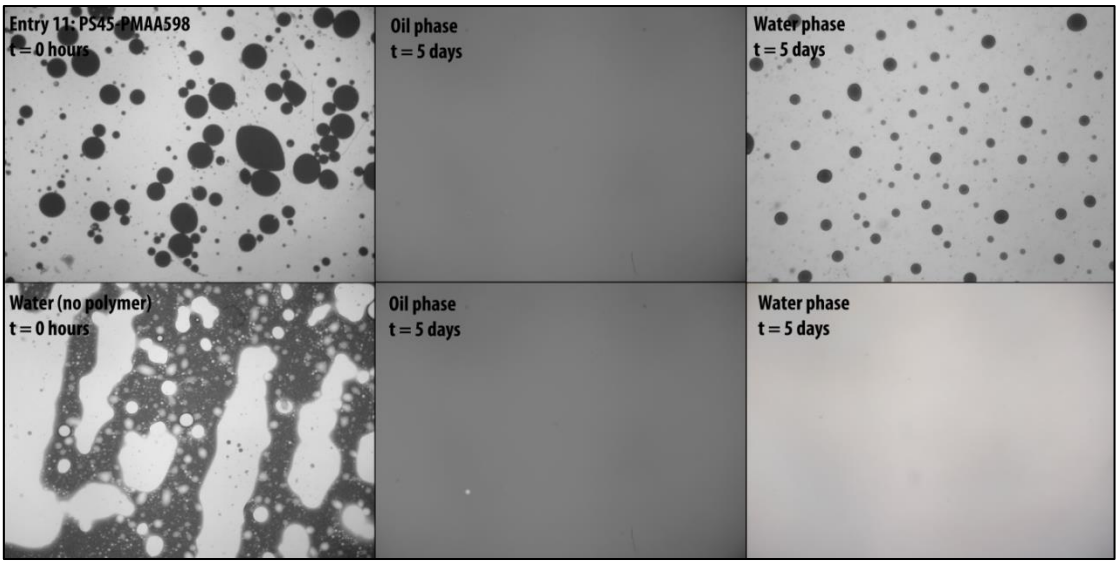

Figure 35: Comparison between the reference (water/oil) and polymer emulsion (entry 11/oil) directly and after 5 days of emulsification

In the second kinetic stability emulsion experiment the molar concentration of the polymer solution was held constant and the effect of the viscosity and structure of the polymer on the emulsion stability was tested. The emulsions were made by the same method as described above. Before the experiment, the viscosity of the polymer solution was measured on a HAAKE Mars III (ThermoScientific) rotational rheometer at shear rate (γ = 9.63 s^{-1} at 20 °C). The results of the stability experiment are shown in Figure 36 with the solution characteristics in appendix IV.

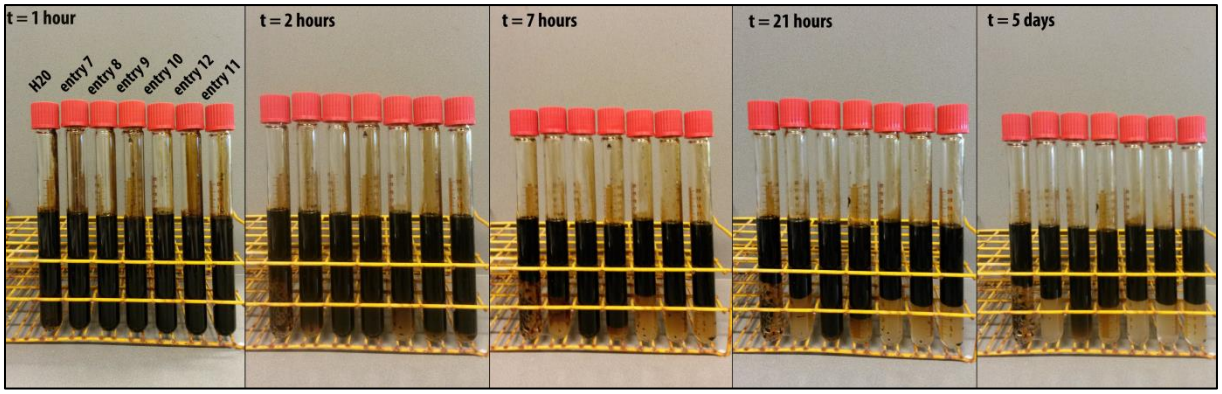

Figure 36: Phase separation of oil and polymer solution (at the same molar concentration) at given times

The kinetic stability experiment showed that a higher viscosity enhances the stability of the emulsion significantly. For example, after 21 hours entry 8 (η = 308.0 mPa.s) shows almost no phase separation where for entry 10 (η = 36.4 mPa.s) phase separation is almost complete. Figure 36 clearly shows that the extend of phase separation correlates to the viscosity. An explanation lies in the diffusion rate, which is directly influenced by the viscosity of the continuous phase as described by the Stokes-Einstein equation:

$$D = \frac{k\,T}{6\pi\eta r} \qquad \text{[Eq. 17]}$$

Where D is the diffusion coefficient of a droplet, η is the continuous phase viscosity, r is the radius of the spherical particle and k the Boltzmann constant. The zeta potential for the polymer solutions was also measured (Appendix V) where a high zeta potential will confer stability due to resisting aggregation. If the zeta potential is small, attractive forces exceed repulsion (steric or electric) and coagulation and flocculation occurs. The zeta potentials for all polymer solutions were very high, but no clear trend could be found with the results of the emulsion stability experiment.

4.3 Oil recovery simulation

The synthesized triblock copolymers were evaluated by oil recovery simulations to determine the performance in the application of Enhanced Oil Recovery. The oil recovery simulations consist of 2D flow-cell and core-flood experiments.

4.3.1 Flow-cell experiments

In the 2D flow-cell, the polymers capability to recover oil out of dead-end zones can be examined, based on the results of oil depletion for chamber 2, 3 and 4 (see Figure 3). The additional oil recovery was eventually calculated using equation 10. The viscosity of the crude oil (at shear rate of 9.63 s^{-1}, 20 °C) used in the flow-cell was 102.2 mPa.s. The concentration of the polymer solutions used for the experiments were adjusted so that the viscosity of the polymer solution matched the viscosity of the crude oil. All triblock copolymers except entry 13 and 14 (not enough polymer) were tested in the flow-cell. The performance of the PS-PMAA triblock copolymers in the 2D flow-cell were compared with a commercial used polymer in EOR applications; partially hydrolyzed polyacrylamide (HPAM, 12000 kDa, 25-30 hydrolysis in mole %). The results of the flow-cell experiments are summarized in Appendix I and in Figure 37.

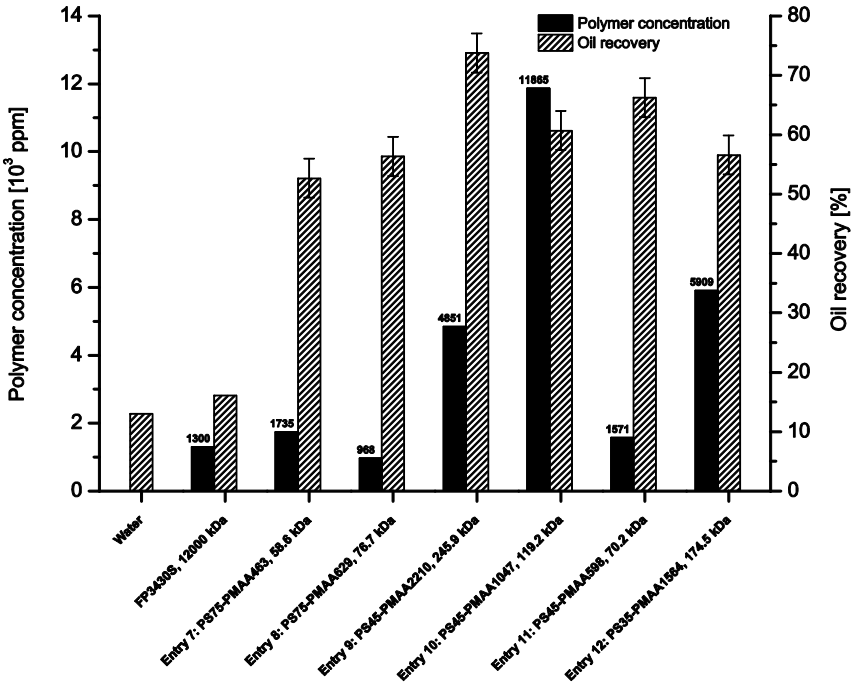

Figure 37: Oil recovery out of dead-end zones in the 2D flow-cell (molecular weight in Da)

From Figure 37, it can be observed that the different polymer solutions give fairly comparable oil recoveries. All the polymers improve the oil recovery roughly between 40-60% compared with water. The first goal of the polymer is to increase the viscosity of the polymer solution in order to decrease the water/oil mobility ratio, which results in an increased displacement efficiency. In these experiments, the viscosity of the oil and polymer solutions are approximately the same which gives interesting opportunities to compare the polymer performance regarding the sweep efficiency, which is affected by other parameters such as the viscoelasticity and/or interfacial tension. Notable, is the fact that the lowest molecular weight polymer solution, entry 7, gives the lowest oil recovery where the highest molecular weight polymer solution, entry 9, gives the highest oil recovery. The molecular weight is primarily determined by the long PMAA blocks and this can give an explanation for the obtained results: the longer arms results in a higher elastic behavior which can increase the microscopic sweep efficiency[22,31]. Elastic behavior provoke shear stresses from interactions between the polymeric chains and the oil droplet resulting into "pulling oil out" (pulling mechanism) of the dead end zones. The latter is in agreement with the observed results. The figure also shows that large differences exist in the used polymer concentrations. Specifically, high concentration were used for the block polymers with a long PMAA block (entry 9, 10 & 12) to match the viscosity of the crude oil. Higher concentrations of polymer, results in more overlap and interaction between the polymer coils. Moreover, the higher concentration may also have influenced the oil recovery while more polymer decreases the interfacial tension significantly. This was also shown in the emulsification experiments

where the emulsions exhibited longer stability for high molecular weight (high concentration) triblock copolymers at the same viscosities.

4.3.2 Core-flood experiment

The oil recovery in porous media using a triblock copolymer (entry 8: PS75-PMAA629) was evaluated by a core-flood experiment. High permeable sandstone cores (Bentheim) were used to evaluate the oil recovery in a reservoir. The physical properties of the Bentheim sandstone cores (5 x 30 cm) are listed in Table 10. The porosity was determined using the buoyancy method, where the bulk volume and the grain volume were measured by immersing the dry sample in mercury[25]. The pore volume (pV) was calculated with the corresponding porosity and the total volume of the core. The brine permeability was calculated using Darcy's law[84].

$$k_{brine} = 1000 * \frac{L}{A} * \eta * Q * \frac{1}{\Delta P} \qquad \text{[Eq. 18]}$$

Where k_{brine} = brine permeability (mD), L = length of the core (cm), A = cross sectional area of the core (cm^2), η = viscosity of the fluid (mPa.s), Q = the flow rate (cm^3/s) and ΔP = pressure drop across the core. The pressure drop across the core was determined by injecting the brine solution (2000 ppm) at different flow rates (50, 100, 200, 250, 350, 450, 550 mL/h). Finally, the average pore radius for a brine flow can be calculated using the following equation.

$$r = \left(\frac{8 * k_{brine}}{\theta}\right)^{\frac{1}{2}} \qquad \text{[Eq. 19]}$$

Where r = the average pore radius for brine flow (μm), k_{brine} = brine permeability (m^2) and θ = the porosity (fraction).

Table 10: Physical properties of the sandstone cores used in the core-flood experiments

	Bentheim (1)	**Bentheim (2)**
Length (cm)	30	30
Diameter (cm)	5	5
Cross sectional area (cm^2)	19.63	19.63
Porosity (%)	24	24
Pore volume (PV, ml)	141.4	141.4
Brine permeability (mD)	2195	457
Average pore radius (μm)	8.49	3.87
Oil saturation (%)	84.88	78.51

For the core-flood experiment entry 8 (PS75-PMAA629) was chosen as amphiphilic triblock copolymer because of the good performance in the flow-cell (add. oil rec. 43.34 %), but mainly for the need for a very low polymer concentration (0.096 wt% in water). The lower the concentration, the more economical feasible the polymer is. The polymer was dissolved in a 2000 ppm brine solution (polymer concentration adjusted so that the viscosity matched the oil viscosity) to compare the results with a commercial polymer FP 3430S (HPAM, 12000 kDa, 25-30 hydrolysis in mole %). The results of the core-flood experiment are given in Table 11 and Figure 38.

Table 11: Oil recovery from Bentheim sandstone cores (brine concentration 2000 ppm)

Entry	Core sample	Polymer conc. (ppm)	Oil sat. [a] (% of PV)	Oil sat. water [b] (%)	Oil sat. polymer [c] (%)	Oil recovery [d] (% OOIP)	ΔP, PF [e] (bars)
PS75-PMAA629	Bentheim (1)	5538	84.88	38.06	32.64	6.38	0.74
FP 3430S	Bentheim (2)	2000	78.51	44.71	40.85	4.01	1.5

a. The oil saturation to begin of the experiment (i.e. the OOIP)
b. The oil saturation after the water flood
c. The oil saturation after the polymer flood
d. Oil recovery based on equation 11
e. The maximum pressure drop during the polymer flood

The use of the commercial linear polymer (FP 3430S) results in an additional oil recovery of 4.01 % after the water flood. In contrast, the use of the triblock copolymer PS75-PMAA629 (entry 8) results in an additional oil recovery of 6.38 %. The higher oil recovery is remarkable given that the viscosity of the displacing fluid is equal for both solutions. The slight increase in oil recovery can be attributed to several parameters such as the elasticity of the polymer solution or to the fact that the triblock copolymer act as a surfactant, lowering the interfacial tension. However, there are some interesting differences between the two experiments. The concentration of the commercial polymer is significantly lower than the concentration of the triblock copolymer to obtain the same viscosity as oil (γ = 102.3 mPa.s). The viscosity of the triblock copolymer in brine solution decreases significantly due to polyelectrolyte screening. The screening effect for the commercial polymer is less pronounced because only 25-30 mole % of the backbone is hydrolyzed. In this experiment the salt concentration is relatively low compared to the salt concentration in oil reservoirs with concentrations over 30.000 ppm[114]. A higher salt concentration results in the need for a higher polymer concentration, which from an economical point of view is not beneficial. Nevertheless, both commercial and triblock copolymer give a high viscosity at low concentrations and enhance the oil recovery significantly as tertiary oil recovery method. The slight increase in oil recovery for the commercial polymer can be attributed by the significant larger pressure drop (1.5 bar), which is high compared to the triblock copolymer (0.7

bar). The increased pressure drop can be caused by the high hydrodynamic polymer layer thickness, but the most plausible solution is the much lower brine permeability of the Bentheim core used in the core-flood experiment for the commercial polymer. As expected, the permeability and the oil recovery are related. Nonetheless, with a lower pressure drop, the triblock copolymer has even a higher oil recovery, which can be attributed to the elastic behavior of the polymer and the capability of lowering the interfacial tension of the oil and water interface.

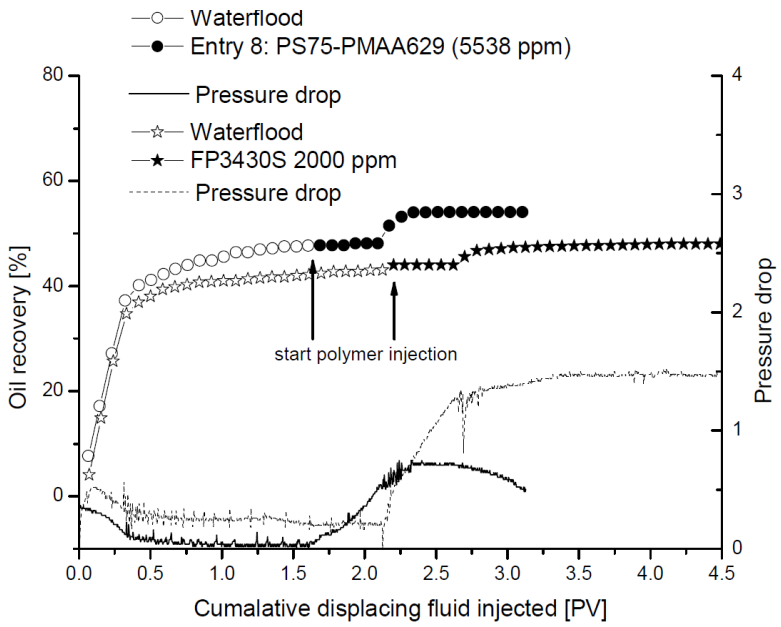

Figure 38: Oil recovery from high permeable Bentheim sandstone cores

The shear viscosity of the polymer solution, PS75-PMAA629, was measured before and after the polymer flood. The results are shown in Figure 39.

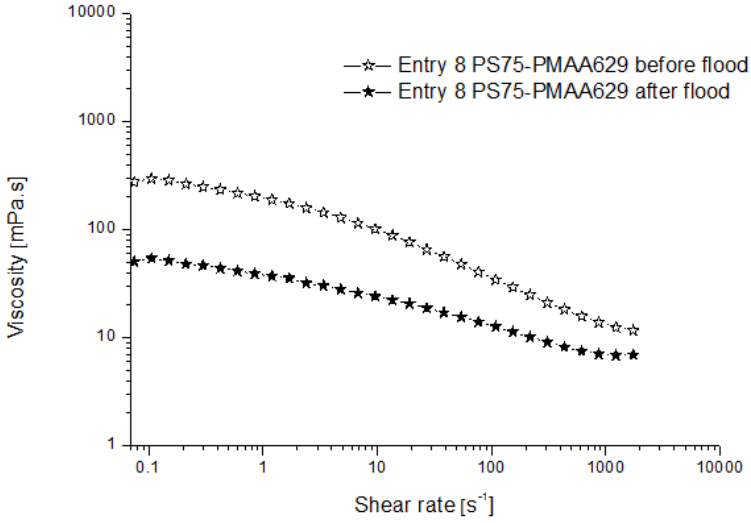

Figure 39: Viscosity as function of the shear rate (PS75-PMAA629) before and after the polymer flood in the core-flood experiment

A significant difference in the viscosity of the polymer solution, before and after polymer flooding in the core-flood experiment exist. An explanation for this interesting observation, could be that the polymer is retained in the reservoir rock surface by mechanical trapping and adsorption[66]. Adsorption for both polymers and hydrophobic modified polymers is reported in literature[73,74]. The blocky structure of the triblock copolymer results in strong hydrophobic interactions which leads to strong adsorption and the formation of multilayers[115,116]. Hydrophobically modified polymers show an unusual adsorption isotherm and the amount of polymer adsorbed on the rock surface is higher than adsorption for homopolymers[18]. Adsorption increases continuously with increasing polymer concentration due to the formation of multilayers, which can only be formed due to the hydrophobic and hydrophilic blocks. Adsorption can result in an increase in oil recovery because it leads to a reduction in permeability in reservoir rocks, which can be measured by the residual retention factor (see equation 5). The calculated RRF values and the corresponding adsorbed polymer layer thickness for the polymers in the core-flood experiments are shown in Table 12.

Table 12: Permeability results of the core-flood experiment

Entry	Core sample	Polymer conc. (ppm)	Brine conc. (ppm)	RRF[a]	e (µm)[b]
PS75-PMAA629	Bentheim (1)	5538	2000	14.78	4.13
FP 3430S	Bentheim (2)	2000	2000	6.25	1.42

a. Residual retention factor based on equation 5
b. The average absorbed polymer thickness based on equation 6

The above results confirm the formation of multilayers for the PS-PMAA triblock copolymers. The adsorbed polymer layer thickness is almost four times higher compared with the commercial hydrolyzed polyacrylamide. The differences can be attributed to the molecular architecture (triblock vs linear) and chemical structure (amphiphilic vs homopolymer). The presence of charges reduces the extent of adsorption onto a surface, but both polymers exhibit charges on the backbone. The reduction in permeability subsequently diverts the injected fluid to poorly swept zones, which increases the oil recovery while improving the sweep efficiency[76]. However, injectivity issues can arise due to the exponential increase in the pressure of the reservoir due to plugging. This phenomena is even more pronounced for low permeable reservoirs. Another explanation for the high difference in viscosity before and after the polymer flood in the stone core, could be mechanical degradation of the polymer due to chain scission[117]. It is known that mechanical degradation occurs in pipes, through valves or stones above a certain pressure drop[118-120]. This phenomena is most pronounced for high molecular weight polymers. The molecular weight of the polymer used in the experiment (Mn = 58.6 kDa) is

quite low and therefore it is uncertain if mechanical degradation attributes to the lower viscosity. For further research on this topic, the molecular weight before and after the core-flood experiment should be measured to determine the presence of this effect.

5. Conclusion

In this work well-defined amphiphilic triblock poly(sodium methacrylate)-polystyrene-poly(sodium methacrylate) (PMAA-*b*-PS-*b*-PMAA) copolymers were synthesized by ATRP. The block copolymers were characterized by a different length of either the hydrophilic or the hydrophobic block to study the influence of the block length on the rheological properties in water. Previous work focused on the rheology of the analogue diblock copolymers constituted by $PMAA^{16}/PAA^{3}$ and PS, but a systematic study on the effect of the block length for triblock copolymers was never considered before. Moreover, this research investigated the performance of the triblock copolymers in oil recovery simulations. To the best of our knowledge, the rheological behavior and the corresponding application in Enhanced Oil Recovery have not been investigated before.

The PMAA-*b*-PS-*b*-PMAA copolymers were successfully synthesized by ATRP. The obtained triblock copolymers form strong viscoelastic gels depending on the polymer composition. It was found that in the concentrated region (1 wt%) short PMAA blocks yield the strongest gels. However, polymers with longer PMAA blocks start to form gels at lower concentrations. The hydrophobic block length only plays a minor role until a certain threshold (35 monomeric units) below which the hydrophobic interactions are too weak resulting in the formation of weak gels. The same results were found by Raffa et al. for the analogous diblock copolymers of PS-$PMAA^{16}$.

The amphiphilic triblock copolymers form star-like micelles (hydrophilic block > hydrophobic block) consisting of a collapsed PS core surrounded by charged hydrated PMAA chains which are fully stretched in solution. At low concentrations non-interacting isolated micelles are present, but after a certain critical concentration the micelles start to interpenetrate and shrink. Eventually a sol-gel transition occurs and an interpenetrating polymer network is formed. The gel structure was examined by negative stain electron microscopy. The images show a micellar structure, which was disordered in all cases. The polymers with a high viscosity at 1 wt% showed a smaller micelle radius and and a more dense packing indicating that a gel network is formed. A mathematical model that describes the micellar radius was used to make estimations of the gel structure. The mathematical model and the experimentally found radius in transmission electron microscopy are in good agreement. It can be concluded that in the gel structure (high concentration) the hydrophilic corona shrinks due to the screening effect exerted by interpenetrating charged coronas. Furthermore, the aggregation number of the triblock copolymers was found to be much lower compared with the analogue diblock copolymers due to steric hindrance.

The triblock copolymers did not exhibit a CMC so it can be concluded that the polymers seems to be present in water as kinetically “frozen” micelles. This can be attributed to the high hydrophobicity and high glass transition temperature of the polystyrene block, which causes a large activation energy barrier for molecular exchange. The ability of the triblock copolymers to stabilize water/oil emulsions

was investigated. Emulsions of crude oil and polymer solutions were stable for a prolonged period of time where the stability was primarily determined by the viscosity, concentration and the molecular structure.

The influence of the ionic strength, pH and the temperature on the rheology has been preliminary investigated. The experiments showed that the pH and ionic strength have a great influence on the rheology. The viscosity decreased significantly upon addition of salt or decreasing the pH due to shielding of the charges on the PMAA block, which leads to chain collapse, shrinking of the corona and weaker intermicellar interactions. The change in conformation from collapsed to stretched by changing the pH was quantified with zeta-potential measurements. The experiments showed that the zeta-potential increases with increasing the pH due to ionization of the PMAA blocks.

Finally, the EOR performance was evaluated by simulating oil recovery in 2D flow-cell and core-flood experiments. The efficiency of the polymers in recovering residual oil out of dead-end pores in the flow-cell showed promising results with an additional oil recovery between 40-60% compared with a water flow. One amphiphilic triblock copolymer (entry 8: PS75-PMAA629) was used to evaluate oil recovery from a Bentheim sandstone core in a core-flood experiment and was compared with a commercial polymer: HPAM. The oil recovery in high permeable Bentheim cores was significantly improved with an additional oil recovery of 6.38 % for the triblock copolymer compared with 4.01 % for the commercial HPAM polymer. Also, the amphiphilic block copolymer displayed a higher RRF and adsorbed polymer layer thickness compared to the commercial polymer, which can increase oil recovery due to an improvement in the sweep efficiency. However, the effect of the salt concentration influences the solution viscosity significantly. Therefore, from an economical point of view, the amphiphilic triblock copolymers are only feasible in low salt concentration reservoirs. Overall, from this study it can be concluded that amphiphilic PS-PMAA triblock copolymers show very interesting rheological properties and enhance the oil recovery more efficiently than the current used HPAM polymer.

In conclusion, a better understanding of the structure-properties relationship of PS-PMAA amphiphilic triblock copolymers in respect to the rheology, which represents the basis of this present work, can provide an useful tool in designing polymers for specific applications for example in the research fields of smart materials and Enhanced Oil Recovery.

6. Recommendations

The following recommendations are made in order to gain more knowledge about the interesting properties of PS-PMAA amphiphilic triblock copolymers.

This study showed that the oil recovery in high permeable Bentheim cores was significantly improved by polymer flooding with a PS-PMAA amphiphilic triblock copolymer. It would also be interesting to test the triblock copolymer in low permeable Berea sandstone cores. It can be expected that the oil recovery is significantly improved due to the high value for the residual retention factor which gives a high pressure drop. However, if the adsorption is too high injectivity issues can arise which is an important parameter that should be investigated. Furthermore, it would be interesting to measure the viscoelasticity of the polymers used in the flow-cell (at equal viscosity). This could give a better understanding to what extent the elasticity of the triblock copolymers attributes to an increase in oil recovery.

Another recommendation would be to investigate with transmission electron microscopy the change in conformation of the PS-PMAA micelle at changing the pH. Fernyhough et al.[5] found for polybutadiene–poly(methacrylic acid) (PMAA) triblock copolymers a morphological change from large vesicles to worm-like micelles to spherical micelles with increasing the pH. The pH responsive behavior yields interesting applications in the field of smart materials. It must be noted that for the PS-PMAA block copolymers the polystyrene block might inhibit change of the structure due to the high glass transition temperature.

Phase inversion was obtained with one of the emulsions (triblock copolymer/oil) after sonication. This interesting phenomena and the mechanism behind is an interesting research field. Moreover, phase inversion is an important industrial process to make stable emulsions for a different products varying from food to pharmaceuticals.

The monomer poly(ethylene glycol) monomethyl ether methacylate (PEGMA) is a very interesting and promising monomer to use as the hydrophilic block in block copolymers. Block copolymers of PEGMA and PS exhibit excellent thickening capabilities without using charged moieties along the backbone (therefore also compatible in high salt reservoirs)[121,122]. Preliminary synthesis reactions with ATRP and RAFT have already been executed by the authors. However, the use of ATRP as polymerization method resulted that the chain extension with PEGMA on the PS-initiator gave very low conversions. When RAFT polymerization was applied, the PEGMA homopolymerized instead of chain extended on the PS initiator.

References

1. Raffa P, Wever DAZ, Picchioni F, Broekhuis AA. Polymeric surfactants: Synthesis, properties, and links to applications. *Chem Rev*. 2015;115(16):8504-8563.

2. Alexandridis P. Amphiphilic copolymers and their applications. *Current Opinion in Colloid & Interface Science*. 1996;1(4):490-501.

3. Tsitsilianis C, Iliopoulos I, Ducouret G. An associative polyelectrolyte end-capped with short polystyrene chains. synthesis and rheological behavior. *Macromolecules*. 2000;33(8):2936-2943.

4. Cohen Stuart MA, Hofs B, Voets IK, de Keizer A. Assembly of polyelectrolyte-containing block copolymers in aqueous media. *Current Opinion in Colloid & Interface Science*. 2005;10(1–2):30-36.

5. Fernyhough C, Ryan AJ, Battaglia G. pH controlled assembly of a polybutadiene–poly (methacrylic acid) copolymer in water: Packing considerations and kinetic limitations. *Soft Matter*. 2009;5(8):1674-1682.

6. Cayre OJ, Chagneux N, Biggs S. Stimulus responsive core-shell nanoparticles: Synthesis and applications of polymer based aqueous systems. *Soft Matter*. 2011;7(6):2211-2234.

7. Hocine S, Li M. Thermoresponsive self-assembled polymer colloids in water. *Soft Matter*. 2013;9(25):5839-5861.

8. Sottmann T. Solubilization efficiency boosting by amphiphilic block co-polymers in microemulsions. *Curr Opin Colloid Interface Sci*. 2002;7(1-2):57-65.

9. Muller H, Leube W, Tauer K, Forster S, Antonietti M. Polyelectrolyte block copolymers as effective stabilizers in emulsion polymerization. *Macromolecules*. 1997;30(8):2288-2293.

10. Muñoz-Bonilla A, van Herk AM, Heuts JP. Preparation of hairy particles and antifouling films using brush-type amphiphilic block copolymer surfactants in emulsion polymerization. *Macromolecules*. 2010;43(6):2721-2731.

11. Ibrahim K, Salminen A, Holappa S, et al. Preparation and characterization of polystyrene-poly(ethylene oxide) amphiphilic block copolymers via atom transfer radical polymerization: Potential application as paper coating materials. *J Appl Polym Sci*. 2006;102(5):4304-4313.

12. Haladjova E, Rangelov S, Tsvetanov CB, Pispas S. DNA encapsulation via nanotemplates from cationic block copolymer micelles. *Soft Matter*. 2012;8(10):2884-2889.

13. York AW, Kirkland SE, McCormick CL. Advances in the synthesis of amphiphilic block copolymers via RAFT polymerization: Stimuli-responsive drug and gene delivery. *Adv Drug Deliv Rev*. 2008;60(9):1018-1036.

14. Bian F, Xiang M, Yu W, Liu M. Preparation and self-assembly behavior of thermosensitive polymeric micelles comprising poly (styrene-b-N, n-diethylacrylamide). *J Appl Polym Sci*. 2008;110(2):900-907.

15. Raffa P, Brandenburg P, Wever DAZ, Broekhuis AA, Picchioni F. Polystyrene-poly(sodium methacrylate) amphiphilic block copolymers by ATRP: Effect of structure, pH, and ionic strength on rheology of aqueous solutions. *Macromolecules*. 2013;46(17):7106-7111.

16. Raffa P, Stuart MCA, Broekhuis AA, Picchioni F. The effect of hydrophilic and hydrophobic block length on the rheology of amphiphilic diblock polystyrene-b-poly(sodium methacrylate) copolymers prepared by ATRP. *J Colloid Interface Sci*. 2014;428:152-161.

17. Winnik M, Yekta A. Associative polymers in aqueous solution. *Curr Opin Colloid Interface Sci*. 1997;2(4):424-436.

18. Maia AMS, Borsali R, Balaban RC. Comparison between a polyacrylamide and a hydrophobically modified polyacrylamide flood in a sandstone core. *Materials Science & Engineering C-Biomimetic and Supramolecular Systems*. 2009;29(2):505-509.

19. Thomas S. Enhanced Oil Recovery - an overview. *Oil Gas Sci Technol*. 2008;63(1):9-19.

20. Zhang Li-juan, Yue Xiang-an. Displacement of polymer solution on residual oil trapped in

dead ends. *Journal of Central South University of Technology*. 2008;15:84-87.

21. Wei B, Romero-Zerón L, Rodrigue D. Oil displacement mechanisms of viscoelastic polymers in Enhanced Oil Recovery (EOR): A review. *Journal of Petroleum Exploration and Production Technology*. 2014;4(2):113-121.

22. Wever DA, Picchioni F, Broekhuis AA. Comblike polyacrylamides as flooding agent in Enhanced Oil Recovery. *Ind Eng Chem Res*. 2013;52(46):16352-16363.

23. Veerabhadrappa SK. *Study of effects of polymer elasticity on Enhanced Oil Recovery by core flooding and visualization experiments*. 2012.

24. Alvarado V, Manrique E. Enhanced Oil Recovery: An update review. *Energies*. 2010;3(9):1529-1575.

25. Wever DAZ. *Synthesis and evaluation of novel linear and branched polyacrylamides for Enhanced Oil Recovery*. [Doctoral dissertation]. Groningen: University of Groningen; 2013.

26. Chuah H, Lin-Vien D, Soni U. Poly (trimethylene terephthalate) molecular weight and Mark–Houwink equation. *Polymer*. 2001;42(16):7137-7139.

27. Taylor KC, Nasr-El-Din HA. Water-soluble hydrophobically associating polymers for improved oil recovery: A literature review. *Journal of Petroleum Science and Engineering*. 1998;19(3-4):265-280.

28. Lund R, Pipich V, Willner L, Radulescu A, Colmenero J, Richter D. Structural and thermodynamic aspects of the cylinder-to-sphere transition in amphiphilic diblock copolymer micelles. *Soft Matter*. 2011;7(4):1491-1500.

29. Burguiere C, Pascual S, Bui C, et al. Block copolymers of poly(styrene) and poly(acrylic acid) of various molar masses, topologies, and compositions prepared via controlled/living radical polymerization. application as stabilizers in emulsion polymerization. *Macromolecules*. 2001;34(13):4439-4450.

30. Hussain H, Amado E, Kressler J. Functional polyether-based amphiphilic block copolymers synthesized by atom-transfer radical polymerization. *Aust J Chem*. 2011;64(9):1181-1193.

31. Wever DAZ, Picchioni F, Broekhuis AA. Polymers for Enhanced Oil Recovery: A paradigm for structure-property relationship in aqueous solution. *Prog Polym Sci*. 2011;36(11):1558-1628.

32. Riess G. Micellization of block copolymers. *Prog Polym Sci*. 2003;28(7):1107-1170.

33. Matyjaszewski K. Atom transfer radical polymerization (ATRP): Current status and future perspectives. *Macromolecules*. 2012;45(10):4015-4039.

34. Wang J, Matyjaszewski K. Controlled/" living" radical polymerization. atom transfer radical polymerization in the presence of transition-metal complexes. *J Am Chem Soc*. 1995;117(20):5614-5615.

35. Chaduc I, Lansalot M, D'Agosto F, Charleux B. RAFT polymerization of methacrylic acid in water. *Macromolecules*. 2012;45(3):1241-1247.

36. Nicolas J, Guillaneuf Y, Lefay C, Bertin D, Gigmes D, Charleux B. Nitroxide-mediated polymerization. *Progress in Polymer Science*. 2013;38(1):63-235.

37. Jagur-Grodzinski J. *Living and controlled polymerization: Synthesis, characterization, and properties of the respective polymers and copolymers.* Nova Publishers; 2006.

38. Tsitsilianis C, Sfika V. Heteroarm star-like micelles formed from polystyrene-block-poly (2-vinyl pyridine)-block-poly (methyl methacrylate) ABC triblock copolymers in toluene. *Macromolecular rapid communications*. 2001;22(8):647-651.

39. Dobrynin AV, Rubinstein M. Theory of polyelectrolytes in solutions and at surfaces. *Progress in Polymer Science*. 2005;30(11):1049-1118.

40. Taribagil RR, Hillmyer MA, Lodge TP. Hydrogels from ABA and ABC triblock polymers. *Macromolecules*. 2010;43(12):5396-5404.

41. Kimerling AS, Rochefort WE, Bhatia SR. Rheology of block polyelectrolyte solutions

and gels: A review. *Ind Eng Chem Res*. 2006;45(21):6885-6889.

42. Korobko A, Jesse W, Lapp A, Egelhaaf S, van der Maarel J. Structure of strongly interacting polyelectrolyte diblock copolymer micelles. *J Chem Phys*. 2005;122(2):024902.

43. Tsitsilianis C, Aubry T, Iliopoulos I, Norvez S. Effect of DMF on the rheological properties of telechelic polyelectrolyte hydrogels. *Macromolecules*. 2010;43(18):7779-7784.

44. Bhatia SR, Mourchid A. Gelation of micellar block polyelectrolytes: Evidence of glassy behavior in an attractive system. *Langmuir*. 2002;18(17):6469-6472.

45. Alexandridis P, Hatton T. Poly(ethylene oxide)-poly(propylene oxide)-poly(ethylene oxide) block-copolymer surfactants in aqueous-solutions and at interfaces - thermodynamics, structure, dynamics, and modeling. *Colloid Surf A-Physicochem Eng Asp*. 1995;96(1-2):1-46.

46. Hamley IW, Daniel C, Mingvanish W, et al. From hard spheres to soft spheres: The effect of copolymer composition on the structure of micellar cubic phases formed by diblock copolymers in aqueous solution. *Langmuir*. 2000;16(6):2508-2514.

47. Milnera M., Stepanek M, Zuskova I, Prochazka K. Experimental study of the electrophoretic mobility and effective electric charge of polystyrene-block-poly(methacrylic acid) micelles in aqueous media. *International Journal of Polymer Analysis and Characterization*. 2007;12(1):23-33.

48. van Stam J, Creutz S, De Schryver F, Jerome R. Tuning of the exchange dynamics of unimers between block copolymer micelles with temperature, cosolvents, and cosurfactants. *Macromolecules*. 2000;33(17):6388-6395.

49. Hales K, Pochan DJ. Using polyelectrolyte block copolymers to tune nanostructure assembly. *Current Opinion in Colloid & Interface Science*. 2006;11(6):330-336.

50. Zhang L, Eisenberg A. Thermodynamic vs kinetic aspects in the formation and morphological transitions of crew-cut aggregates produced by self-assembly of polystyrene-b-poly (acrylic acid) block copolymers in dilute solution. *Macromolecules*. 1999;32(7):2239-2249.

51. Choucair A, Lavigueur C, Eisenberg A. Polystyrene-b-poly (acrylic acid) vesicle size control using solution properties and hydrophilic block length. *Langmuir*. 2004;20(10):3894-3900.

52. Garnier S, Laschewsky A. New amphiphilic diblock copolymers: Surfactant properties and solubilization in their micelles. *Langmuir*. 2006;22(9):4044-4053.

53. Exerowa D, Platikanov D. Thin liquid films from aqueous solutions of non-ionic polymeric surfactants. *Adv Colloid Interface Sci*. 2009;147-48:74-87.

54. Zhou J, Wang L, Ma J. Recent research progress in the synthesis and properties of amphiphilic block co-polymers and their applications in emulsion polymerization. *Designed Monomers and Polymers*. 2009;12(1):19-41.

55. Kilpatrick Peter K. Water-in-crude oil emulsion stabilization: Review and unanswered questions. *Energy and Fuels*. 2012;26(7):4017-4026.

56. Eow JS, Ghadiri M, Sharif A, Williams T. Electrostatic enhancement of coalescence of water droplets in oil: A review of the current understanding. *Chem Eng J*. 2001;84(3):173-192.

57. Tadros Tharwat T. Principles of emulsion stabilization with special reference to polymeric surfactants. *J Cosmet Sci*. 2006 Mar-Apr;57(2):153-69.

58. Burguiere C, Pascual S, Coutin B, et al. Amphiphilic block copolymers prepared via controlled radical polymerization as surfactants for emulsion polymerization. *Macromol Symp*. 2000;150:39-44.

59. Davis K, Charleux B, Matyjaszewski K. Preparation of block copolymers of polystyrene and poly (t-butyl acrylate) of various molecular weights and architectures by atom transfer radical polymerization. *J Polym Sci Pol Chem*. 2000;38(12):2274-2283.

60. Birshtein T. M., Mercurieva AA, Leermakers FAM, Rud OV. Conformations of polymer

and polyelectrolyte stars. *Polymer Science Series A*. 2008;50(9):992-1007.

61. Rud O. V., Mercurieva AA, Leermakers FAM, Birshtein TM. Collapse of polyelectrolyte star. theory and modeling. *Macromolecules*. 2012;45(4):2145-2160.

62. Muggeridge A, Cockin A, Webb K, et al. Recovery rates, Enhanced Oil Recovery and technological limits. *Philos Trans R Soc A-Math Phys Eng Sci*. 2014;372(2006):20120320.

63. Shah DO. *Improved oil recovery by surfactant and polymer flooding.* Elsevier; 2012.

64. Yu W, Lashgari HR, Wu K, Sepehrnoori K. CO2 injection for Enhanced Oil Recovery in bakken tight oil reservoirs. *Fuel*. 2015;159:354-363.

65. Shah A, Fishwick R, Wood J, Leeke G, Rigby S, Greaves M. A review of novel techniques for heavy oil and bitumen extraction and upgrading. *Energy Environ Sci*. 2010;3(6):700-714.

66. Kamal MS, Sultan AS, Al-Mubaiyedh UA, Hussein IA. Review on polymer flooding: Rheology, adsorption, stability, and field applications of various polymer systems. *Polymer Reviews*. 2015;55(3):491-530.

67. Olajire AA. Review of ASP EOR (alkaline surfactant polymer Enhanced Oil Recovery) technology in the petroleum industry: Prospects and challenges. *Energy*. 2014;77:963-982.

68. Standnes DC, Skjevrak I. Literature review of implemented polymer field projects. *Journal of Petroleum Science and Engineering*. 2014;122:761-775.

69. Zhang Lijuan, Yue Xiang'an, Guo Fenqiao. Micro-mechanisms of residual oil mobilization by viscoelastic fluids. *Pet Sci*. 2008;5(1):56-61.

70. Buchgraber M, Clemens T, Castanier LM, Kovscek AR. The displacement of viscous oil by associative polymer solutions. . 2009.

71. Nazar M, Shah S, Khosa M. Microemulsions in Enhanced Oil Recovery: A review. *Petrol Sci Technol*. 2011;29(13):1353-1365.

72. Schramm LL, Stasiuk EN, Marangoni DG. 2 surfactants and their applications. *Annual Reports Section" C"(Physical Chemistry)*. 2003;99:3-48.

73. Atesok G, Somasundaran P, Morgan L. Charge effects in the adsorption of polyacrylamides on sodium kaolinite and its flocculation. *Powder Technol*. 1988;54(2):77-83.

74. Nilsson L, Bergenståhl B. Adsorption of hydrophobically modified anionic starch at oppositely charged oil/water interfaces. *J Colloid Interface Sci*. 2007;308(2):508-513.

75. Lake LW. *Enhanced Oil Recovery*. United States: Old Tappan, NJ: Prentice Hall Inc.; 1989.

76. Zaitoun A, Kohler N. Two-phase flow through porous media: Effect of an adsorbed polymer layer. . 1988.

77. Eghbali E, Colombani O, Drechsler M, Müller AH, Hoffmann H. Rheology and phase behavior of poly (n-butyl acrylate)-b lock-poly (acrylic acid) in aqueous solution. *Langmuir*. 2006;22(10):4766-4776.

78. Lee SC, Lee HJ. pH-controlled, polymer-mediated assembly of polymer micelle nanoparticles. *Langmuir*. 2007;23(2):488-495.

79. Dai S, Ravi P, Tam KC, Mao BW, Gang LH. Novel pH-responsive amphiphilic diblock copolymers with reversible micellization properties. *Langmuir*. 2003;19(12):5175-5177.

80. Pelet JM, Putnam D. High molecular weight poly (methacrylic acid) with narrow polydispersity by RAFT polymerization. *Macromolecules*. 2009;42(5):1494-1499.

81. Wever DA, Polgar LM, Stuart MC, Picchioni F, Broekhuis AA. Polymer molecular architecture as a tool for controlling the rheological properties of aqueous polyacrylamide solutions for Enhanced Oil Recovery. *Ind Eng Chem Res*. 2013;52(47):16993-17005.

82. Wever Diego Armando Z., Ramalho G, Picchioni F, Broekhuis AA. Acrylamide-b-N-isopropylacrylamide block copolymers: Synthesis by atomic transfer radical polymerization in water and the effect of the

hydrophilic-hydrophobic ratio on the solution properties. *J Appl Polym Sci*. 2014;131(2).

83. Niu Y, Jian O, Zhu Z, Wang G, Sun G, Shi l. Research on hydrophobically associating water-soluble polymer used for EOR. *Society of Petroleum Engineers*. 2001.

84. Takeuchi S, Nakashima S, Tomiya A. Permeability measurements of natural and experimental volcanic materials with a simple permeameter: Toward an understanding of magmatic degassing processes. *J Volcanol Geotherm Res*. 2008;177(2):329-339.

85. Braunecker WA, Matyjaszewski K. Controlled/living radical polymerization: Features, developments, and perspectives. *Progress in Polymer Science*. 2007;32(1):93-146.

86. Rager T, Meyer W, Wegner G, Winnik M. Influence of chain length and salt concentration on block copolymer micellization. *Macromolecules*. 1997;30(17):4911-4919.

87. Thomas DB, Convertine AJ, Hester RD, Lowe AB, McCormick CL. Hydrolytic susceptibility of dithioester chain transfer agents and implications in aqueous RAFT polymerizations. *Macromolecules*. 2004;37(5):1735-1741.

88. Thomas DB, Convertine AJ, Myrick LJ, et al. Kinetics and molecular weight control of the polymerization of acrylamide via RAFT. *Macromolecules*. 2004;37(24):8941-8950.

89. Hietala S, Mononen P, Strandman S, et al. Synthesis and rheological properties of an associative star polymer in aqueous solutions. *Polymer*. 2007;48(14):4087-4096.

90. Flory P, Fox T. Treatment of intrinsic viscosities. *J Am Chem Soc*. 1951;73(5):1904-1908.

91. Valint Jr P, Bock J. Synthesis and characterization of hydrophobically associating block polymers. *Macromolecules*. 1988;21(1):175-179.

92. Borisova O., Billon L, Zaremski M, Grassl B, Bakaeva Z. Synthesis and pH- and salinity-controlled self-assembly of novel amphiphilic block-gradient copolymers of styrene and acrylic acid. *Soft Matter*. 2012;8(29):7649-7659.

93. Vlassopoulos D, Fytas G, Pispas S, Hadjichristidis N. Spherical polymeric brushes viewed as soft colloidal particles: Zero-shear viscosity. *Physica B: Condensed Matter*. 2001;296(1–3):184-189.

94. Katsampas I, Tsitsilianis C. Hierarchical self-organization of ABC terpolymer constituted of a long polyelectrolyte end-capped by different hydrophobic blocks. *Macromolecules*. 2005;38(4):1307-1314.

95. Hamley IW. *Block copolymers in solution: Fundamentals and applications.* John Wiley & Sons; 2005.

96. Raju VR, Menezes EV, Marin G, Graessley WW, Fetters LJ. Concentration and molecular-weight dependence of viscoelastic properties in linear and star polymers. *Macromolecules*. 1981;14(6):1668-1676.

97. Wever DAZ, Picchioni F, Broekhuis AA. Branched polyacrylamides: Synthesis and effect of molecular architecture on solution rheology. *Eur Polym J*. 2013;49(10):3289-3301.

98. Peter P, Plessis C, Riess G. Controlled latex agglomeration by formulation of anionic surfactant complexes: Poly(ethylene) block copolymers. *Comptes Rendus Chimie*. 2003;6(11-12):1403-1410.

99. Theodoly O O, Jacquin M, Muller P, Chhun S. Adsorption kinetics of amphiphilic diblock copolymers: From kinetically frozen colloids to macrosurfactants. *Langmuir*. 2009-1-20;25(2):781-93.

100. Moffitt M, Khougaz K, Eisenberg A. Micellization of ionic block copolymers. *Acc Chem Res*. 1996;29(2):95-102.

101. Huh J, Kim K, Ahn C, Jo W. Micellization behavior of star-block copolymers in a selective solvent: A brownian dynamics simulation approach. *J Chem Phys*. 2004;121(10):4998-5004.

102. Malhotra A, Coupland JN. The effect of surfactants on the solubility, zeta potential, and viscosity of soy protein isolates. *Food Hydrocoll*. 2004;18(1):101-108.

103. Hunter RJ. *Zeta potential in colloid science: Principles and applications.* Vol 2. Academic press; 2013.

104. Lyklema J. *Fundamentals of interface and colloid science: Soft colloids.* Vol 5. Academic press; 2005.

105. O'Brien RW, White LR. Electrophoretic mobility of a spherical colloidal particle. *Journal of the Chemical Society, Faraday Transactions 2: Molecular and Chemical Physics*. 1978;74:1607-1626.

106. Borisov O, Zhulina E. Effect of salt on self-assembly in charged block copolymer micelles. *Macromolecules*. 2002;35(11):4472-4480.

107. Osada Y, Gong J, Tanaka Y. Polymer gels (reprinted from functional monomers and polymers, pg 497-528, 1997). *Journal of Macromolecular Science-Polymer Reviews*. 2004;C44(1):87-112.

108. Ruiz-Perez L, Pryke A, Sommer M, et al. Conformation of poly(methacrylic acid) chains in dilute aqueous solution. *Macromolecules*. 2008;41(6):2203-2211.

109. Sun Y, Peng Z, Liu X, Tong Z. Synthesis and pH-sensitive micellization of doubly hydrophilic poly (acrylic acid)-b-poly (ethylene oxide)-b-poly (acrylic acid) triblock copolymer in aqueous solutions. *Colloid Polym Sci*. 2010;288(9):997-1003.

110. Ruckenstein E. Microemulsions, macroemulsions, and the bancroft rule. *Langmuir*. 1996;12(26):6351-6353.

111. Zhao J, Pispas S, Zhang G. Effect of sonication on polymeric aggregates formed by poly (ethylene oxide)-Based amphiphilic block copolymers. *Macromolecular Chemistry and Physics*. 2009;210(12):1026-1032.

112. Huang Jing, Xu J, Chen K, Wang T, Cui C. Synthesis of triblock copolymers via RAFT polymerization and their application as surfactants for crude oil-in-water emulsion. *Industrial and Engineering Chemistry Research*. 2015;54(5):1564-1575.

113. Munoz-Bonilla A, Ali SI, del Campo A, Fernandez-Garcia M, van Herk AM, Heuts JPA. Block copolymer surfactants in emulsion polymerization: Influence of the miscibility of the hydrophobic block on kinetics, particle morphology, and film formation. *Macromolecules*. 2011;44(11):4282-4290.

114. Wang Guijiang, Ouyang J, Yi X. Study of copolymer performance in polymer flooding of the daqing oil field. *Chem Technol Fuels Oils*. 2011;47(4):263-267.

115. Page M, Lecourtier J, Noïk C, Foissy A. Adsorption of polyacrylamides and of polysaccharides on siliceous materials and kaolinite: Influence of temperature. *J Colloid Interface Sci*. 1993;161(2):450-454.

116. Ren H, Li Y, Zhang S, Wang J, Luan Z. Flocculation of kaolin suspension with the adsorption of N, N-disubstituted hydrophobically modified polyacrylamide. *Colloids Surf Physicochem Eng Aspects*. 2008;317(1):388-393.

117. Seright RS, Fan T, Wavrik K, Balaban RdC. New insights into polymer rheology in porous media. *SPE Journal*. 2011;16(01):35-42.

118. Thomas A, Gaillard N, Favero C. Some key features to consider when studying acrylamide-based polymers for chemical Enhanced Oil Recovery. *Oil & Gas Science and Technology–Revue d'IFP Energies nouvelles*. 2012;67(6):887-902.

119. Al Hashmi AR, Al Maamari RS, Al Shabibi IS, Mansoor AM, Zaitoun A, Al Sharji HH. Rheology and mechanical degradation of high-molecular-weight partially hydrolyzed polyacrylamide during flow through capillaries. *Journal of Petroleum Science and Engineering*. 2013;105:100-106.

120. Seright RS, Seheult M, Talashek T. Injectivity characteristics of EOR polymers. *Spe Reservoir Evaluation & Engineering*. 2009;12(5):783-792.

121. Sun L, Liu J, Zhao H. Reactive polymeric micelles with disulfide groups in the coronae. *Polymer Chemistry*. 2014;5(22):6584-6592.

122. Zhao W, Gody G, Dong S, Zetterlund PB, Perrier S. Optimization of the RAFT polymerization conditions for the in situ formation of nano-objects via dispersion polymerization in alcoholic medium. *Polymer Chemistry*.2014.

Appendix I

Entry	PS-PMAA	Polymer concentration [wt%]	Viscosity [mPa.s]	Oil recovery [%]	Additional oil recovery [b] [%]	Flow-cell picture
Water flood	-	-	-	13.0	0	
FP3430	HPAM	0.13	72	16.1	3.1	
7	PS75-PMAA463	0.17	105.8	52.7	39.7	
8	PS75-PMAA629	0.096	104.6	56.3	43.3	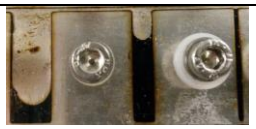
9[c]	PS45-PMAA2210	0.48	93.7	73.8	60.8	
10	PS45-PMAA1047	1.19	97.8	60.7	47.7	
11	PS45-PMAA598	0.16	106.6	66.2	53.2	
12	PS35-PMAA1564	0.59	102.3	56.6	43.6	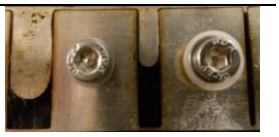

a. Additional oil recovery calculation according to equation 10

b. SNF polyacrylamide (HPAM, Mn ≈ 12000 kDa, 25-30 hydrolysis in mole %); Viscosity oil in experiment 70 mPa.s

c. Performed in duplo. Standard deviation oil recovery = 3.29 %

Appendix II

The figure below shows the viscosity versus the shear rate at different weight concentration for the synthesized triblock copolymers.

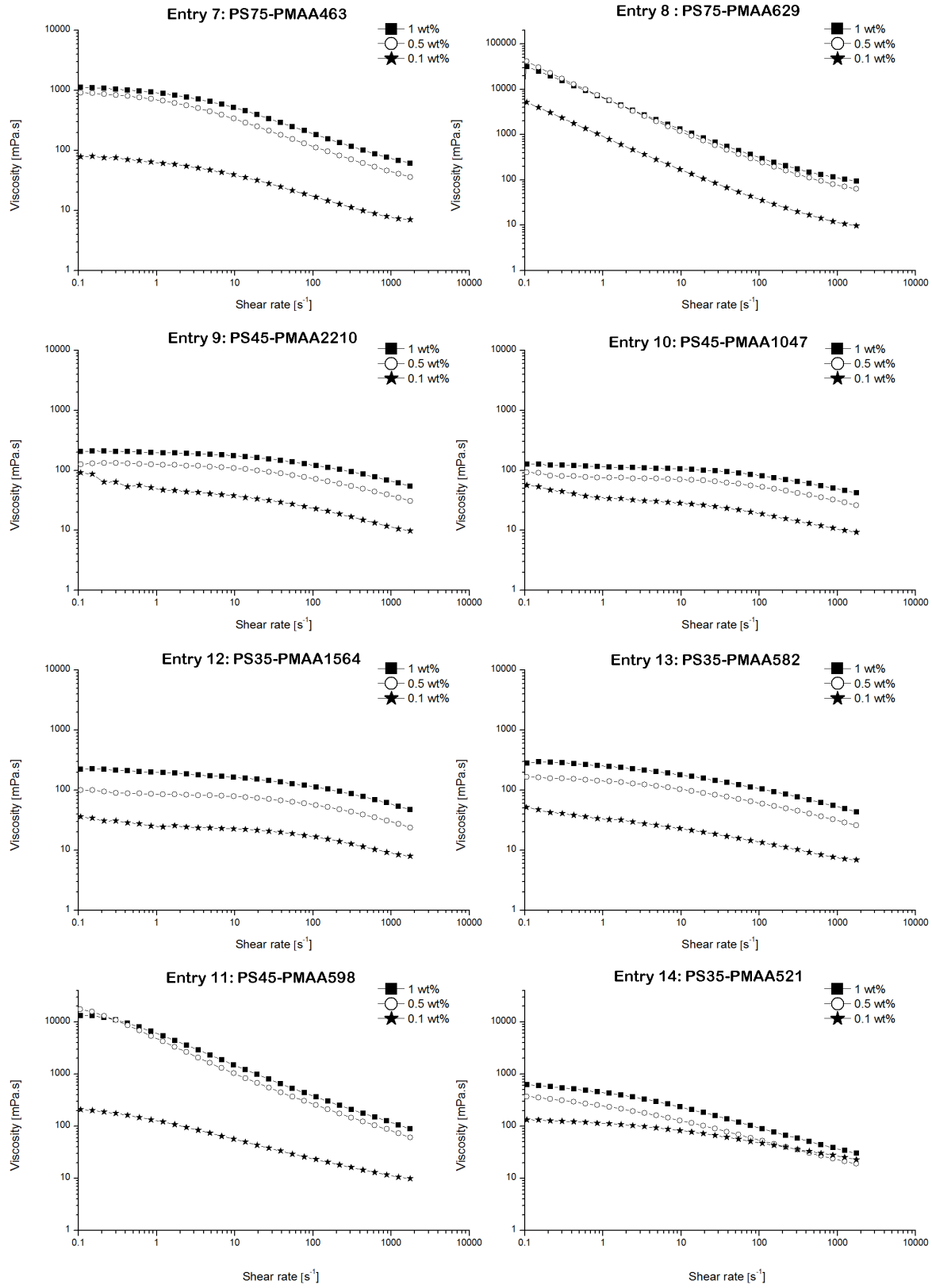

Appendix III

The figure below shows the G' and G'' versus the frequency for 1.0, 0.5 and 0.1 wt% polymer solutions.

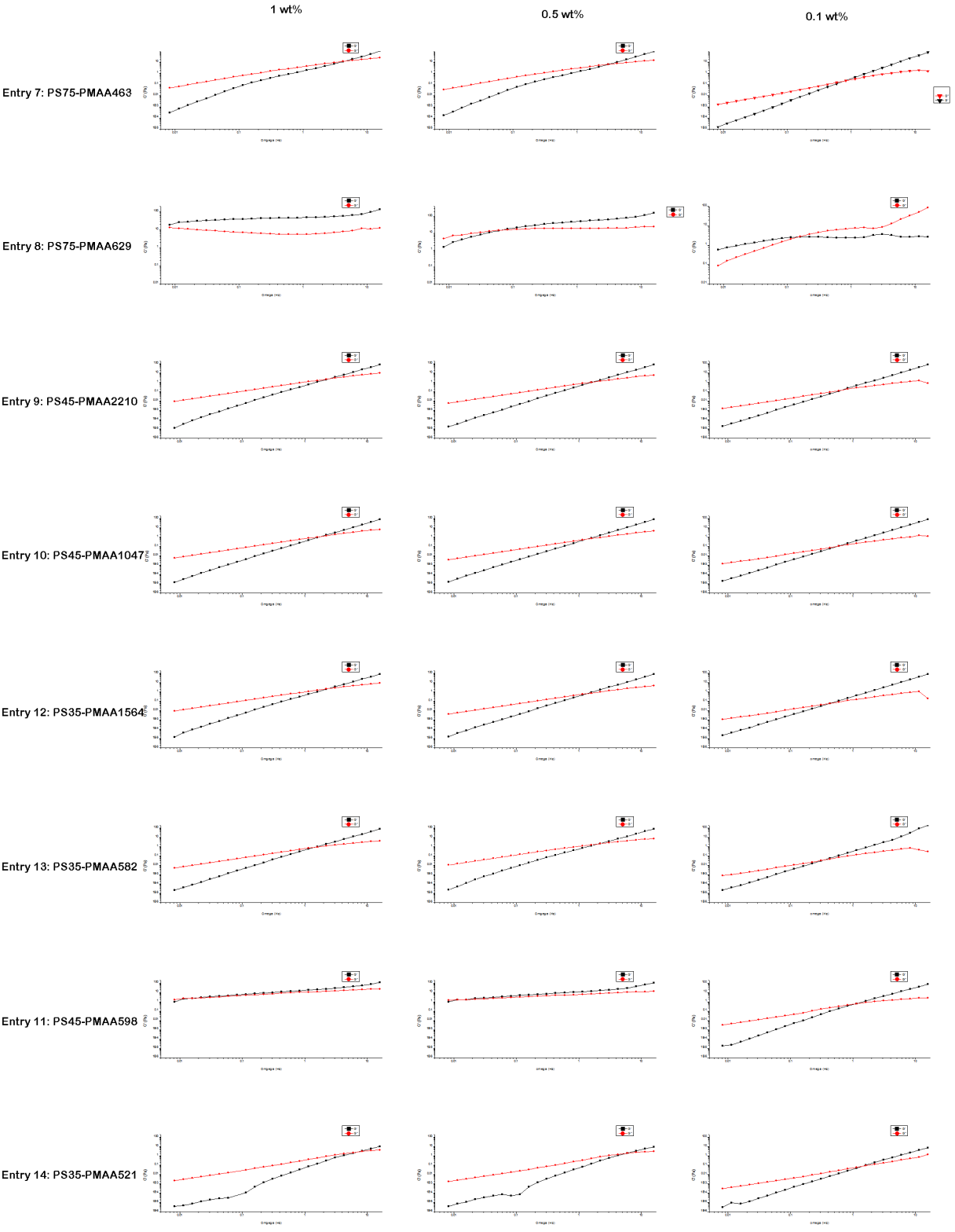

Appendix IV

Zeta potential results for the amphiphilic triblock copolymer systems

Entry	Molar concentration (M)	Viscosity (mPa.s)	pH (-)	d_{mic} (μm)	Zeta potential (mV)	mobility
7	$2.0\ 10^{-5}$	40.4	9.07	11.77	-74.17	-5.79
8	$2.0\ 10^{-5}$	308.0	9.03	40.21	-67.50	-5.27
9	$2.0\ 10^{-5}$	113.2	9.30	50.35	-69.64	-5.44
10	$2.0\ 10^{-5}$	36.4	9.34	13.42	-75.37	-5.89
11	$2.0\ 10^{-5}$	100.2	9.06	42.82	-72.95	-5.70
12	$2.0\ 10^{-5}$	81.5	9.25	35.41	-73.54	-5.75

Zeta potential results for entry 11: PS45-PMAA598 at different pH

pH	Molar concentration (M)	d_{mic} (μm)	Zeta potential (mV)	mobility
9.06	$2.0\ 10^{-5}$	42.82	-72.95	-5.75
8.40	$2.0\ 10^{-5}$	13.59	-62.74	-4.90
6.16	$2.0\ 10^{-5}$	1.16	-48.41	-3.78
4.17	$2.0\ 10^{-5}$	0.38	-22.58	-1.76
3.18	$2.0\ 10^{-5}$	9.82	-6.19	-0.40
1.16	$2.0\ 10^{-5}$	5.24	-0.9	-0.07

Appendix V

Stability experiment 1: stability of the emulsion at the same viscosity

Entry	Molar concentration (M)	Viscosity (mPa.s)
7	$2.90\ 10^{-5}$	105.8
8	$1.25\ 10^{-5}$	104.6
9	$1.95\ 10^{-5}$	93.7
10	$9.98\ 10^{-5}$	97.8
11	$2.28\ 10^{-5}$	106.6
12	$3.38\ 10^{-5}$	102.3

Stability experiment 2: stability of the emulsion at the same molar concentration

Entry	Molecular weight (g/mol)	conc. (M)[a]	Viscosity (mPa.s)	Zeta potential (mV)
7	58638	$2.0\ 10^{-5}$	40.4	-74.17
8	76708	$2.0\ 10^{-5}$	308.1	-67.50
9	245904	$2.0\ 10^{-5}$	113.2	-69.64
10	119211	$2.0\ 10^{-5}$	36.4	-75.37
11	70210	$2.0\ 10^{-5}$	100.2	-72.95
12	174548	$2.0\ 10^{-5}$	81.5	-73.54

Appendix VI

Negative stain electron microscope images (1 wt%):

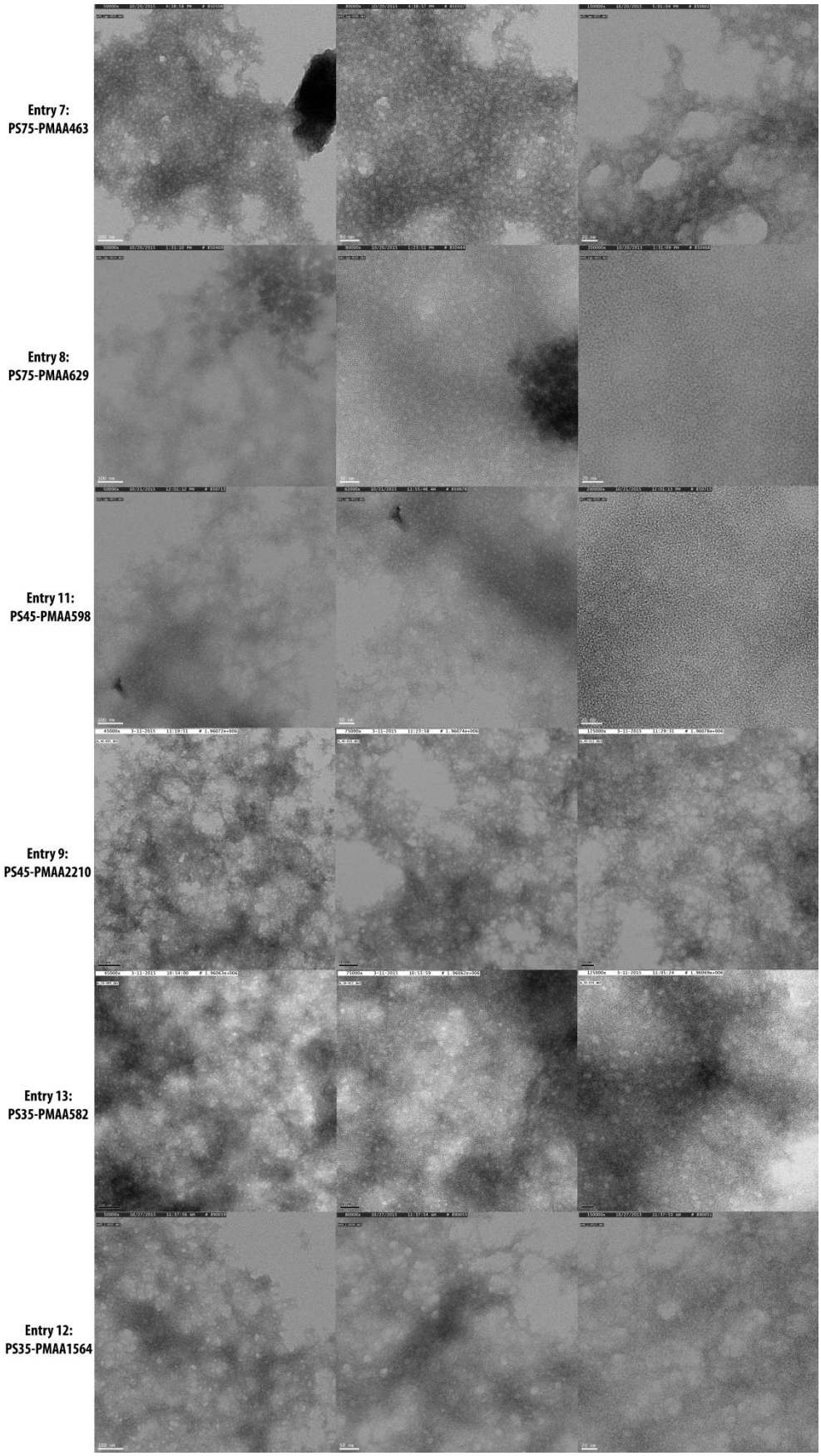

This page intentionally left blank